The Effects of Manufacturing on the Structural Integrity of Gr/PEEK Composite Parts

by

THOMAS ACKLEY WILSON

S.B., Massachusetts Institute of Technology
(1988)

SUBMITTED IN PARTIAL FULFILLMENT OF THE
REQUIREMENTS FOR THE DEGREE OF

MASTER OF SCIENCE
IN
AERONAUTICS AND ASTRONAUTICS

at the

MASSACHUSETTS INSTITUTE OF TECHNOLOGY

September 1990

Signature of Author_____
Department of Aeronautics and Astronautics
August 27th, 1990

Certified by_____
Professor Michael J. Graves
Boeing Assistant Professor of Aeronautics and Astronautics
Thesis Supervisor

Accepted by_____
Professor Harold Y. Wachman
Chairman, Departmental Graduate Committee

The Effects of Manufacturing on the Structural Integrity of Gr/PEEK Composite Parts

by

Thomas A. Wilson

Submitted to the Department of Aeronautics and Astronautics
on August 28, 1990 in partial fulfillment of the
requirements for the Degree of Master of Science

Abstract

The effects of manufacturing on the quality, structural integrity, and predictability of the structural integrity of APC-2 Gr/PEEK parts were investigated. The manufacturing process itself was examined through quality, repeatability, longevity, and practicality. Small plates, large plates and right angle bends were formed with an inexpensive heat blanket surrounded by an insulator in an unheated but pressurized autoclave. From the large plates and bends were cut 20 tensile coupons and 4 bend specimens. The tensile coupons had layups (%0°/%±45°/%90°) of 1) 100/0/0, 70/20/10, 50/40/10, and 30/60/10 of 20 plies and 2) 0/0/100 of 10 plies, while the bends were 100/0/0 of 10 plies. Quality was ascertained by visual observation, microscopic evaluation of the edges and consolidation distance, the distance that plies blend together during consolidation. Structural integrity was determined by comparing the measured ply properties to referenced values. The predictability of the structural integrity of the coupons was determined by applying the measured ply properties and Laminated Plate Theory to the measured 70/20/10, 50/40/10, and 30/60/10 laminate properties. The predictability of the structural integrity of the bends was determined by applying the measured ply properties to an energy method derived stiffness and comparing to load-deflection data. The quality and repeatability of the manufacturing process was evaluated by the magnitude and consistency of the temperature gradient across the part during processing. For the particular manufacturing procedure used, the heat blanket process could form Gr/PEEK parts, although not very well. Quality, repeatability, and longevity make the process impractical. However, if the insulation around the assembly during consolidation was improved, the increase in quality and repeatability may make the process practical. When using the heat blanket in an unheated autoclave, an insulator must surround the assembly, creating a partial oven within the autoclave, to reduce the temperature gradient. The small plates had good quality, while the large plates and bends had poor quality. The large plates had good structural integrity after manufacturing as defined by stiffness. The predictability of the structural integrity for the large plates and bends was good.

Thesis Supervisor: Michael J. Graves
Title: Boeing Assistant Professor of Aeronautics and Astronautics

Acknowledgements

I am very thankful for having Michael as my advisor and the chance to learn from and work with him. His intelligence, knowledge, availability and friendship have been deeply appreciated. His innovative and constructive management approach was greatly appreciated during the difficult times and frustrations of developing the manufacturing technology within this investigation.

My parents have played a large role in this thesis. Their support, love and emphasis on education helped me develop to the point of dealing with MIT and its pressures, which included this thesis. By providing emotional stability and support at home, in addition to maintaining their principles in this current age, I was able to concentrate on education and athletics. Thankyou Mom and Dad!!

I am thankful for the opportunity to be taught by Professor Mar and Professor Dugundji in my graduate years. Their wealth of knowledge, experience and amicable personalities made learning about composite materials thorough and challenging, yet enjoyable as well. I am deeply grateful to Professor Crawley for helping me find employment. In addition, I am thankful for the Gr/PEEK material obtained from Boeing by Professor Lagace.

I am thankful for the opportunity to learn about machining and other experimental issues from Al Supple, Don Weiner and Earl Wassmouth. I wouldn't know how to use a milling machine, drill press, band saw, or how to tap holes in aluminum and steel without their help.

Kevin Saeger and Pierre Minguet deserve special mention in the development of some parts of the analytical section on the bends. Special thanks to fellow graduate students Ken Bonello, Narendra Bhat, Teresa Guy, Claudia Ranniger, Randy Notestine, James Williamson, Adam Sawicki, Ed Wolf, Wilson Tsang and Luca Marmorini. In addition, the help of undergraduates Matthew Beaumont and John Woyak during the mechanical testing was greatly appreciated.

Finally and most importantly, I would like to thank my Fortress, Redeemer, and the One in whom I trust, my Lord and Savior Jesus Christ. As Isaiah 40:30-31 (NIV) says, "Even youths grow tired and weary, and young men stumble and fall; but those who hope in the Lord will renew their strength. They will soar on wings like eagles; they will run and not grow weary, they will walk and not be faint." To this end, this thesis is dedicated to the Praise and Glory of God.

Foreword

This work was performed in the Technology Laboratory for Advanced Composites (TELAC) of the Department of Aeronautics and Astronautics at the Massachusetts Institute of Technology. This work was sponsored by a Leaders for Manufacturing Program Junior Faculty Grant. Special thanks to The Boeing Company for donating the Gr/PEEK.

Table of Contents

Table of Contents (continued)

Table of Contents (continued)

List of Figures

List of Figures (continued)

List of Tables

List of Tables (continued)

Nomenclature

A	Cross sectional area
BX/Y/Z	Bend specimen of laminate type X/Y/Z
TX/Y/Z	Tensile coupon of laminate type X/Y/Z
E_L	Longitudinal ply stiffness
E_T	Transverse ply stiffness
E_{11}	Longitudinal stiffness in principal axes of an orthotropic material
$E_{\alpha\beta\sigma\gamma}$	Stiffness
$S_{\alpha\beta\sigma\gamma}$	Compliance
F	Horizontal force perpendicular to cross-sectional area
G_{LT}	In-plane shear stiffness
G_{XZ}	Out-of-plane shear stiffness
h	Thickness of bend specimen
I	Moment of inertia
L	Total horizontal length of bend specimen
ℓ	Length of straight section of bend specimen
M	Moment
P	End load applied to a bend specimen
PX/Y/Z	Small plate of laminate type X/Y/Z
R	"Goodness" of fit using least squares linear regression method
r	Radius of curved section of bend specimen
s	Distance along the centerline transverse to the cross sectional area within the beam
t_{ply}	Ply thickness
V	Vertical force tangent to the cross sectional area
X/Y/Z	X, Y, Z = % of plies with fibers in the 0°, ±45°, and 90° direction, respectively
ε_A	Strain in rosette axes along the loading direction
ε_{AC}	Shear strain in rosette axes
ε_B	Strain 45° counter-clockwise from ε_A
ε_C	Strain in rosette axes perpendicular to the loading direction
ε_L	Strain in fiber direction

Nomenclature (continued)

ε_T	Strain perpendicular to fiber direction
ε_{11}	Principal strain in loading direction
ε_{22}	Principal strain perpendicular to loading direction
$\varepsilon_{\alpha\beta}$	Strain
δ	Deflection due to an end load
ν_{LT}	Poisson's ratio
Π	Total potential energy of system
θ_P	Amount of rotation to principal axes as measured with the rosette strain gage
σ_L	Stress in fiber direction
σ_T	Stress perpendicular to fiber direction
σ_{11}	Stress applied by MTS machine
$\sigma_{\alpha\beta}$	Stress

Chapter 1
INTRODUCTION

1.1 The Global Picture

The world economy has changed significantly within the last decade. Not only has the world economy played a major role in the political changes in Eastern Europe and the Soviet Union, epitomized by the destruction of the Berlin Wall, but also the economic competitiveness of the United States.

Germany and Japan have completed their recovery from World War II and are challenging the U.S. economically through engineering excellence and the economical application of high technology to market oriented products. Due to the loss of market share in the consumer electronic and automotive industries to foreign competition, U.S. firms are concerned about losing market share in their respective industries. U.S. firms site manufacturing quality and the economical and expedient application of high technology to market oriented products as the weak link which should be improved for the U.S. to remain economically competitive.

Eleven "blue chip" companies formed a partnership with the MIT engineering and business schools to address the problem of manufacturing. This partnership supports research in manufacturing, especially the incorporation of high technology into economical consumer products. Composite materials fall into the category of high technology; and the economical manufacturing of composite parts is one example of applying high technology to consumer products.

1.2 Filamentary Composite Materials

Even though filamentary composite materials have existed for a long time in building construction, such as steel bars reinforcing concrete or fiberglass hulls for boats, they are gaining the most use and publicity in airplanes and spacecraft. Eliminating weight where high strength is unnecessary and the capability for aeroelastic and mechanical property tailoring permit filamentary composite materials to perform as well as their metallic counterparts for less weight. The result of these beneficial qualities is an increase in capability of the aerospace vehicle. In addition, these materials can be tailored to meet a variety of hygrothermal conditions. The Hubble Space Telescope, for example, demands precision when directing its cameras or lenses at objects far away. The tailorability of Gr/Epoxy is used to reduce the hygrothermal effects. Filamentary composite materials appeal to engineers when circumstances demand a high priority on vehicle performance, weight reduction or precision.

Composite materials have been applied to military aircraft and in a small but noticeable role to commercial aircraft. The AV-8B Harrier and the A-6E have composite wing assemblies. The reduced weight with the same stiffness and strength as compared to the conventional metallic material allows the Harrier to perform as a fighter yet light enough for vertical takeoff capability. The F-117A stealth fighter has composite trailing edges to increase the stiffness of the wing. ATF, LHX, and Bell's new bearingless rotor system on the AH-1W are expected to use or are using composite structures. In addition, the Defense Department has cited composite materials as a critical technology to be researched. The commercial business jet Beech Starship 1 uses composite materials on its

primary structure, while the commercial passenger aircraft Boeing 757 and 767 use composite materials for their secondary structures.

Although composite materials can be composed of many different material systems, the most common in the aerospace industry are filamentary composite materials. These materials consist of high strength fibers (e.g. Graphite) in a polymeric matrix, usually a thermoplastic (e.g. PEEK) or thermoset (e.g. Epoxy). The fibers permit composites to be strong in specific directions parallel to the fiber orientations and carry extensional loading. The matrix maintains fiber placement, carries shear loading, and enables the fibers to share tensile loading. A composite material is formed by consolidating plies with the fibers in various directions through heat, pressure and vacuum.

1.3 Cost of Manufacturing Composite Parts

Although filamentary composite materials have higher strength/weight and stiffness/weight ratios in the loading directions than their familiar metallic counterparts, such as aluminum, their application has been relatively restricted to high priority military or space programs. The main reason for this phenomenon is due to the emphasis placed on performance as opposed to cost. The cost is currently too high for making composite parts commercially, primarily due to a lack of comprehensive knowledge of failure behavior and manufacturing cost.

Without a reasonable model for delamination and in-plane failure, engineers will tend to "over" design the part due to excessive safety margins, resulting in extra weight and cost. A review of various methods

used to predict failure of filamentary composite materials can be found in [1].

Equally contributing to the excessive cost is manufacturing the composite parts. Such familiar composites as Graphite/Epoxy (Gr/Ep) and Graphite/Poly-Ether-Ether-Keytone (Gr/PEEK) cost two to ten times more than aluminum per pound for the raw material. In addition, manufacturing composite parts is difficult due to the inherent nature of the material, such as the inextensible continuous fibers, fiber movement during formation and the propensity for voids and delaminations.

This investigation addressed the manufacturing side of the problem by using potentially economical processes to form flat plate and right angle bend composite parts.

1.4 Manufacturing Effects on Mechanical Properties of Composites

Not only does manufacturing affect cost, but also the mechanical performance of the composite part. If a low resin pressure is present during the consolidation process, voids may develop and cause reduction in the mechanical strength [2,3,4]. For Gr/PEEK, the cooling rate after consolidation affects crystallinity and the fracture toughness of the resin [5]. A high crystalline resin has less toughness but more stiffness; an amorphous resin has more toughness and less stiffness. Fast cooling rates create an amorphous resin, while slow cooling rates form a crystalline resin. The room humidity during lay-up has an effect on the amount of voids, and therefore strength, on the final composite part [2]. Consolidation of a composite part at the wrong temperature can cause buckling of the plies, burning of the surface, or a general lack of consolidation. Tooling

properties affect the final composite part. If the male or female die changes shape due to the high temperature, the part geometry might be altered, resulting in a change of mechanical performance.

In general, manufacturing affects the mechanical performance of the part in many ways. The manufacturing process should be known, as well as the material system and stacking sequence, to determine mechanical properties. This experiment addressed the effect of the manufacturing process on the structural state of the final part.

1.5 A Comparison of Gr/PEEK and Gr/Epoxy

Most filamentary composite materials containing a polymeric matrix can be broken down into two types, thermoplastics and thermosets. Thermoplastics are characterized by long chemical chains, creating a "soft" matrix, and are in their final chemical state before consolidation. Thermosets are characterized by three dimensional cross linking, creating a "hard" matrix, and require a chemical reaction, often called polymerization, during the consolidation process. Gr/PEEK is a thermoplastic, while Gr/Epoxy is a thermoset.

For effective use of Gr/PEEK or Gr/Epoxy, an emphasis is placed on reducing weight while maintaining strength and stiffness, or tailoring to reduce hygrothermal effects for precision. In addition, planar stresses are often present; otherwise, the composite material is not being used effectively, since out-of-plane stresses load the composite in its weakest direction.

Gr/PEEK has several advantages over Gr/Epoxy, especially with regards to fracture toughness and manufacturing cost. The high fracture

toughness and damage resistance of Gr/PEEK parts cause a reduction in repair costs and weight as compared to Gr/Epoxy parts. The reduction in weight is a result of designing with higher allowable strains. Long term manufacturing cost for Gr/PEEK is lower than for Gr/Epoxy. Gr/PEEK has no critical storage temperature, an unlimited shelf life, and post forming capabilities, reducing cost and scrap. The ability to post form after initial consolidation is the property of Gr/PEEK that was exploited in this investigation. Gr/Epoxy has a short shelf life, must be refrigerated during storage, and cannot be post formed due to the epoxy's inherent three dimensional chemical bonds. Gr/PEEK does not go through polymerization during the consolidation process, as opposed to Gr/Epoxy. Polymerization dramatically lengthens the processing time, resulting in higher cost.

Gr/PEEK has several disadvantages as compared to Gr/Epoxy. The viscosity of the PEEK matrix is significantly higher than the viscosity of the uncured epoxy matrix. High viscosity causes problems when forming composite parts, because a matrix with high viscosity will tend to create unwanted fiber movement during processing more than low viscosity matrix materials. The forming temperature of Gr/PEEK is much higher than Gr/Epoxy, 399°F (750°F) as compared to 177°F (350°F). Since most currently available autoclaves cannot reach 399°F (750°F), another expensive autoclave must be purchased or an internal heat source within the autoclave must be built.

Due to the savings in long term manufacturing cost and desirable mechanical properties, Gr/PEEK warrants further investigation. Gr/PEEK was the material system used for this study. The chemical formula for PEEK is [6]:

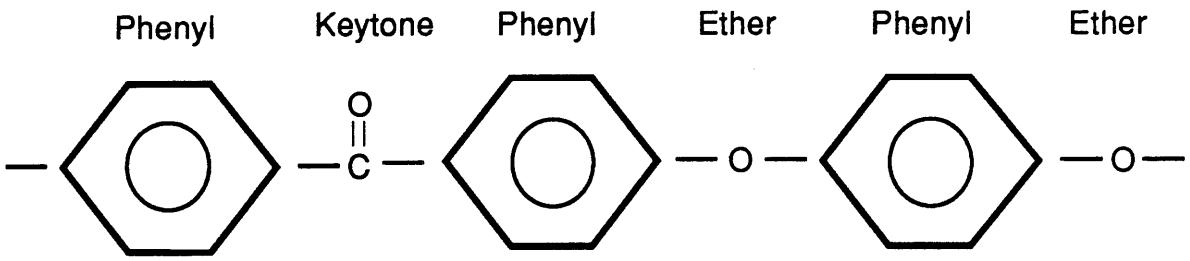

Figure 1.1 Chemical formula for PEEK.

The phenyls provide the strength and high melting temperature, while the keytones and ethers provide flexibility and ease of processing.

1.6 Definition of Terms

Several terms employed throughout the experiment are defined below:

1. Quality of Specimens: The state of the part after manufacturing as defined by visual inspection and observation, such as burning, amount of consolidation, delamination, and voids.

2. Structural Integrity: The ability of a structure to perform inservice as defined by its mechanical performance. Mechanical performance is specified by the important or critical structural properties that enable the part to perform its designed task, such as strength, stiffness, and fracture toughness.

3. Predictability of Structural Integrity: The ability to determine the structural integrity of a part after manufacturing.

4. Quality of Heat Blanket Processes: The ability of the manufacturing process to minimize the temperature gradient across the part during processing. Even though many issues determine the quality, the temperature gradient is the dominant one.

5. Repeatability of Heat Blanket Processes: The ability of the manufacturing process to reproduce a consistent temperature gradient during consolidation with a constant processing procedure. Once again, many issues determine repeatability. However, the consistency of the temperature gradient is the dominant one.

6. Longevity: The length of time that the manufacturing process can produce parts similar to the parts produced at the beginning of production.

7. Practicality: The amount of ease with which the manufacturing process can be implemented as defined by cost, quality, repeatability and longevity of the process.

These terms evaluated the structural state of the Gr/PEEK parts after manufacturing and the manufacturing process itself. Structural integrity dominates this study over the other issues listed above. Structural integrity determines whether a part should be rejected if the criteria is solely based on mechanical performance. Although quality and structural integrity are closely related, they are distinct concepts. Quality may affect certain mechanical properties, but it does not necessarily affect the critical mechanical properties that enable the structure to meet the design requirements. In other words, part rejection is not based on quality, but on structural integrity. However, it is recognized that a good appearance, or quality, of a part may be essential for successful commercial marketing.

1.7 Purpose and Goals of Investigation

This investigation addressed the relationship of a manufacturing process to the structural state of the parts produced from that process. Specifically, an unheated autoclave with a capability of 204°C (400°F) was used with an external heating source, a heat blanket capable of 538°C (1000°F), to produce Gr/PEEK composite parts between 360-438°C (680-

820°F). Since most autoclaves in universities and companies are designed to 316°C (600°F) for Gr/Epoxy production, an inexpensive heat blanket is financially preferable to a new expensive autoclave capable of producing Gr/PEEK composite parts.

Gr/PEEK small and large flat plates were produced by laying a heat blanket on top of the composite material, surrounding the entire assembly with insulation, and inserting into an autoclave. Gr/PEEK right angle bends were formed by clamping unconsolidated Gr/PEEK plies to a right angle iron bend and then processing in a method similar to the flat plates. Finally, an attempt was made to thermoform right angle bends from a flat, consolidated sheet of Gr/PEEK using heat, pressure, vacuum and a stiff diaphragm.

These processes and parts were evaluated by the following: 1) quality of the specimens, 2) structural integrity of the specimens, 3) predictability of the structural integrity of the specimens, 4) quality of the manufacturing process, 5) repeatability of the manufacturing process, 6) longevity of the manufacturing process, and 7) the practicality of the manufacturing process.

The quality of the specimens was measured through visual inspection of the surface, microscopic evaluation of the edges, and consolidation distance of the plies during processing.

The structural integrity of the large plates was found by determining E_L, E_T, ν_{LT}, and G_{LT} using 0°, 90° and ±45° tensile coupons and comparing to other references.

Predictability of the structural integrity for the large plates was determined by applying Classical Laminated Plate Theory to the tensile coupon layups. The compliance matrix [S] in conjunction with the applied

stresses during the test generated theoretical stress-strain curves. These curves were then compared to the experimental values of the 70/20/10, 50/40/10 and 30/60/10 tensile coupons. The compliance matrix was found by inverting the [E] matrix, which is determined by Classical Laminated Plate Theory. The 0°, ±45°, and 90° tensile coupons generated the ply properties necessary for Classical Laminated Plate Theory. For the case of the bend specimens, an energy derived stiffness was compared to the experimental stiffness due to an end load.

The quality of the manufacturing process was evaluated by the magnitude of the temperature gradient as revealed by in-plane thermocouples. The repeatability of the manufacturing process was evaluated by the consistency of the temperature gradient across the part as revealed by in-plane thermocouples using an identical processing procedure. The longevity of the manufacturing process was examined through the visual observation of the degradation of the heat blanket as parts were made and the number of heating cycles that could be done before failure of the heat blanket. Finally, the practicality of the manufacturing process was determined by cost, quality, repeatability and longevity of the manufacturing process. This study should give an idea of whether the manufacturing processes investigated are reasonable for producing Gr/PEEK parts.

The remainder of this thesis is broken down into six parts. Chapter Two contains the manufacturing procedures used to make the specimens and the development of the manufacturing procedures. The analytical models used to make conclusions are derived in Chapter Three, while Chapter Four and Chapter Five describe the testing procedure and the results from manufacturing and mechanical testing. A discussion of the

results is contained in Chapter Six. Chapter Seven presents the conclusions and recommendations. References and Appendices are included at the end.

1.8 Previous Work

Although manufacturing composite parts are in preliminary developmental stages, some work has addressed the forming and mechanical properties of Gr/PEEK plates and bends. Articles on Gr/PEEK plates and bends usually fall into one or both of the following categories: 1) theoretical strength and/or stiffness and 2) processing.

Several researchers have worked on the fabrication of composite right angle bends. Soll [7] investigated the forming of two-dimensional parts from consolidated sheets using matched die molds. She determined the part quality after formation by surface features, micrography through the part thickness, fracture strength and final angle of the bend. She found that tension applied during forming and slower processing speeds created good quality parts. She also found that poor surface features revealed fiber misalignment, resulting in reduced fracture strength. The Center for Composite Materials at the University of Delaware has investigated the use of diaphragm forming to make composite parts. Mallon et al. [8] described the current methods of thermoforming composite parts, including matched die forming, hydroforming, rubber forming, and in the most detail, diaphragm forming. He also specified properties of the mold and diaphragm material that would optimize processing. O'Bradaigh [9] designed an innovative autoclave to produce composite bends. He then investigated the effects of processing on the mechanical strength by non-

destructive methods and theoretical stiffness predictions. He found that the optimum temperature range to form right angle bends was between 360°C (680°F) and 390°C (734°F). He also checked if interply slip occurred, a necessary deformation for successful part formation. Smiley et al. [10] developed a theoretical analysis that described composite deformation in diaphragm forming. He then compared his analysis to the experimental results for verification. Hoggatt, et al. [11] compared the manufacturing cost of aerospace parts made of Gr/Epoxy and Gr/Polysulfone, a thermoplastic composite material. He found that the Gr/Epoxy was cheaper for the first part, reflecting the lower fixed cost. Fixed cost is independent of the number of parts made. By the tenth part, however, the Gr/Polysulfone saved an average of 33%, reflecting the lower variable costs, which depend on the number of parts made. The conclusion was that production cost offsets material and tooling cost after the tenth part. Hoggatt also examined the use of diaphragm forming. He found that the cycle time to produce a part depended on heat transfer and the thickness of the part. He also concluded that diaphragm forming created "extremely accurate and reproducible parts."

Theoretical predictions for the strength of composite bends has been done by Brent, Chang and Sun. Brent [12] developed an elasticity solution for a composite bend and then compared his solution to finite element models. He used the elasticity analysis with two failure theories to predict composite bend strength. He fabricated thermoplastic and thermoset composite bends and tested them to failure. He then compared the predicted behavior to the experimental results and found good agreement. Chang et al. [13] did a theoretical analysis on the strength of composite bends. Chang predicted the stresses using the Finite Element Method and

the strength by the Chang-Springer and Tsai-Hill criterions. Chang then illustrated the effects of geometry and ply orientation on the strength of the bend. Sun, et al. [14] studied failure in composite angle structures both experimentally and analytically through the use of the Hill and augmented Hill-Tsai failure criteria. Sun found that there were two possible failure modes: 1) initial transverse matrix cracking due to bending stress, and 2) final delamination due to through-the-thickness normal stress in the curved region. The 3-D Hill failure criterion predicted failure correctly in the investigation.

Several investigations have involved the manufacturing of flat plates. The Technology Laboratory for Advanced Composites (TELAC) made Gr/PEEK specimens and listed an experimental manufacturing procedure in Appendix B of the TELAC Manufacturing Course [15] notes. These notes were the starting point for the processing of Gr/PEEK flat plates in this investigation. The composite material rested on a thin steel caul plate with fiberglass air breather and Kapton coated with Frekote 700. On top of the composite was Kapton coated with Frekote 700, followed by fiberglass air breather, Kapton vacuum bagging, a heat blanket and insulator. The vacuum bag was sealed onto the caul plate by the application of semi-tacky high temperature vacuum tape along the outer perimeter of the caul plate. This assembly was inserted into the autoclave. The autoclave provided a .34 MPa (50 psi) pressure and a 762 mm (30 in) vacuum, while the heat blanket provided the heat for the high temperature of 393°C (740°F) needed to process Gr/PEEK. Vacuum was applied by a hose that connected to the caul plate from the autoclave. Although not providing any heat during the manufacturing process, the autoclave had a capability of 204°C (400°F) and 1.2 MPa (175 psi) when processing Gr/PEEK. The Gr/PEEK was processed

at 388-398°C (730-749°F) with a pressure of .34 MPa (50 psi) for about 15 minutes. The temperature cycle was the following: 1) 149°C (300°F) for 10 minutes, 2) 260°C (500°F) for 10 minutes, 3) 371°C (700°F) for 10 minutes, and 4) 466°C (870°F) for 30 minutes. The temperature was monitored by thermocouples. Horton et al. [16] studied the damage tolerance of Gr/PEEK. In the process, tensile coupons were made. The manufacturing process was similar to the one listed in the TELAC manufacturing notes except for the following: 1) no heat blanket or insulator was necessary since the autoclave could reach 393°C (740°F), and 2) the Gr/PEEK was heated to 393°C (740°F) at .90 MPa (130 psi) for 20 minutes, followed by 1.4 MPa (200 psi) for 30 minutes. Springer [5] processed Gr/PEEK plates. He applied a temperature of 399°C (750°F) and a pressure of 1.4 MPa (200 psi) for 10 minutes plus some time to reach equilibrium.

The current investigation was similar to Soll's, Brent's and O'Bradaigh's theses. Right angle bends were formed and then analyzed for their structural integrity and quality. The predicted behavior was related to the experimental results to develop conclusions about the experiment. This investigation was different in three major respects: 1) a unique but inexpensive manufacturing process was used, 2) the manufactured flat plates were examined through three distinct concepts: quality, structural integrity and predictability of the structural integrity, and 3) a thorough investigation of the manufacturing processes was employed during the experiment, including quality, repeatability, longevity and practicality.

Chapter 2
SPECIMEN MANUFACTURE

2.1 Overview

The most difficult and time consuming section of the investigation was specimen manufacture. Starting from the TELAC manufacturing notes, educated trial and error was applied to produce the best possible specimens using the heat blankets. Manufacturing procedures were developed in incremental steps by varying as few processing variables at a time while changing enough processing variables for rapid development. The effort required to form the large plates and right angle bends was minimal because of the previous experience gained in producing the small plates. Manufacturing procedures for the specimens were highly dependent on the materials. Table 2.1 lists these materials and their associated manufacturers and distributors. The following subsections describe the methods or development of the methods employed to form the small plates, large plates, and right angle bends.

2.2 Laminate Stacking Sequence

The large plates consisted of 100/0/0, 70/20/10, 50/40/10, 30/60/10, 0/100/0 and 0/0/100 laminates. The 0/0/100 laminates were 10 plies thick, while the rest were 20 plies thick. All the laminates were symmetric about the midplane. Table 2.2 lists the stacking sequence of the six different laminates. The numbers inside the table represent the angles of fibers in each ply with respect to the lengthwise, or longitudinal, direction of the

laminate. This type of nomenclature, X/Y/Z, was used instead of nomenclature involving stacking sequence for the following two reasons: 1) indicating stacking sequence would make the nomenclature too cumbersome and 2) ease of communication with industry.

Table 2.1 Materials used for manufacturing specimens.

Material	Manufacturer	Distributor
Kapton	Dupont	Northern Fiberglass
Gr/PEEK	ICI	Donated from Boeing
High Temp. Vac. Tape	Schnee Morehead	Northern Fiberglass
High Temp. Flash Tape	Ideal Tape	Northern Fiberglass
Fiberglass Air Breather	B.G.F. Industries	Northern Fiberglass
Frekote 700	Dexter	R. P. Morrison
F-57	Axel Plastics	Axel Plastics
Heat Blanket	Briskheat	Briskheat
Insulator	Briskheat	Briskheat
Glass Tabs	3M	3M
Adhesive	American Cynamid	American Cynamid
Strain Gages	Micro-Measurements	Andruss Peskin
Aluminum (Mold)	Alcoa	Mohawk Aluminum
Iron (Mold)	Bethlehem Steel	Ryerson

The small plates and right angle bends consisted of 100/0/0 laminates that were 10 plies thick. The small plates and right angle bends had the same stacking sequence as the 100/0/0 tensile coupons.

Table 2.2 Laminate stacking sequences from the outer surface (#1) to the midplane (#10).

Ply Number	Laminate					
#	100/0/0	70/20/10	50/40/10	30/60/10	0/100/0	0/0/100
1.	0	+45	+45	+45	+45	90
2.	0	0	-45	-45	-45	90
3.	0	0	90	90	+45	90
4.	0	-45	0	+45	-45	90
5.	0	0	0	0	+45	90
6.	0	0	+45	-45	-45	--
7.	0	90	0	0	+45	--
8.	0	0	0	+45	-45	--
9.	0	0	-45	-45	+45	--
10.	0	0	0	0	-45	--

2.3 Heat Blankets

The heat blankets were the critical elements in processing all the specimens. Two large heat blankets with the same specifications and one small heat blanket were used for the investigation. Their specifications are

listed in Table 2.3. The specifications include the dimensions, the heating capability, and the type of electrical input.

The dimensions for each blanket, 787 mm (31 in) by 1397 mm (55 in) and 305 mm (12 in) by 330 mm (13 in), were chosen because these were the dimensions of the caul plate that the blankets would heat during processing. 1.24 Watts/cm^2 (8 Watts/in^2) was the heating specification because this amount of power would heat the system yet not burn the blanket in the process. Previous lab experience revealed that 1.86 Watts/cm^2 (12 Watts/in^2) was too powerful for the materials within the blanket. After consultation with the manufacturer, 1.24 Watts/cm^2 (8 Watts/in^2) was chosen as the optimal power.

Table 2.3 Specifications for heat blankets.

Type of Blanket	Specifications	Price
Large	Samox Blanket 787 mm X 1397 mm 1.24 Watts/cm^2 480 V, 3 Phase	$750
Small	Samox Blanket 305 mm X 330 mm 1.24 Watts/cm^2 480 V, 3 Phase	$395

Understanding the fabrication of the blanket was essential to processing the specimens. Figure 2.1 is an illustration of the large heat blanket. The small heat blanket was similar. The blanket was heated by electricity. Three large wires connected to the autoclave at one end, while

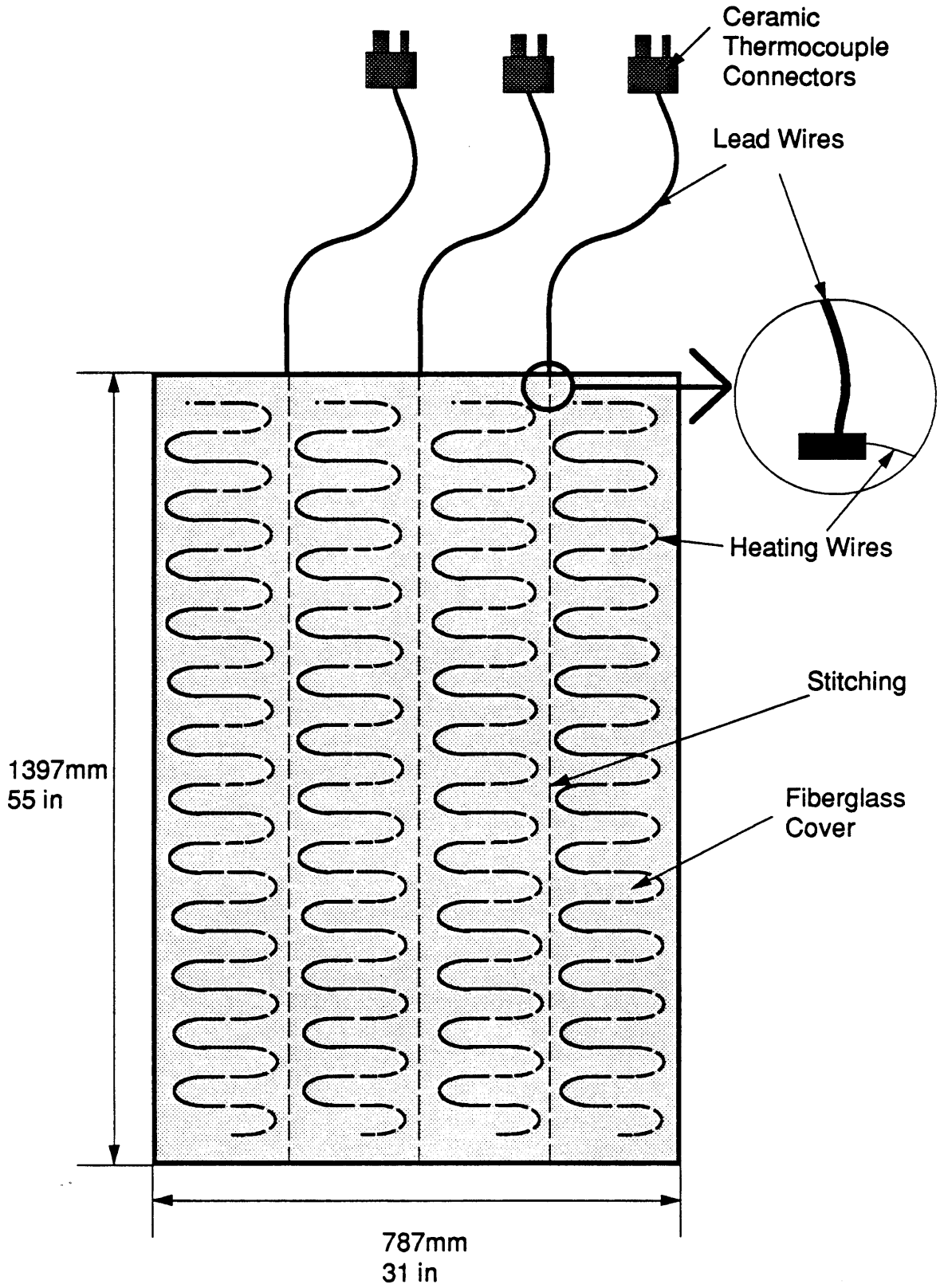

Figure 2.1 Large Heat Blanket.

the other end connected to the thin heating wires within the blanket. One end of the large wires was constrained at the edge of the blanket by tight sewing, while the other end was inserted into the autoclave power supply by ceramic thermocouple connectors wrapped in blue flash tape. The connection from the large wires to the thin heating wires was very fragile. The insulated heating wires extended in strips along the length of the blanket. The heating wires were placed in tight, repeated "S" shapes within the strips. Sewing separated one strip from another. As a result, significant heating occurred under the wires, but little heating occurred under the sewing. This created a temperature gradient throughout the blanket. Thermocouples were placed underneath the wires instead of the sewing to read the highest temperatures during processing.

2.4 Trial and Error Experience with Consolidation Process

A series of tests were run to determine the characteristics of the different components of the consolidation equipment. A total of 18 tests were completed.

Test #1

Initially, a large heat blanket was tested on a steel caul plate, with dimensions 838 mm (33 in) by 1448 mm (57 in) by 10 mm (.125 in), to determine if the blanket was working properly after receiving from the manufacturer and if the consolidation temperature could be reached. A reading of 490°C (914°F) was achieved without incident.

Test #2

The next step attempted to consolidate 6 laminates according to the

TELAC manufacturing notes, which were developed for a heat blanket of 1.86 Watts/cm^2 (12 Watts/in^2).

Two small squares of fiberglass air breather were pinned over the 2 vacuum holes in the caul plate using high temperature flash tape. Fiberglass air breather was placed over the steel caul plate and secured in place using high temperature flash tape. The breather covered the caul plate to 51 mm (2 in) from the edges. This space was used for the vacuum tape. Kapton release film was secured to the fiberglass air breather using high temperature flash tape. Frekote 700, acting as a mold release, was sprayed onto the Kapton release film. Mold release was necessary for removal of the Kapton release film from the laminates after processing. The six laminates were placed on the Kapton release film, 2 along the width and 3 along the length of the caul plate. The longitudinal direction of the laminates was parallel to the lengthwise direction of the caul plate. The laminates were separated by approximately 25.4 mm (1 in). Kapton coated with Frekote 700 covered the top of the laminates and was pinned down at the corners by high temperature flash tape. Fiberglass air breather and the Kapton vacuum bag were placed on top of the Kapton release film. The vacuum bag was sealed using high temperature vacuum tape along the edge of the caul plate. Two thermocouples were clamped to the Kapton release film underneath the laminates by high temperature flash tape. The wires were placed between the laminates along the centerline of the caul plate 381 mm (15 in) inward from the front and approximately 127 mm (5 in) from the back. The front was defined as the end at which the vacuum hose from the autoclave connected to the caul plate. Two thermocouples were clamped onto the surface of the blanket that touched the Kapton vacuum bag. The thermocouples were placed on the centerline of the

blanket, 305 mm (12 in) from the front. The front of the heat blanket was defined as the end at which the 3 wire leads exited the blanket. A 838 mm (33 in) by 1448 mm (57 in) insulator covered the top surface of the blanket. The entire assembly was inserted into an autoclave.

Heat, pressure and vacuum were used to consolidate the laminates. The heat blanket was the sole source of heat; the autoclave did not contribute to the heating process. The heating cycle was as follows: 1) 149°C (300°F) with 10 minute hold, 2) 260°C (500°F) with 10 minute hold, 3) 371°C (700°F) with 10 minute hold, and 4) 466°C (870°F) with 30 minute hold. This allowed the caul plate to reach 388-398°C (730-749°F) in the front after the thirty minute hold. The autoclave provided the pressure and vacuum. The pressure and vacuum, .34 MPa (50 psi) and 762 mm Hg (30 in Hg), were applied for the entire consolidation process. For specific procedures, please consult the TELAC manufacturing notes, Appendix B.

While using this procedure during the 366°C (870°F) heating section, a catastrophic fire occurred when the blanket temperature was 382°C (720°F). The fire burned everything except the insulator. The caul plate was significantly warped.

The cause of the fire was never determined exactly; however, the following tests were conducted.

Test #3

This test determined if the small heat blanket was working properly after receiving from the manufacturer. A new caul plate was machined with the same length and thickness as the previous caul plate, except the width was 394 mm (16 in). The small heat blanket was placed on top of the steel caul plate and tested to 371°C (700°F) without incident.

Test #4

Test #4 attempted to examine the reaction of Kapton to temperatures near 371°C (700°F). Kapton was placed between the steel caul plate and a steel top plate. The steel top plate had dimensions 356 mm (14 in) by 305 mm (12 in) by 3 mm (.125 in). Two thermocouples were pinned to the Kapton using high temperature flash tape. The heat blanket was placed over the steel top plate. The Kapton reached only 338°C (640°F) with the heat blanket on continuous full power. The Kapton was not damaged. Since Gr/PEEK laminates require 360°C (680°F) to 393°C (740°F) for processing, an insulator was necessary to retain heat and to lengthen the life of the blanket. Initially, the top plate was used to protect the heat blanket in case a fire occurred.

Test #5

Test #5 used the same processing procedure as in test #4 to find the reaction of Kapton to temperatures near 371°C (700°F), except for the addition of an insulator. The Kapton reached 382°C (720°F) while the blanket was set at 510°C (950°F) for 30 minutes. Since the Kapton was not damaged by the extreme heat, it was assumed that the Kapton could not have been the cause of the fire. After consultation with the manufacturer, it was learned that Kapton did not have a flash point. Kapton thermally degrades by charring and then disintegrates. The heating process used for this test rose in 28°C (50°F) increments starting at 149°C (300°F) and then holding for either 2, 3, 5, or 10 minutes.

Test #6

This test attempted to consolidate a laminate that was processed similar to the TELAC manufacturing notes, except no autoclave pressure was applied and a different caul plate and a different heat blanket were used. A 762 mm Hg (30 in Hg) vacuum was applied during processing, creating an applied pressure on the laminate. In addition, no mold release was sprayed on the Kapton release film. Autoclave pressure and Frekote 700, the mold release, were not used because they were suspected as being possible causes of the fire. The laminate layup for this test through test #18 was 100/0/0 of 10 plies. Four thermocouples were placed on the 4 corners of the composite laminate. A steel top plate covered the surface of the Kapton vacuum bag. Even though the blanket was at a temperature of 510°C (950°F) for more than an hour, the thermocouples next to the laminate reached approximately 243°C (470°F).

Test #7

Test #7 attempted to consolidate a laminate by substituting a copper plate for the steel top plate. The copper top plate was used because a possibility existed that the steel top plate was inhibiting heat transfer. The same procedure was used as in test #6, but with a different thermocouple arrangement within the vacuum bag. One thermocouple was placed at the center of the laminate on top of the Kapton release film. The second thermocouple was placed near the corner of the laminate on the Kapton release film underneath the laminate. The third was placed in between a corner and the center of the laminate on the Kapton release film above the laminate. The laminate reached 316°C (600°F) after the blanket was set at 510°C (950°F) for 2.5 hours. After removing the assembly from the

autoclave, the copper had changed structurally and was a lighter, duller color.

Test #8

Test #8 probed the effect of the laminate on heat transfer within the assembly. The processing procedure was the same as before, except the top plate and laminate were not present. After the blanket was set at 466°C (870°F) for 40 minutes, the Kapton reached 404°F. The presence of a laminate did not have an effect on reaching the proper temperature range. The blanket was set at 466°C (870°F) instead of 510°C (950°F) because the latter would burn the Kapton.

Test #9

Test #9 attempted to determine the effects of the vacuum on heat transfer using the same procedure as test #8, except no vacuum was applied while heating the assembly. Vacuum was applied when the maximum temperature was reached. The effect of the presence of a laminate inside the assembly is unknown. After the blanket had been set to 466°C (870°F) for one hour, the assembly reached 343°C (650°F). This test indicated that vacuum might be removing heat from the system after comparing to test #8.

Test #10

Test #10 determined the effect of a bottom plate underneath the laminate on the heat transfer of the system. Test #10 was similar to test #9. In addition, a steel top plate and laminate were present. A steel bottom plate, with the same dimensions as the top plate, was placed above the caul

plate underneath the laminate. The blanket was set at 510°C (950°F) for 15 minutes. The laminate reached 490°C (914°F), which was significantly above processing temperature. An explanation for reaching such a high temperature was that the steel plate underneath the laminate "pushed" the laminate into the heat blanket; as a result, a higher temperature was reached.

Test #11

Test #11 and Test #12 investigated the effects of vacuum on heat transfer. Test #11 was similar to the previous test, except vacuum was applied continuously and the heating cycle of test #2 was used. In addition, the thermocouple arrangement was different. One thermocouple was placed on top of the Kapton release film underneath the laminate and next to the corner of the laminate. The second thermocouple was placed in the same place, except near the middle of an edge of the laminate instead of the corner. After the blanket was set at 466°C (870°F) for 30 minutes, the laminate reached 375°C (707°F). The Kapton condition was good except around the thermocouple wires.

Test #12

Test #12 was similar to test #11 except vacuum was not applied until processing. After the blanket was at 466°C (870°F) for 35 minutes, the laminate reached 423°C (793°F). After comparing this test with the previous test, the vacuum seemed to reduce the temperature. All of the tests conducted so far did not satisfy the vacuum test, which meant losing more than 127 mm Hg (5 in Hg) of vacuum within 5 minutes. As vacuum

was being drawn to maintain 762 mm Hg (30 in Hg), the heat was carried out of the assembly.

Test #13

Test #13 was identical to test #12, but with the objective of keeping the laminate at 416°C (780°F) by manual control. This test was successful.

Test #14

This test determined if the second large heat blanket was operating correctly after receiving from the manufacturer. A new large caul plate, with dimensions 838 mm (33 in) by 1448 mm (57 in) by 3 mm (.125) was machined. The second large heat blanket was tested successfully at 466°C (870°F) for 15 minutes.

Test #15

Test #15 attempted to consolidate a single laminate using the large heat blanket and vacuum on continuously. The fiberglass air breather, Kapton release film, laminate and Kapton vacuum bag were applied similarly to test #2. Two thermocouples were placed at the center of two edges of the laminate. After the blanket reached 466°C (870°F) for 30 minutes, the laminate reached 311°C (592°F). The effect of the presence of a steel top plate during the test is unknown.

Test #16

Test #16 attempted to consolidate a laminate using a processing procedure that was identical to the previous test except that vacuum was not applied until reaching the consolidation temperature and a bottom steel

plate was placed underneath the laminate. The effect of the presence of a top plate is unknown. After the blanket was at 466°C (870°F) for 30 minutes, the laminate reached 387°C (728°F). Inspection of the laminate, after removal from the autoclave, revealed that only half reached temperature. The blanket was applying temperature unevenly. The plan at this point was to repeat processing until the entire laminate was exposed to processing temperatures near 382°C (720°F).

Test #17

Test #17 was identical to #16 except the laminate was flipped so that the other side would reach temperature. This test was successful.

Test #18

Test #18 attempted the consolidation of 6 laminates with multiple stacking sequences. The Kapton film release, Kapton vacuum bag, vacuum tape and fiberglass air breather were applied similarly to the previous test. The laminates were placed 2 along the width and 3 along the length of the caul plate. The laminates were 70/20/10, 50/40/10, 30/60/10, 0/100/0, and 2 of 100/0/0. A distance of 25.4 mm (1 in) separated each laminate. Three thermocouples were pinned along the centerline of the caul plate, near the edges of the laminates, by high temperature flash tape. Two thermocouples were placed behind the first two laminates seen from the front of the caul plate. The other thermocouple was placed behind the last row of laminates seen from the back of the caul plate. The effect of the presence of top plates or bottom plates is unknown. After the blanket reached 493°C (920°F) for 25 minutes using a heating cycle similar to test #2, the laminates reached 342°C (647°F).

After removing the assembly from the autoclave, it was revealed that massive ply buckling had occurred for laminates 70/20/10, 50/40/10, 30/60/10 and 0/100/0, but not for the 2 100/0/0 laminates.

The ply buckling occurred because of 1) temperature gradients and 2) the difference in the coefficient of thermal expansion between adjacent plies. The matrix has a large coefficient of thermal expansion relative to the fibers. Therefore, plies with different fiber orientations have different values for the coefficient of thermal expansion. The blanket heated the laminates in strips, through electricity, underneath the heating coils. Some parts of the ply surfaces within each laminate reached temperature and bonded to an adjacent ply. When the partially bonded plies within each laminate cooled down, one ply would want to contract more than the other, while at the same time each ply was clamped to one another due to the partial consolidation. As a result, the plies buckled with respect to one another with very little or no damage to the fibers. Concisely, thermally induced strains caused mechanical stresses that resulted in plies buckling relative to one another. All the laminates, except the 100/0/0s, suffered ply buckling. The 100/0/0 laminates did not exhibit ply buckling because each ply had the same coefficient of thermal expansion. This phenomena did not occur before test #18, because the 100/0/0 laminate was used in all the previous tests. This phenomena indicated that laminates, except unidirectional laminates, are pre-stressed by thermal strains inducing mechanical stresses. Properly consolidated laminates do not exhibit ply buckling because the matrix clamps one ply to another. The pre-stressed condition of a laminate should not affect the tensile stiffness of a specimen because of the linear relationship of the stress-strain curve. Below a certain point of stress, no matter what value of stress is chosen, the

corresponding strain will result in the same stiffness as for another chosen stress.

2.5 Small Plates

Due to the result of ply buckling in test #18, it was decided that successful processing would require a reduction in the temperature gradient while consolidating the laminates. This was partially accomplished by creating an oven within the autoclave. Seven small plates of the laminate 100/0/0 with a thickness of 10 plies were formed using this procedure.

A small 305 mm (12 in) by 356 mm (14 in) by 3 mm (.125 in) caul plate was machined. A small square of fiberglass air breather was pinned over the vacuum hole in the caul plate with high temperature vacuum tape. Fiberglass air breather was held in place over the steel caul plate using high temperature flash tape. The fiberglass air breather covered the caul plate to 51 mm (2 in) from the edges. This space was used for the vacuum tape. Kapton release film was applied to the fiberglass air breather using high temperature flash tape. F-57 was sprayed onto the Kapton release film. F-57 was only applied to specimen P100/0/0-7. F-57 was not applied to P100/0/0-1 thru P100/0/0-6 because enough confidence in the procedure had not been established. The mold release was necessary for removal of the Kapton release film from the laminate after processing. A laminate with dimensions 127 mm (5 in) by 203 mm (8 in) and layup 100/0/0 was placed on the Kapton release film. Four thermocouples were pinned down to the Kapton release film, near each corner of the laminate, using high temperature flash tape. The thermocouple wires were stripped of the

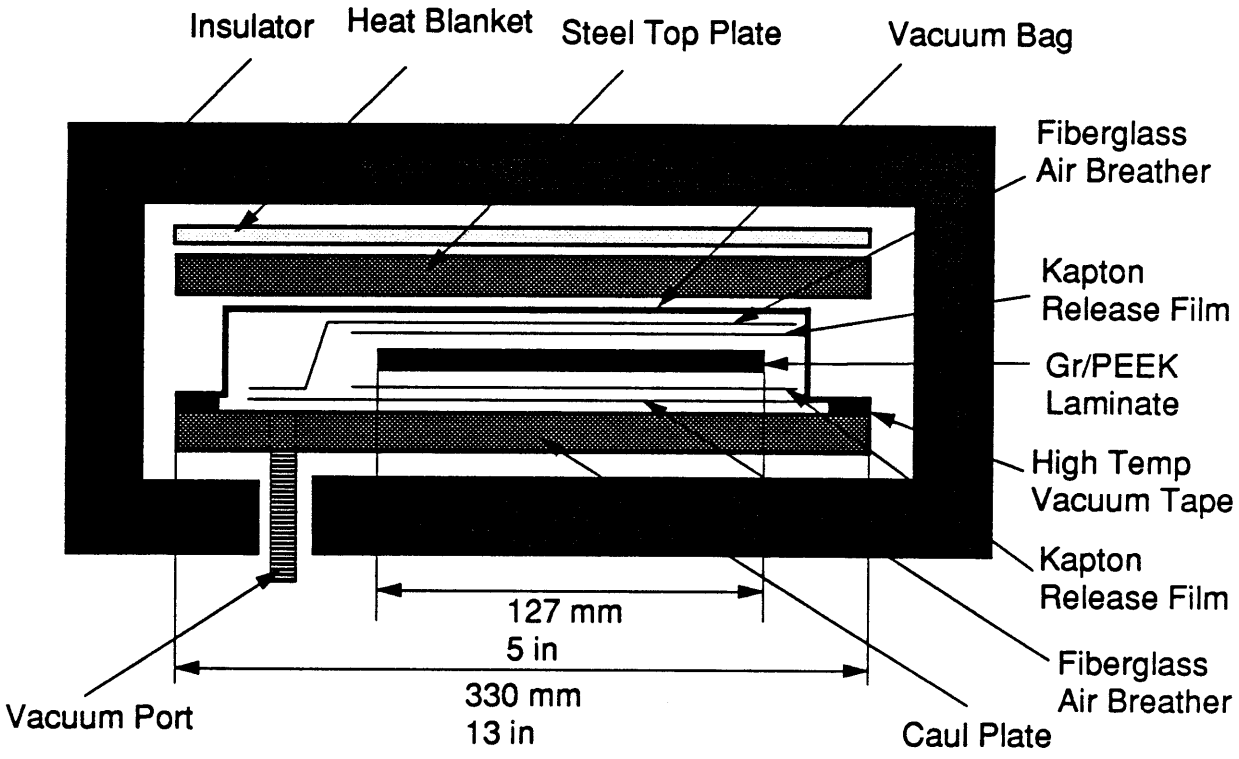

Figure 2.2 Side view of the composite assembly for small plates.

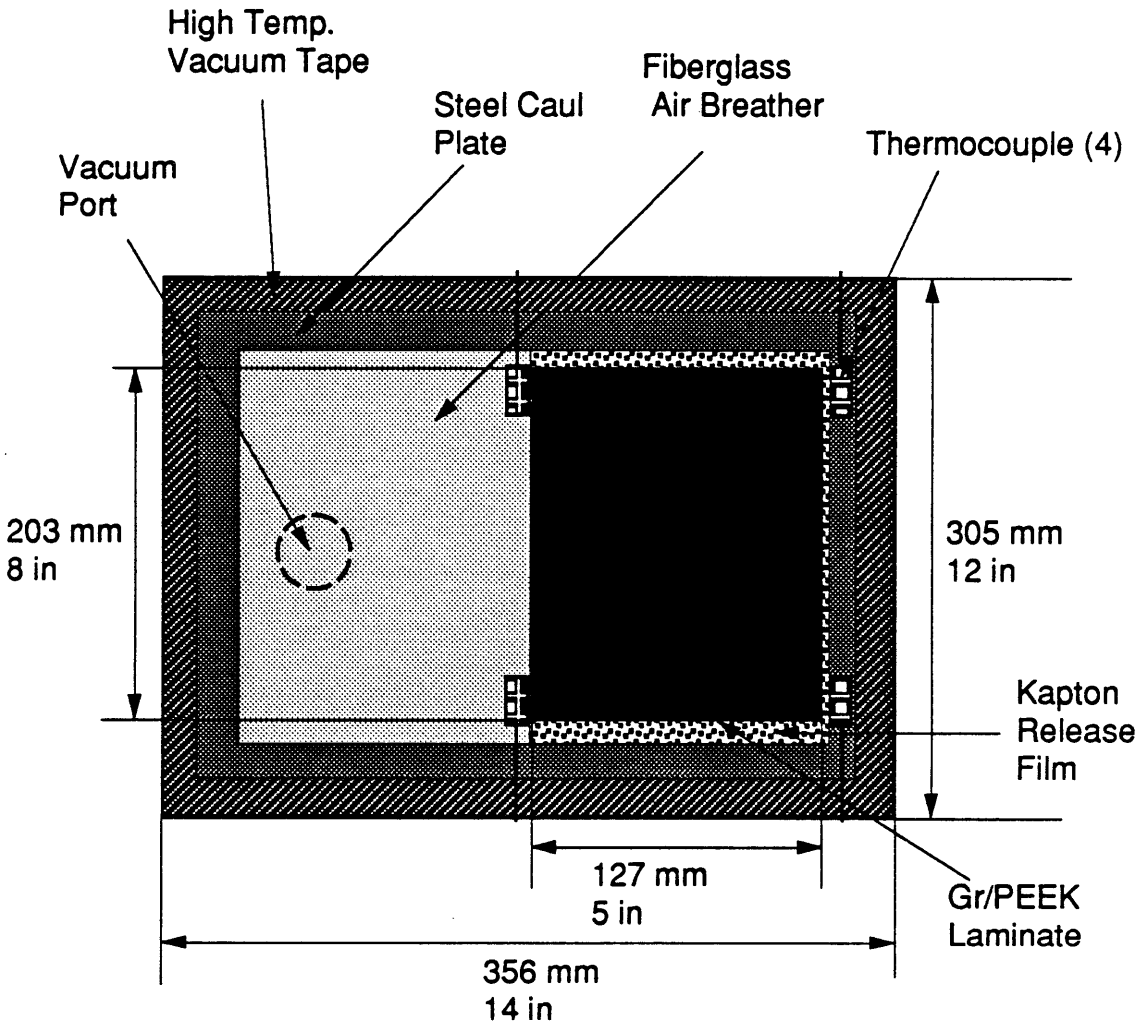

Figure 2.3 Top view of composite assembly for small plates revealing laminate.

fiberglass coating over the vacuum tape. This was done to eliminate possible vacuum leaks. Kapton release film coated with F-57 covered the top of the laminate and was pinned down at the corners using high temperature flash tape. Fiberglass air breather and the Kapton vacuum bag were placed on top of the Kapton release film. The vacuum bag was sealed using high temperature vacuum tape along the edge of the caul plate. A steel top plate, with dimensions 305 mm (12 in) by 356 mm (14 in) by 3 mm (.125 in), was placed on the Kapton vacuum bag. The steel top plate was used to spread out the high temperature under the coils and protect the Kapton vacuum bag from temperature spikes within the blanket. Two thermocouples were pinned to the small heat blanket approximately 102 mm (4 in) from the front of the blanket. These thermocouples monitored the temperature of the blanket. The front of the blanket was defined as the end at which the lead wires exited the blanket. The small heat blanket had dimensions 305 mm (12 in) by 330 mm (13 in) with a power of 1.24 Watts/cm^2 (8 Watts/in^2). The blanket was placed on the steel top plate. An insulator surrounded the entire assembly, which created an oven. The whole system was inserted into an autoclave. Please see Figures 2.2 and 2.3 for details.

The autoclave provided the pressure and vacuum. The heat blanket supplied the only source of heat; the autoclave did not contribute to the heating process. The pressure and vacuum were set at .34 MPa (50 psi) and 762 mm Hg (30 in Hg). The nominal heating cycle was as follows: 1) 300°F for 10 minute hold, 2) 500°F for ten minute hold, 3) 700°F for 10 minute hold, 4) 880°F for 10 minute hold, and 5) 900-920°F for 105 minute hold. The final temperature hold varied from one specimen to another. The goal of the final hold was to raise the temperature high enough to 1) heat the assembly

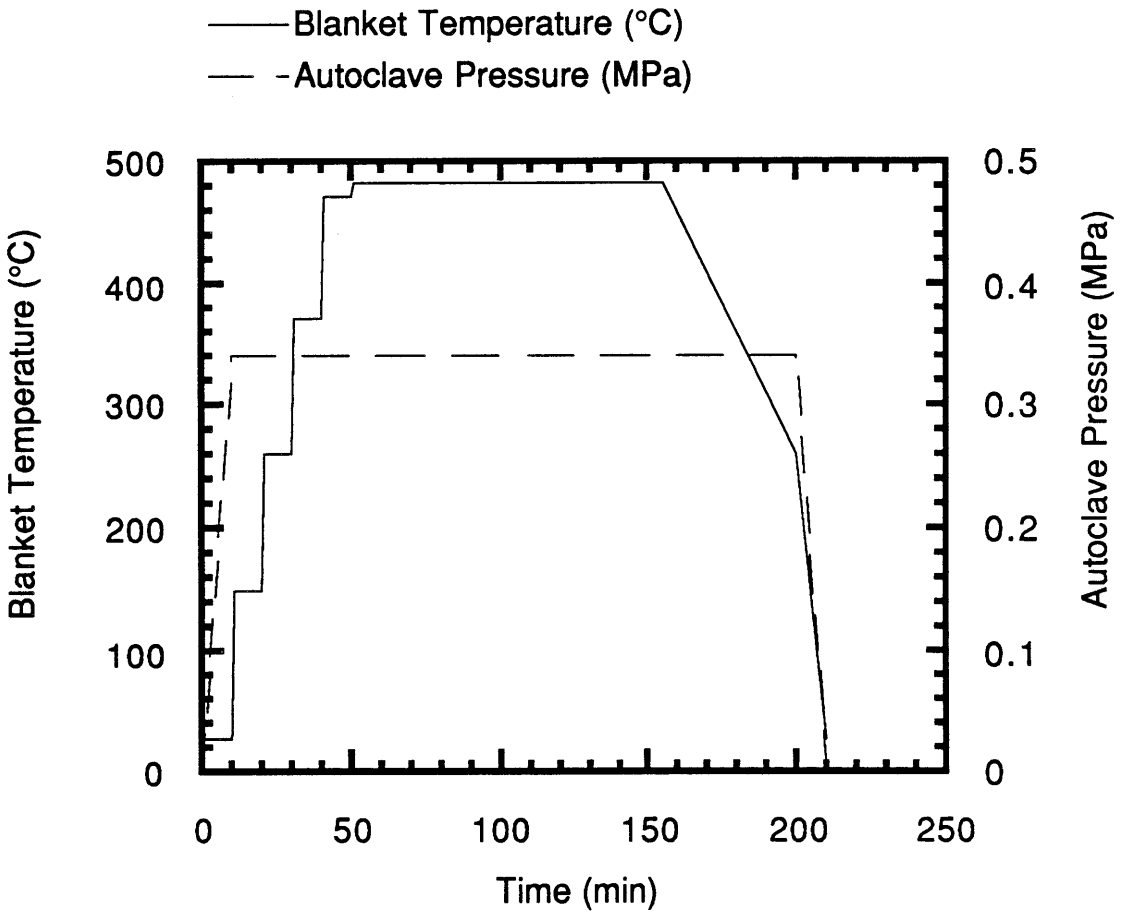

Figure 2.4 Temperature and pressure during consolidation for the small plates.

quickly to reduce processing time, and 2) heat the cool parts of the assembly above the minimum processing temperature. If the processing window, the range between the Kapton burn temperature of 427°C (800°F) and the lowest consolidation temperature of 360°C (680°F), of 49°C (120°F) could not be achieved, the temperature that averaged the differences between the two extremes was applied. If the temperature gradient within the system was greater than 67°C (120°F), a possibility existed that some material would not be properly consolidated. Figure 2.4 gives a graphical illustration of the temperature and pressure during consolidation.

The quality and repeatability of the manufacturing process, as defined by the magnitude and consistency of the ΔT, the maximum difference in temperature measured by the four in-plane thermocouples, during consolidation, is listed in Table 2.4. This processing window was not discovered until specimen P100/0/0-4.

Table 2.4 Magnitude and consistency of the temperature gradient across the part for small plate processing.

Specimen	ΔT (°C) during processing
P100/0/0-4	50
P100/0/0-5	74
P100/0/0-6	63
P100/0/0-7	102
Average	72
Coefficient of Variation	30.6%

Table 2.5 Thickness measurements for small plates.

Specimen	Thickness (mm)						
	1	2	3	4	5	6	Av.
P100/0/0-1	1.36	1.34	1.38	1.48	1.52	1.48	1.43
P100/0/0-2	2.65	2.07	1.33	1.47	1.47	1.43	1.74
P100/0/0-4	1.36	1.33	1.31	1.42	1.43	1.41	1.38
P100/0/0-5	1.27	1.26	1.31	1.46	1.46	1.45	1.37
P100/0/0-6	1.33	1.38	1.32	1.42	1.41	1.38	1.37
P100/0/0-6	1.20	1.21	1.23	1.43	1.38	1.42	1.31

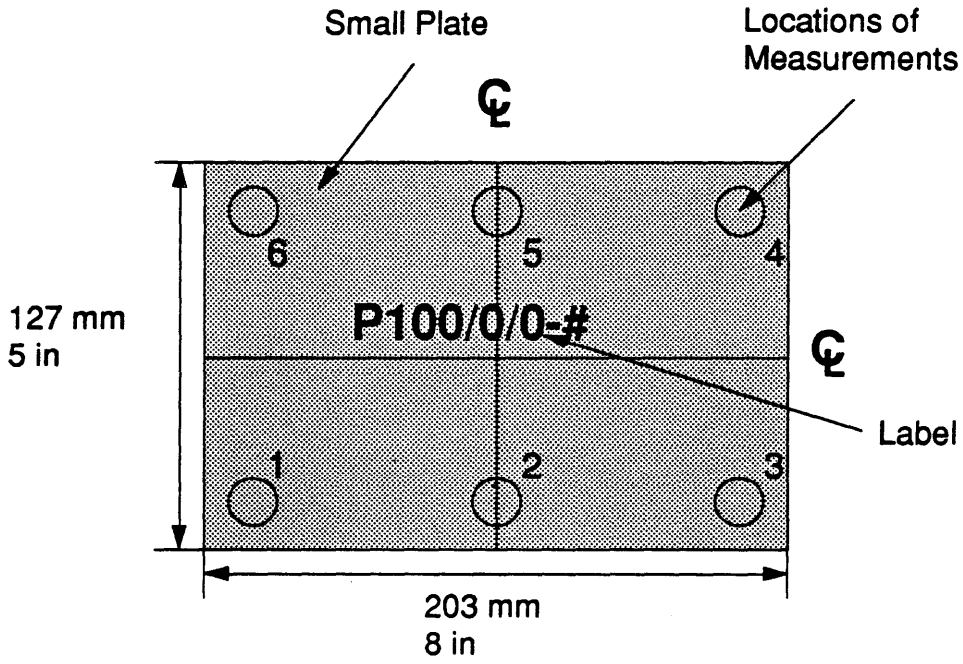

Figure 2.5 Locations of thickness measurements for small plates.

After the processing was completed, the blanket was turned off. Pressure and vacuum were applied until the temperature of the laminate was well below the minimum consolidation temperature. The cooling rate was approximately 3°C/min (5°F/min). Rapid cooling was not possible due to the insulation around the assembly.

The measured thicknesses for the specimens after manufacturing are shown in Table 2.5. Figure 2.5 illustrates where the measurements were taken on the small plates. Specimen P100/0/0-3 was used for thermoforming and is not listed in Table 2.5.

2.6 Large Plates (Tensile Coupons)

Large composite plates were consolidated by employing the manufacturing technology of the small plates. An oven was partially created by placing an insulator above and below the caul plate. The large composite plates were reconsolidated from test #18 described in Section 2.4. Initially, the plates had significant ply buckling. After consolidating the large plates, the ply buckling was gone.

A large steel caul plate, 838 mm (33 in) by 1448 mm (57 in) by 3 mm (.125 in), was placed on top of an insulator with dimensions 838 mm (33 in) by 1448 mm (57 in). A small square of fiberglass air breather was pinned over the vacuum hole in the caul plate with high temperature flash tape. Fiberglass air breather was held in place over the steel caul plate using high temperature flash tape. The fiberglass air breather covered the caul plate to 51 mm (2 in) from the edges. This space was used for the vacuum tape. Kapton release film was applied to the fiberglass air breather using high temperature flash tape. Two coats of F-57 were sprayed onto the

Kapton release film and the lower surface of the laminate. The mold release was necessary for removal of the Kapton release film from the laminate after processing. One or 2 laminates would be processed at a time. The laminates' dimensions were 305 mm (12 in) by 356 mm (14 in) with a thickness of 10 or 20 plies. Four thermocouples were placed on the outer four corners of the laminate or laminates. An extra thermocouple was used in multiple spots, depending on the placement of the laminates. These thermocouples were pinned to the Kapton release film using high temperature flash tape. The thermocouple wires were stripped of the fiberglass insulation over the vacuum tape. This prevented possible vacuum leaks. The top of the laminate was coated twice with F-57 mold release. Kapton release film coated twice on the bottom surface with F-57 mold release covered the top of the laminate and was pinned down at the corners using high temperature flash tape. A steel shim was placed on top of the Kapton film release. The steel shim prevented the slight waviness that was present on the top surface of the small plates. Fiberglass air breather and the Kapton vacuum bag were placed on top of the Kapton release film. The vacuum bag was sealed using high temperature vacuum tape along the edge of the caul plate. Steel top plates were placed over the vacuum bag. The steel top plates were used to spread out the high temperature under the heat blanket coils and protect the Kapton vacuum bag from temperature spikes within the blanket. Two thermocouples were pinned to the large heat blanket approximately 381 mm (15 in) from the front. These thermocouples monitored the temperature of the blanket. The front of the blanket was defined as the end at which the 3 wire leads exited. The large heat blanket had dimensions 787 mm (31 in) by 1397 mm (55 in) with a power of 1.24 Watts/cm^2 (8 Watts/in^2). The blanket was placed on the

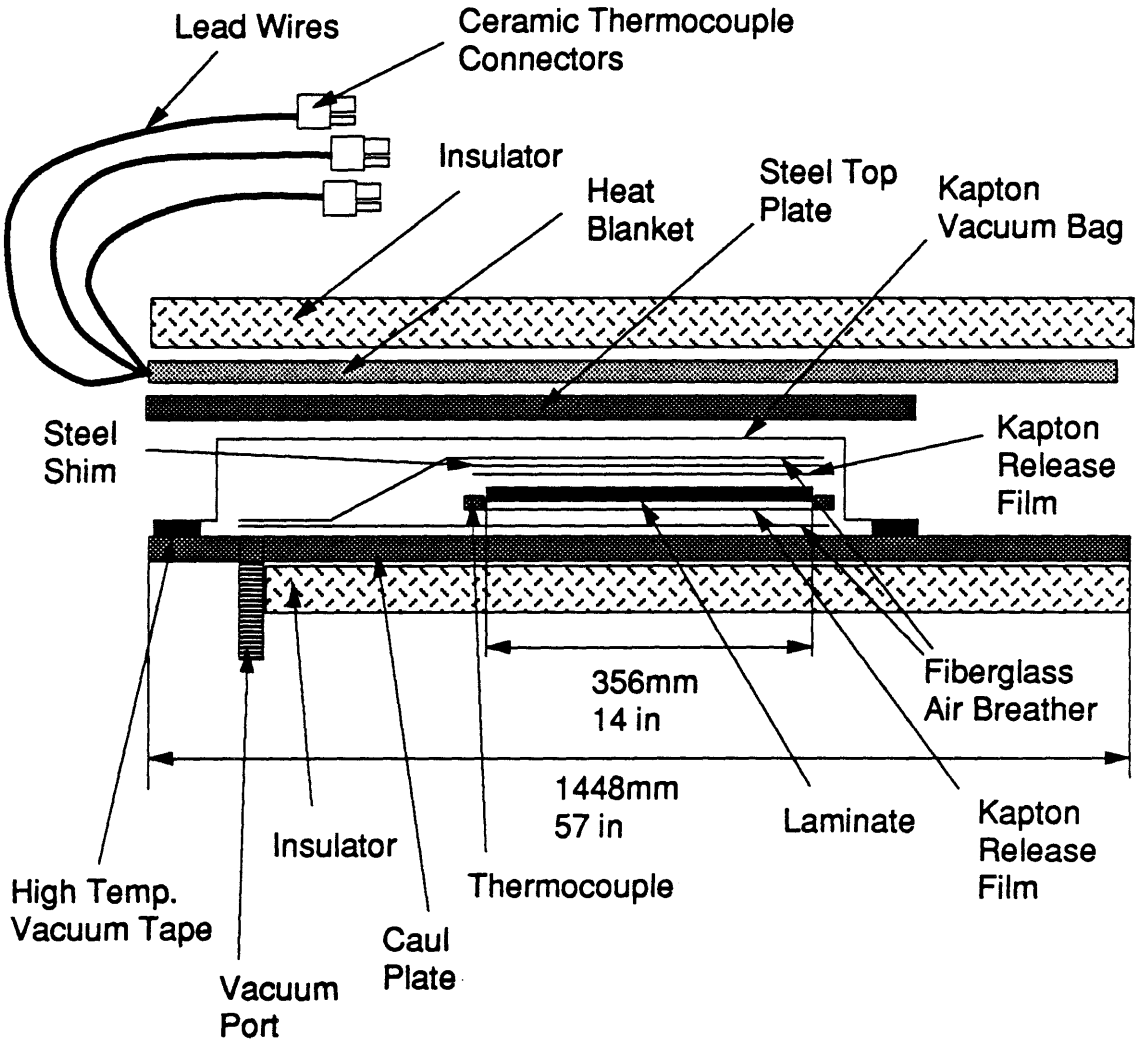

Figure 2.6 Side view of the composite assembly for large plates.

steel top plates. An insulator was placed on top of the blanket. The whole assembly was placed in an autoclave. Please see Figure 2.6.

The autoclave provided the pressure and vacuum. The heat blanket supplied the only source of heat; the autoclave did not contribute to the heating process. The pressure and vacuum were set at .34 MPa (50 psi) and 762 mm Hg (30 in Hg). The nominal heating cycle was as follows: 1) 149°C (300°F) for 10 minute hold, 2) 260°C (500°F) for 10 minute hold, 3) 371°C (700°F) for 10 minute hold, 4) 471°C (880°F) for 10 minute hold, and 5) 482-493°C (900-920°F) for 50 minute hold. The final hold varied in temperature and time for each specimen. The goal of the final hold was to raise the temperature high enough to 1) heat the assembly quickly to reduce processing time, and 2) heat the cool parts of the assembly above the minimum processing temperature. If the processing window, the range between the Kapton burn temperature of 427°C (800°F) and the lowest consolidation temperature of 360°C (680°F), of 67°C (120°F) could not be achieved, the temperature that averaged the differences between the two extremes was applied. If the temperature gradient within the system was greater than 67°C (120°F), a possibility existed that some material would not be properly consolidated. Figure 2.7 gives a graphical illustration of the temperature and pressure during consolidation.

The quality and repeatability of the process, as defined by the magnitude and consistency of ΔT for each processing cycle, is given in Table 2.6.

The temperature gradient was large and caused a 41% loss of material after processing. The reason for the high gradient was due to the caul plate bending during consolidation. The caul plate was exposed to the cool autoclave temperature on the lower surface at the back edge. The top

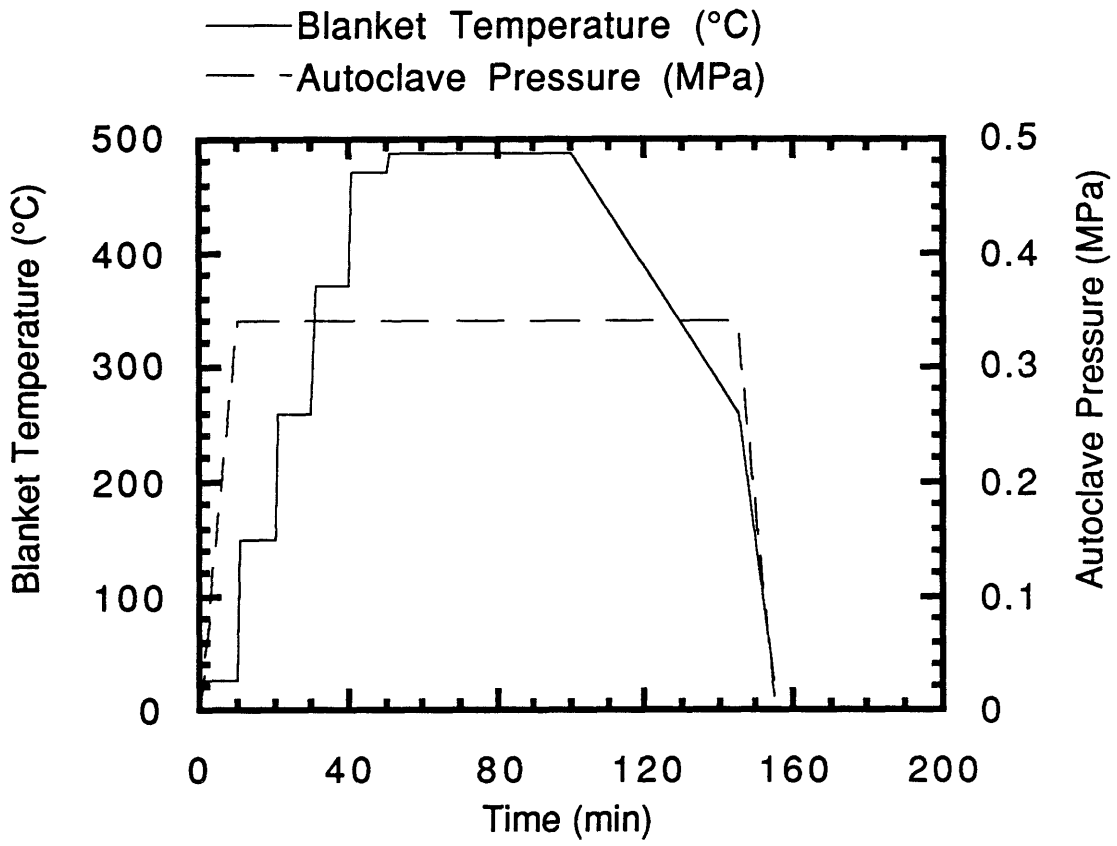

Figure 2.7 Temperature and pressure during consolidation for the large plates.

Table 2.6 Magnitude and consistency of the temperature gradient across the part for large plate processing.

Laminate	ΔT (°C) during processing
100/0/0	83
70/20/10	--
50/40/10, 30/60/10	102
0/100/0	80
0/0/100	71
Average	84
Coefficient of Variation	15.5%

edge of the caul plate was exposed to the hot blanket. As a result, a temperature gradient existed through the thickness of the caul plate. The top part of the caul plate was in compression, because the top part wanted to expand, due to the heat, but was constrained by the lower, "cool" part of the caul plate. This phenomena resulted in an internal bending moment, causing a curvature. Since the heavy steel top plates covered the front end, the back end would rise. This limited the effectiveness of the insulators on both surfaces of the assembly.

The good surfaces of the consolidated laminates were cut into tensile coupons with a diamond circular blade. The nominal dimensions of the coupons were 51 mm (2 in) by 330 mm (13 in) long. Tables 2.7 and 2.8 list the thicknesses and widths of the tensile coupons. Figure 2.8 illustrates where the measurements were taken.

Glass/Epoxy tabs were milled to protect the coupons from the loading grips of the MTS machine. The width of each tab was customized to the

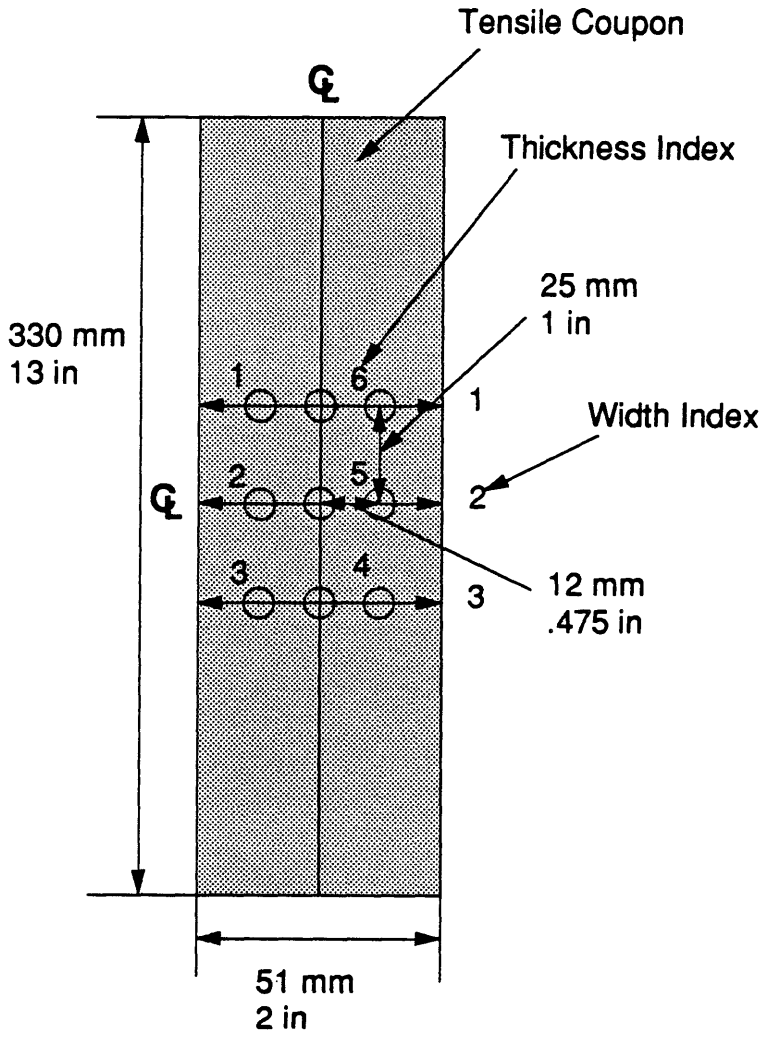

Figure 2.8 Locations of thickness and width measurements for tensile coupons.

Table 2.7 Thickness measurements for tensile coupons.

Specimen	Thickness (mm)						
	1	2	3	4	5	6	Av.
T100/0/0-9	2.95	2.97	2.92	2.82	2.82	2.79	2.88
T100/0/0-10	2.95	3.00	3.00	2.87	2.92	2.90	2.94
T100/0/0-11	2.69	2.72	2.72	3.05	2.92	2.84	2.82
T100/0/0-12	2.72	2.77	2.84	2.82	2.79	2.74	2.78
T70/20/10-19	2.69	2.69	2.67	2.69	2.69	2.67	2.68
T70/20/10-20	2.72	2.72	2.72	2.79	2.74	2.69	2.73
T50/40/10-17	2.87	2.87	2.90	3.07	3.10	2.87	2.95
T50/40/10-18	2.87	2.84	2.84	2.87	2.95	2.87	2.87
T30/60/10-13	2.82	2.87	2.84	2.87	2.92	2.90	2.87
T30/60/10-14	2.92	2.87	2.84	2.79	2.87	2.82	2.85
T30/60/10-15	2.74	2.77	2.77	2.95	2.87	2.82	2.82
T30/60/10-16	2.82	2.77	2.82	2.79	2.77	2.82	2.80
T0/100/0-1	2.72	2.72	2.74	2.69	2.72	2.72	2.72
T0/100/0-2	2.82	2.87	2.82	2.84	2.95	2.87	2.86
T0/100/0-3	2.79	2.74	2.74	2.82	2.84	2.79	2.79
T0/0/100-4	1.32	1.37	1.37	1.37	1.37	1.32	1.35
T0/0/100-5	1.32	1.35	1.37	1.37	1.37	1.32	1.35
T0/0/100-6	1.32	1.35	1.37	1.47	1.45	1.42	1.40
T0/0/100-7	1.45	1.42	1.50	1.50	1.45	1.44	1.46
T0/0/100-8	1.37	1.37	1.37	1.37	1.35	1.35	1.36

Table 2.8 Width measurements for tensile coupons.

Specimen	Width (mm)			
	1	2	3	Av.
T100/0/0-9	58.93	58.95	59.06	58.98
T100/0/0-10	56.41	56.46	56.52	56.46
T100/0/0-11	56.39	56.62	56.79	56.60
T100/0/0-12	56.85	56.57	56.39	56.60
T70/20/10-19	51.41	51.36	51.28	51.35
T70/20/10-20	48.49	48.41	48.29	48.40
T50/40/10-17	54.69	54.61	54.53	54.61
T50/40/10-18	50.72	50.70	50.90	50.78
T30/60/10-13	53.82	53.85	53.90	53.86
T30/60/10-14	58.62	58.62	58.67	58.64
T30/60/10-15	58.14	58.17	58.19	58.17
T30/60/10-16	58.60	58.60	58.57	58.59
T0/100/0-1	52.48	52.30	52.15	52.31
T0/100/0-2	60.30	60.55	60.76	60.54
T0/100/0-3	58.67	58.83	58.95	58.82
T0/0/100-4	53.16	52.91	52.63	52.90
T0/0/100-5	59.03	59.16	59.31	59.17
T0/0/100-6	51.05	50.95	50.83	50.94
T0/0/100-7	53.14	53.32	53.52	53.32
T0/0/100-8	52.93	53.21	53.26	53.14

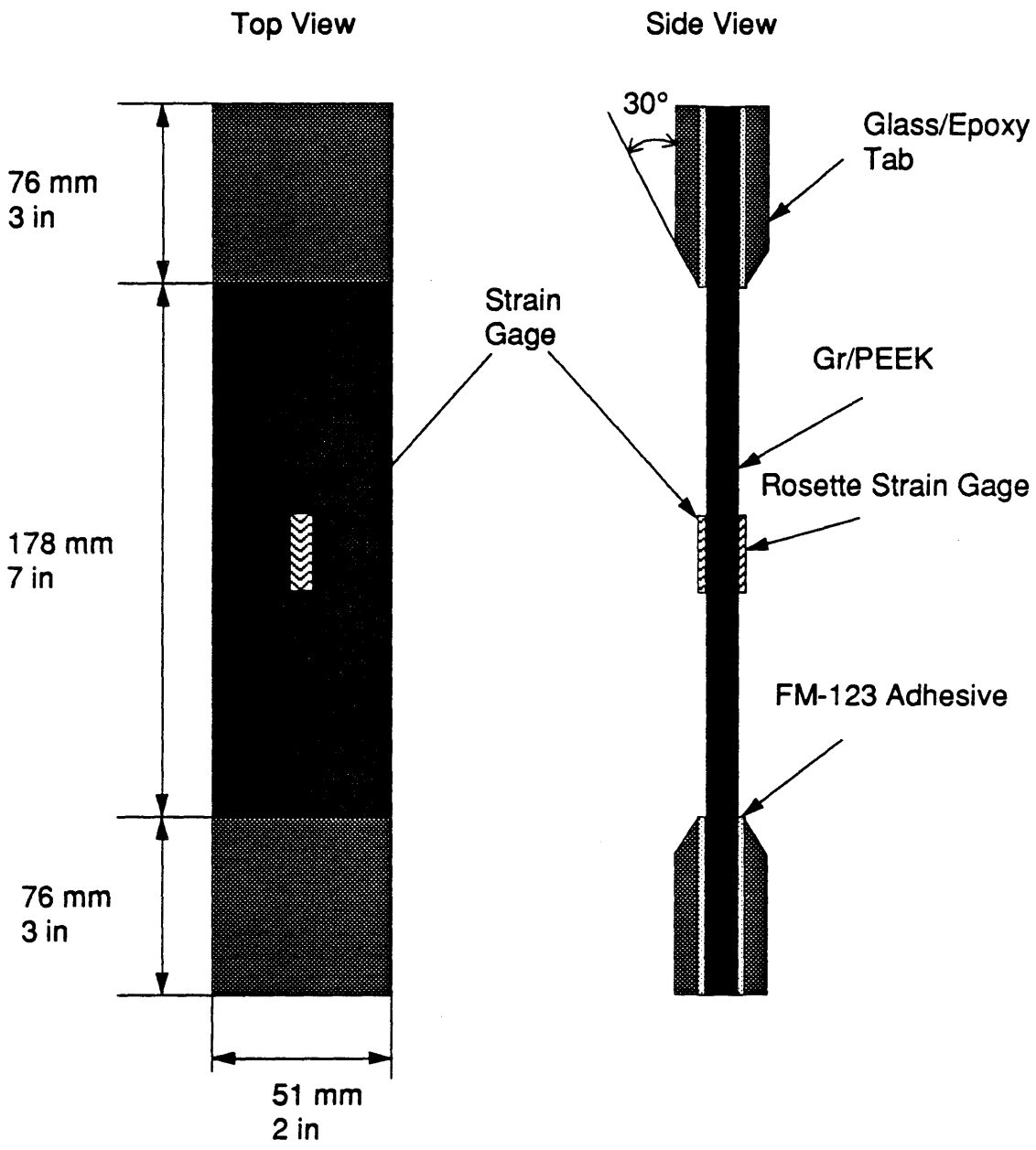

Figure 2.9 Illustration of a typical tensile coupon.

specimen. The length of the tabs was nominally 76 mm (3 in). The thickness of the tabs for the 20 ply 100/0/0, 70/20/10, 50/40/10,30/60/10 and 0/100/0 was 17 plies. The thickness for the tabs for the 10 ply 0/0/100 was 9 plies. The tabs were bevelled on the inner, vertical edge that faced the center of the laminate. FM-123 adhesive was applied to the surface of the glass tabs. After heating the adhesive with a heat gun, the glass tabs were applied to the coupons. The tensile coupons were inserted into an autoclave; and heat, pressure and vacuum were applied. The temperature, pressure and vacuum were set at 107°C (225°F), 69 kPa (10 psi) and 762 mm Hg (30 in Hg) for 2 hours. Please consult the TELAC manufacturing notes for specific details. A nominal tensile coupon is illustrated in Figure 2.9.

A rosette, consisting of 3 strain gages 45° apart, was applied to the flat surface of the tensile coupons that pressed against the caul plate during consolidation. The 3 gages on the rosette were aligned 0°, 45° and 90° with respect to the longitudinal axis of the coupon. The rosette was applied for two reasons: 1) to graph the stress-strain curve in principal axes, thereby eliminating any error in gage application to the coupon, and 2) to find G_{LT} by strain transformation laws. The rosette part number was EA-06-125RA-120. Another single gage was applied on the other surface in the longitudinal direction. This gage was used to illuminate any discrepancies between longitudinal strains on the two surfaces of the coupon. If discrepancies existed, a possibility of extension-bending or extension-twisting could exist. The single gage part number was EA-06-125AD-120. Both gages were applied to the coupon surface using the standard TELAC procedure. Strain gage wires were attached to the strain gages. The wires connected to the strain gage box during the mechanical testing. Please consult the TELAC manufacturing notes for details.

2.7 Male Mold

Two molds were machined to make right angle Gr/PEEK bends. The male mold was an iron bend, 13 mm (.5 in) thick with sides of approximately 152 mm (6 in). The length was 305 mm (12 in). A belt sander was used to smooth the original sharp corner of the bend, since it could cause fiber damage during forming. A hole was drilled into the iron bend to allow for vacuum during processing. Figure 2.10 illustrates the male mold. This mold was employed to make the right angle bend specimens.

The female mold is described and illustrated in Appendix A. The mold was not used to make any specimens. The male mold was chosen over the female mold, because the male mold would allow easy layup before processing and easy heating during processing. In addition, the male mold was made of iron instead of aluminum. The male mold required 3 days of machining at a cost of $137, while the female mold required 3 months of machining at a cost of $440.

2.8 Processing of Right Angle Bends with Male Mold

Two methods were attempted to make right angle bends, 1) layup in final part form and 2) stiff diaphragm thermoforming. The bend specimens were formed using the first method. The second method was attempted once unsuccessfully.

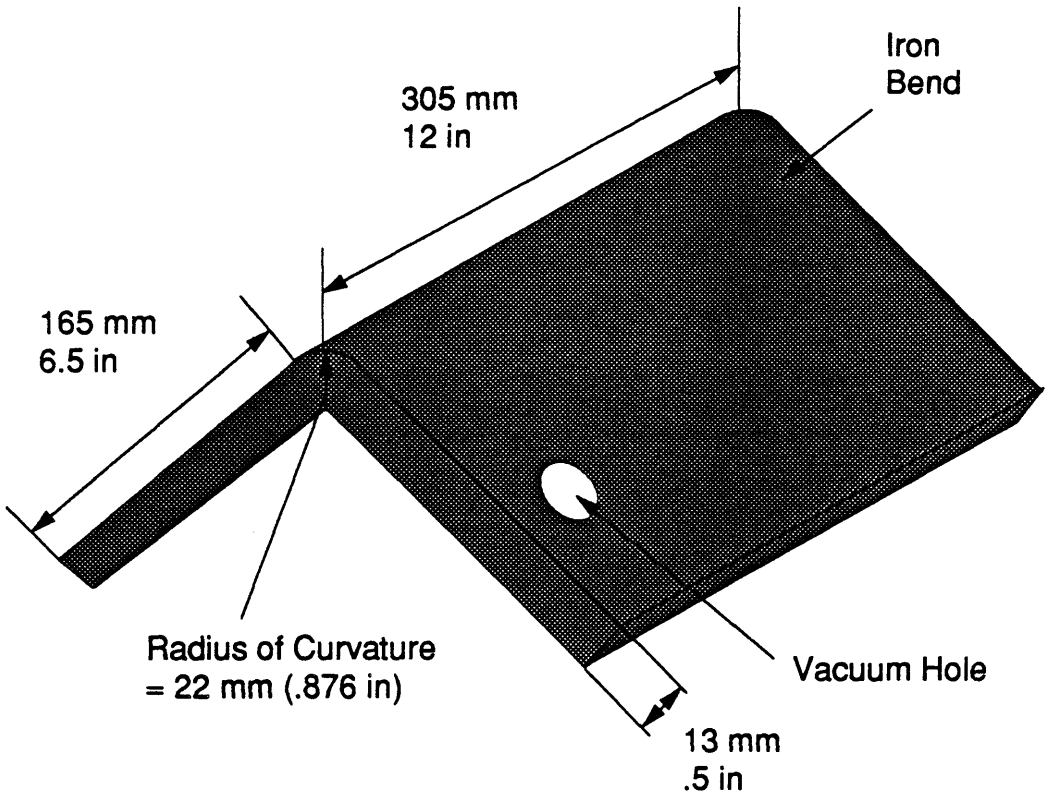

Figure 2.10 Illustration of male mold.

2.8.1 Layup in Final Part Form

A small square of fiberglass air breather was pinned over the vacuum hole in the iron bend with high temperature flash tape. Fiberglass air breather was held in place over the iron bend by high temperature flash tape. The fiberglass air breather covered the iron bend to 51 mm (2 in) from the edges. This space was used for the vacuum tape. Kapton release film was applied to the fiberglass air breather using high temperature flash tape. No mold release was used, because the ability of F-57 to act as a mold release was unknown at this time. As a result, Kapton was present on both surfaces of the bend specimens. The fiberglass air breather and Kapton film release were applied to the iron bend using high temperature flash tape. A ply of Gr/PEEK was clamped to the Kapton release film along its small edge using high temperature flash tape. Each ply was 127 mm (5 in) by 203 mm (8 in). Another ply was pinned onto the clamped ply using a large soldering iron on the corners. This procedure was repeated until ten plies were attached to the mold. One laminate was processed at a time. A thermocouple was placed at each corner of the pre-consolidated plies. A total of four thermocouples were used inside the assembly. These thermocouples were pinned to the Kapton release film using high temperature flash tape. The thermocouple wires were stripped of the fiberglass insulation over the vacuum tape. Kapton release film covered the top of the pre-consolidated plies and was pinned down at the corners using high temperature flash tape. Fiberglass air breather and the Kapton vacuum bag were placed on top of the Kapton release film. The vacuum bag was sealed using high temperature vacuum tape along the edge of the iron bend. Two thermocouples were pinned to the small heat blanket approximately 102 mm (4 in) from the front. These thermocouples

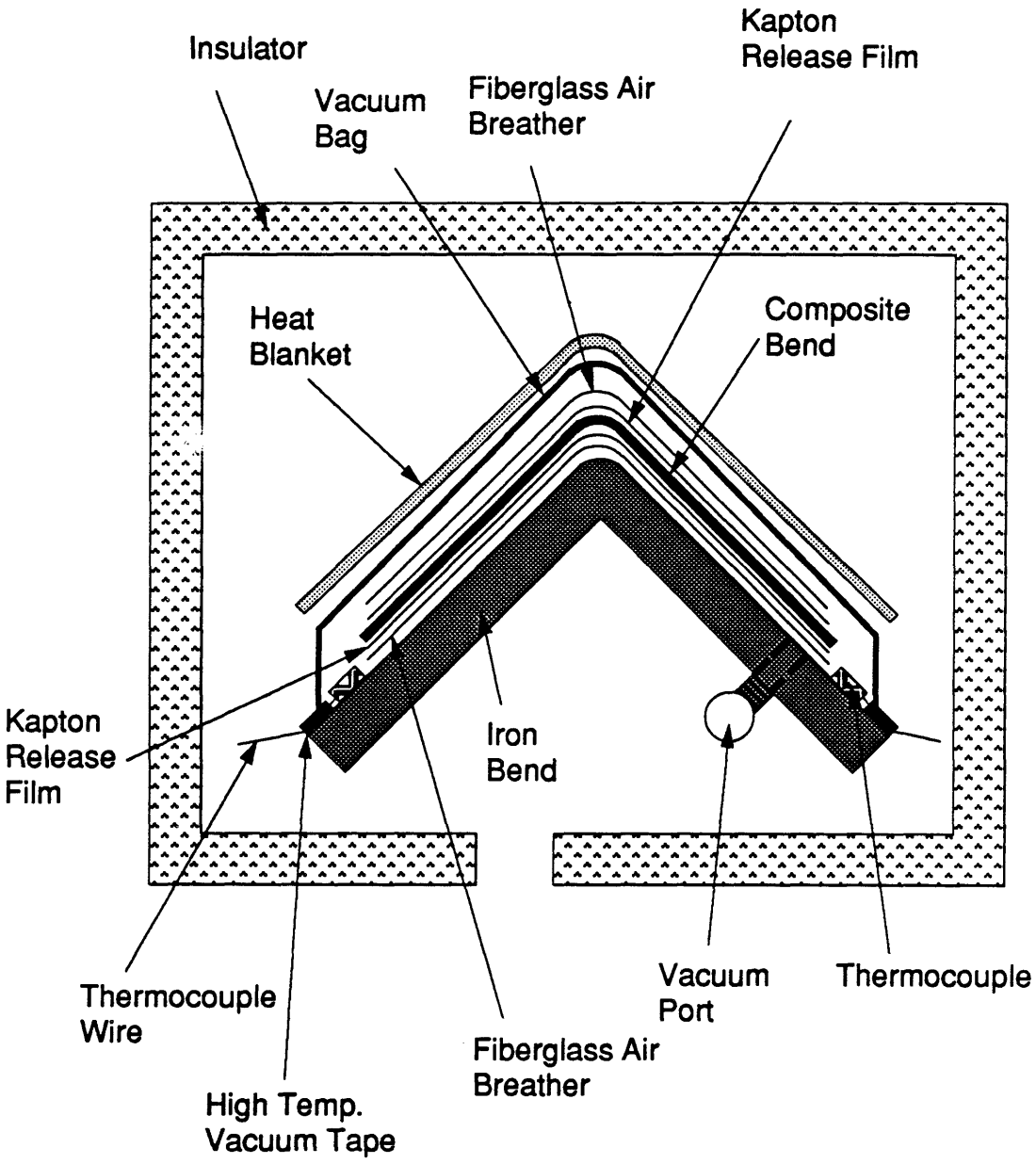

Figure 2.11 Side view of the composite assembly for bend specimens.

monitored the temperature of the blanket. The front of the blanket was defined as the end at which the 3 wire leads exited. The small heat blanket had dimensions 305 mm (12 in) by 330 mm (13 in) with a power of 1.24 Watts/cm^2 (8 Watts/in^2). The blanket was placed on the Kapton vacuum bag. An insulator surrounded the entire assembly creating a partial oven. The whole system was placed in an autoclave. Please see Figure 2.11.

The autoclave provided the pressure and vacuum. The heat blanket supplied the only source of heat; the autoclave did not contribute to the heating process. The pressure and vacuum were set at .34 MPa (50 psi) and 762 mm Hg (30 in Hg). The nominal heating cycle was as follows: 1) 149°C (300°F) for 10 minute hold, 2) 260°C (500°F) for 10 minute hold, 3) 371°C (700°F) for 10 minute hold, and 4) 471°C (880°F) for 80 minute hold. The final hold varied in temperature and time for each specimen. The goal of the final hold was to raise the temperature high enough to 1) heat the assembly quickly to reduce processing time, and 2) heat the cool parts of the assembly above the minimum processing temperature. If the processing window, the range between the Kapton burn temperature of 427°C (800°F) and the lowest consolidation temperature of 360°C (680°F), of 67°C (120°F) could not be achieved, the temperature that averaged the differences between the two extremes was applied. If the temperature gradient within the system was greater than 67°C (120°F), a possibility existed that some material would not be properly consolidated. Figure 2.12 gives a graphical illustration of the temperature and pressure during consolidation.

The quality and repeatability of the manufacturing process, as defined by the magnitude and consistency of the temperature gradient during consolidation, are given in Table 2.9.

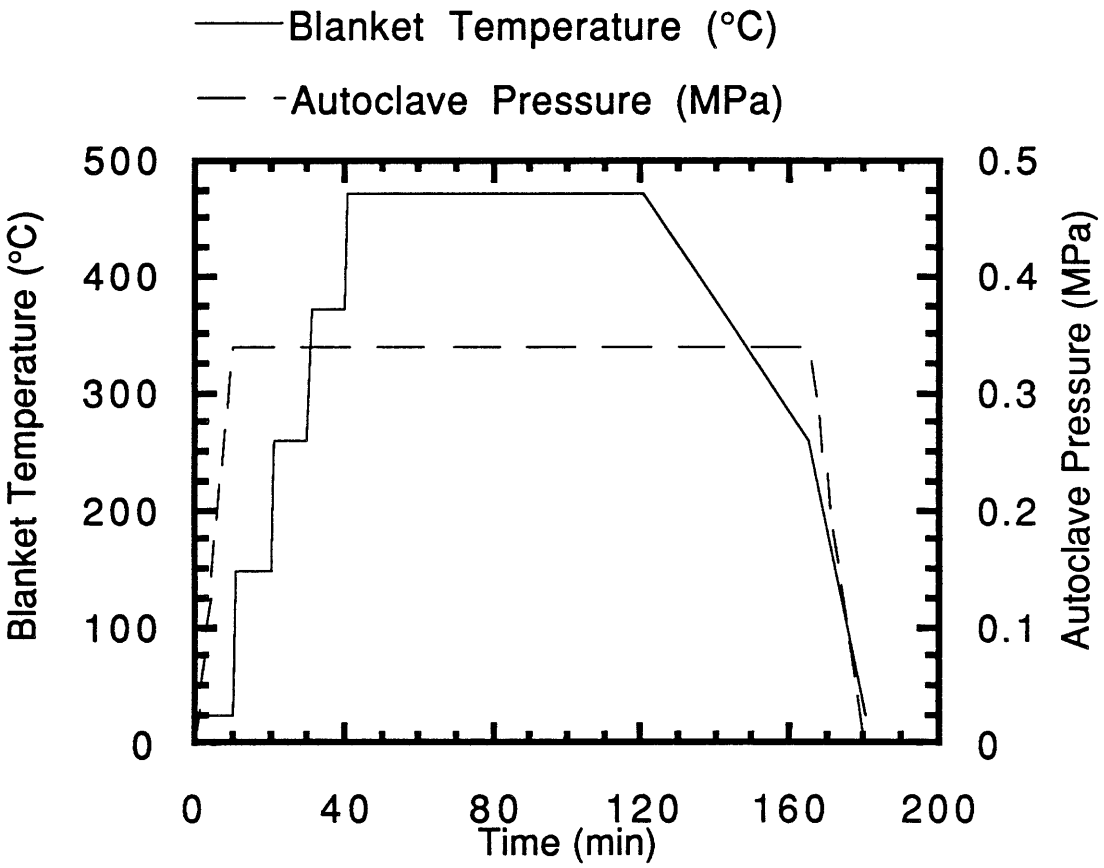

Figure 2.12 Temperature and pressure during consolidation of the bend specimens.

Table 2.9 Magnitude and consistency of the temperature gradient across the part for bend specimen processing.

Bend	ΔT(°C)
B100/0/0-1,2	96
B100/0/0-3,4	58
Average	77
Coefficient of Variation	34.9%

The two bends were cut into specimens with a diamond circular blade. The nominal dimensions of the bend specimens were 51 mm (2 in) wide with sides of length 89 mm (3.5 in). Tables 2.10 and 2.11 list the thickness and width of each bend specimen. Figure 2.13 illustrates a bend specimen and the locations of the measurements. After processing, one side of the bend was longer than the other side. The length of the bend specimens' sides and radius of curvature are tabulated in Table 2.12. Two 13 mm (.5 in) holes were drilled into the center of the short side of the bends for mechanical testing. The two holes were drilled 13 mm (.5 in) and 38 mm (1.5 in) from the end of the curvature in the bend using a diamond drill. A small piece of aluminum, with nominal dimensions 6 mm (.25 in) by 51 mm (2 in) by 3 mm (.125 in), was glued to the upper surface of the long side at the edge using room temperature epoxy. A small slit, of length 2 mm (.0625 in), was cut into the aluminum. The slit held the piano wire during testing. Please see Figure 2.13 for details.

Table 2.10 Thickness measurements for bend specimens.

Specimen	Thickness (mm)						
	1	2	3	4	5	6	Av.
B100/0/0-1	1.35	1.35	1.45	1.49	1.42	1.42	1.41
B100/0/0-2	1.47	1.52	1.50	1.32	1.42	1.37	1.44
B100/0/0-3	1.42	1.52	1.50	1.45	1.25	1.37	1.42
B100/0/0-4	1.32	1.32	1.32	1.47	1.47	1.35	1.38

Table 2.11 Width measurements of bend specimens.

Specimens	Width (mm)			
	1	2	3	Av.
B100/0/0-1	54.81	52.86	52.71	53.46
B100/0/0-2	53.42	54.94	54.86	54.41
B100/0/0-3	50.06	49.48	49.91	49.82
B100/0/0-4	58.04	57.86	57.28	57.73

Table 2.12 Side lengths and radius of curvature for bend specimens.

Specimens	Side Length		Radius of Curvature (mm)
	Long Side (mm)	Short Side (mm)	
B100/0/0-1	89	81	21
B100/0/0-2	91	80	23
B100/0/0-3	90	84	23
B100/0/0-4	91	82	22

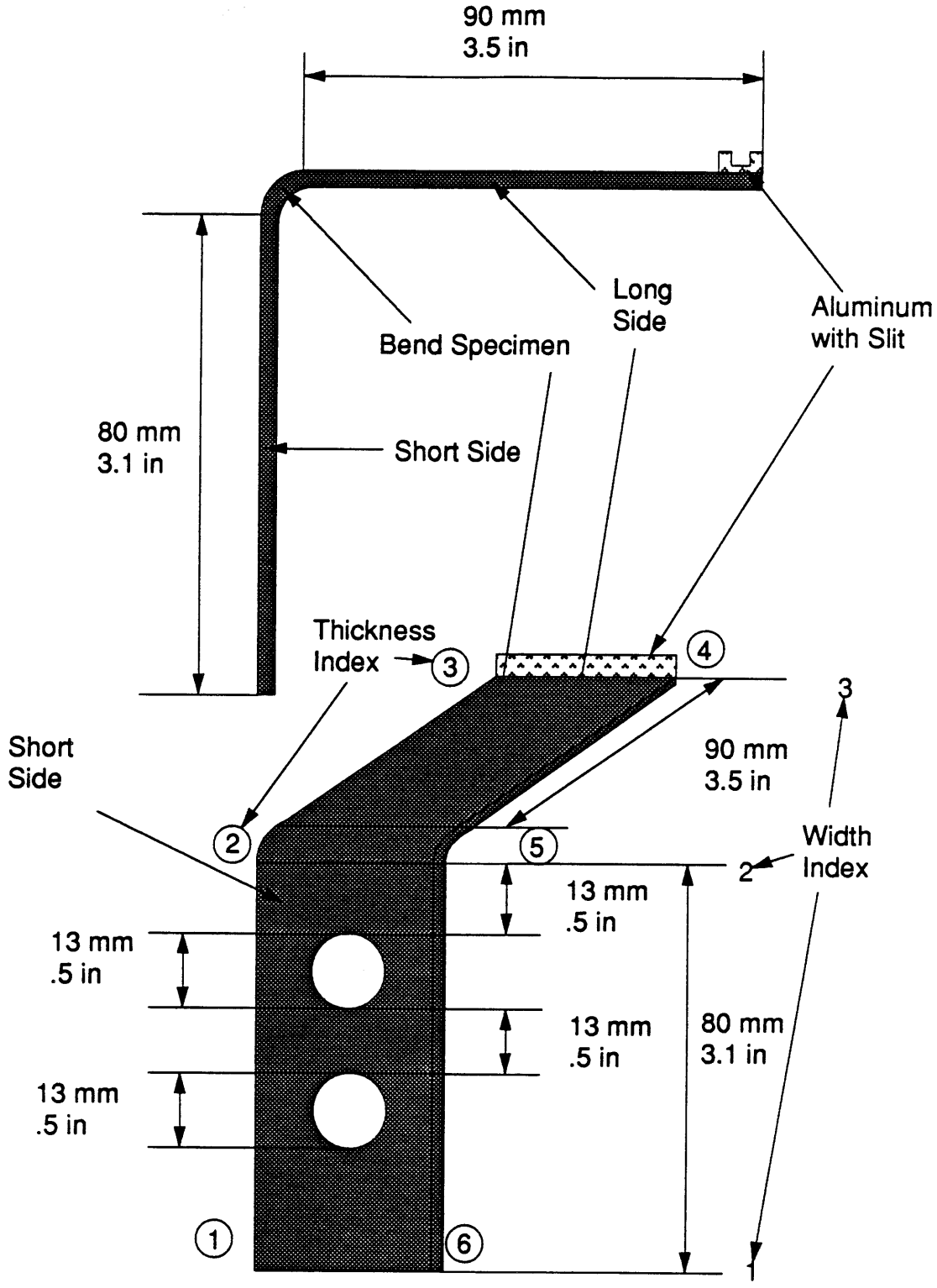

Figure 2.13 Illustration of a typical bend specimen.

2.8.2 Stiff Diaphragm Thermoforming

Forming a right angle bend from a consolidated plate of Gr/PEEK was attempted once, unsuccessfully, by stiff diaphragm thermoforming. The procedure using thermoforming was similar to the bends formed in final part form, except for the consolidated sheet of Gr/PEEK and the vacuum bag. Thermoforming uses heat, pressure and vacuum to form parts. The stiff diaphragm was the vacuum bag. A small sheet, 127 mm (5 in) by 203 mm (8 in), of 10 Gr/PEEK consolidated plies was taped along the width direction onto the male mold's vertex. This sheet was specimen P100/0/0-3. The sheet was symmetrical about the mold with respect to the length. The vacuum bag surrounded the sheet and was sealed by high temperature vacuum tape along the edge of the mold. The vacuum bag was "folded" along the edges by extra vacuum tape to allow for surface discontinuities within the assembly. The assembly was surrounded by an insulator and inserted into an autoclave. A pressure and vacuum of .41 MPa (60 psi) and 762 mm Hg (30 in Hg) were applied after reaching processing temperature. Applying pressure and vacuum before reaching the processing temperature would load the sheet in bending, possibly damaging it. The higher pressure was used to help the vacuum bag push against the sheet. The heating cycle was as follows. 1) 260 °C (500°F) for 10 minute hold, and 2) 471°C (880°F) for 40 minute hold. The reduced heating cycle was employed to reduce the possibility of the vacuum bag burning. The heat softens the sheet while the vacuum bag pushes against it. This combination of heat and pressure should produce a bend. Thermoforming using this method did not work due to the heat blanket burning the Kapton vacuum bag and the laminate.

Chapter 3
ANALYTICAL MODELS

Analytical models calculated the stiffness of a tensile coupon and right angle bend. Classical Laminated Plate Theory was used for the former, while an energy method was used for the latter.

3.1 Laminated Plate Theory

Determining E_L, E_T, ν_{LT}, and G_{LT} from the experimental data using Hooke's law for orthotropic materials enabled one to investigate the structural integrity of the material after manufacturing. The following equations and the output from the coupon tests were used to find the necessary single ply material constants E_L, E_T, ν_{LT}, and G_{LT}.

$$\varepsilon_L = \frac{1}{E_L}[\sigma_L - \nu_{LT}\sigma_T] \tag{3.1.1}$$

$$\varepsilon_T = \frac{1}{E_T}[\sigma_T - \nu_{TL}\sigma_L] \tag{3.1.2}$$

$$\frac{\nu_{LT}}{E_L} = \frac{\nu_{TL}}{E_T} \tag{3.1.3}$$

$$\varepsilon_{LT} = \frac{\sigma_{LT}}{2G_{LT}} \tag{3.1.4}$$

Uniaxial loading in the L-direction of the 100/0/0 tensile coupons reduced equations 3.1.1, 3.1.2 and 3.1.3 to :

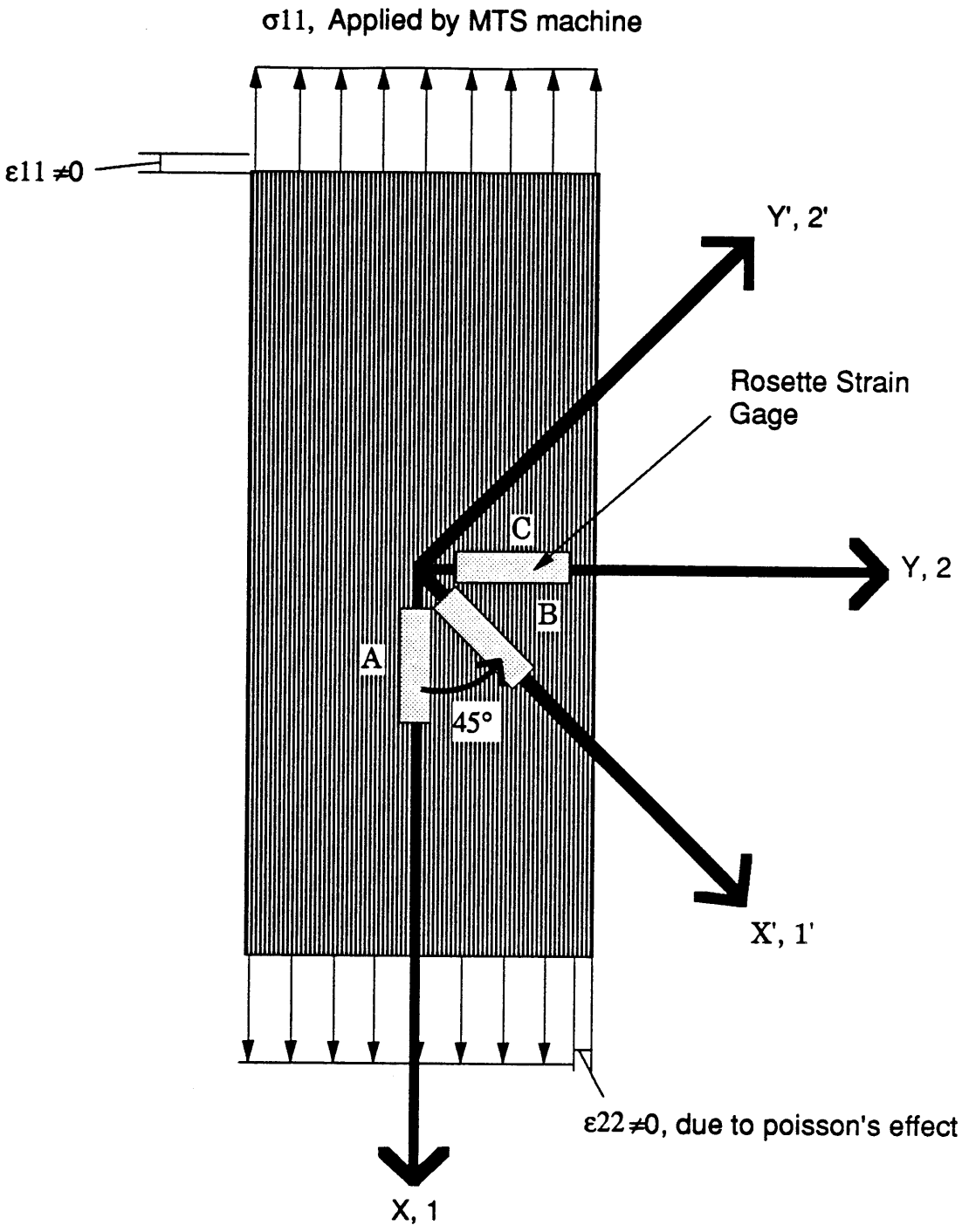

Figure 3.1 Stress-strain state during tensile coupon test in principal axes (no shear).

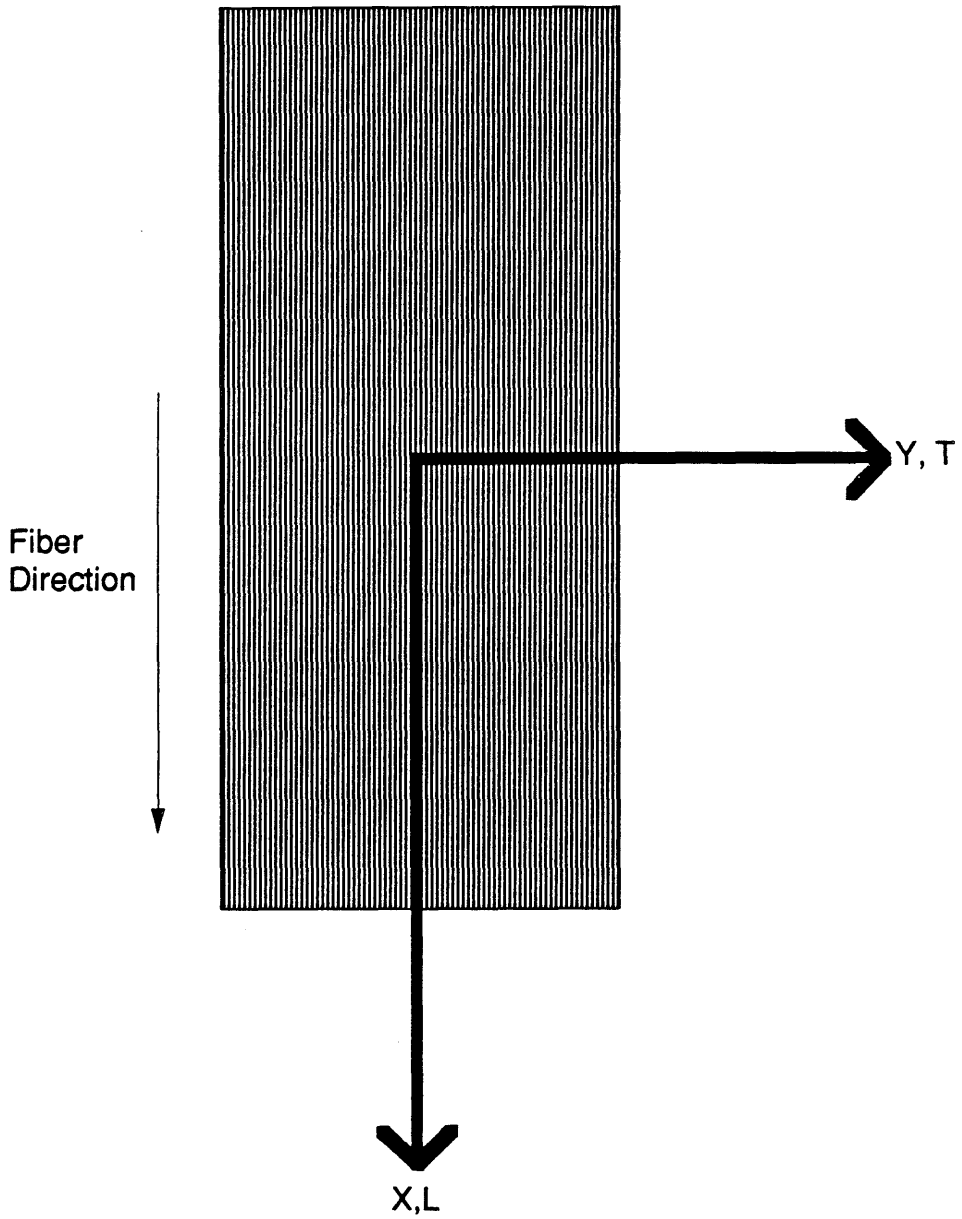

Figure 3.2 Axis system used to determine ply properties.

$$\varepsilon_L = \frac{1}{E_L}[\sigma_L] \tag{3.1.5}$$

$$\nu_{LT} = -\frac{\varepsilon_T}{\varepsilon_L} \tag{3.1.6}$$

from which E_L and ν_{LT} were calculated.

Uniaxial loading in the T-direction of the 0/0/100 tensile coupons reduced equation 3.1.2 to:

$$\varepsilon_T = \frac{1}{E_T}[\sigma_T] \tag{3.1.7}$$

from which E_T was calculated. Please see Figures 3.1 and 3.2.

G_{LT} was calculated with the use of transformation laws. To find the shear stress σ_{LT}, the uniaxial loading of the 0/100/0 tensile coupons was transformed by the following equation:

$$\sigma_{LT} = -\cos\theta \sin\theta \sigma_{11} \tag{3.1.8}$$

where:

$\theta = 45°$

σ_{11}= Longitudinal applied stress

ε_{LT} was determined using the following Mohr's circle transformation equation [18] and the 0/100/0 coupon test with a rosette strain gage. The rosette gage results can be interpreted to give the complete two dimensional state of strain for the material.

$$\varepsilon_{LT} = \frac{\varepsilon_{22} - \varepsilon_{11}}{2} \tag{3.1.9}$$

where:

ε_{11}, ε_{22} are Principal strains

The transformed stresses and strains were used to calculate G_{LT} by the following equation:

$$G_{LT} = \frac{\sigma_{LT}}{2\varepsilon_{LT}} \tag{3.1.10}$$

Classical Laminated Plate Theory was used to calculate the stiffnesses for the 70/20/10, 50/40/10, and 30/60/10 tensile coupons using the measured ply properties. The following variables for a single ply were calculated:

$$E^*_{1111} = \frac{E_L}{1 - \nu_{TL}\nu_{LT}}$$
$$E^*_{1122} = \frac{\nu_{LT}E_L}{1 - \nu_{TL}\nu_{LT}}$$
$$E^*_{2222} = \frac{E_T}{1 - \nu_{TL}\nu_{LT}}$$
$$E^*_{1212} = G_{LT} \tag{3.1.11}$$

These values were inserted into the following invariant equations:

$$I_1 = \frac{1}{4}\left[E^*_{1111} + E^*_{2222} + 2E^*_{1122}\right]$$
$$I_2 = \frac{1}{8}\left[E^*_{1111} + E^*_{2222} - 2E^*_{1122} + 4E^*_{1212}\right]$$
$$R_1 = \frac{1}{2}\left[E^*_{1111} - E^*_{2222}\right]$$
$$R_2 = \frac{1}{8}\left[E^*_{1111} + E^*_{2222} - 2E^*_{1122} - 4E^*_{1212}\right] \qquad (3.1.12)$$

These values were used to calculate the ply stiffnesses in non-principal axes using equation 3.1.13:

$$E^{[\theta]}_{1111} = I_1 + I_2 + R_1\cos 2\theta + R_2\cos 4\theta$$
$$E^{[\theta]}_{2222} = I_1 + I_2 - R_1\cos 2\theta + R_2\cos 4\theta$$
$$E^{[\theta]}_{1122} = I_1 - I_2 - R_2\cos 4\theta$$
$$E^{[\theta]}_{1212} = I_2 - R_2\cos 4\theta$$
$$E^{[\theta]}_{1112} = -\frac{1}{2}R_1\sin 2\theta - R_2\sin 4\theta$$
$$E^{[\theta]}_{2212} = -\frac{1}{2}R_1\sin 2\theta + R_2\sin 4\theta \qquad (3.1.13)$$

The stiffness matrix for the laminate was generated by adding the stiffnesses of each ply together and then dividing by the number of plies:

$$E_{\alpha\beta\sigma\gamma} = \frac{1}{n_{plies}}\sum^{Plies} E_{\alpha\beta\sigma\gamma} \qquad (3.1.14)$$

The matrix equation obtained was:

$$\begin{Bmatrix} \sigma_{11} \\ \sigma_{22} \\ \sigma_{12} \end{Bmatrix} = \begin{bmatrix} E_{1111} & E_{1122} & E_{1112} \\ E_{1122} & E_{2222} & E_{2212} \\ E_{1112} & E_{2212} & E_{1212} \end{bmatrix} \begin{Bmatrix} \varepsilon_{11} \\ \varepsilon_{22} \\ 2\varepsilon_{12} \end{Bmatrix} \tag{3.1.15}$$

The stiffness matrix was inverted to the compliance matrix:

$$\begin{Bmatrix} \varepsilon_{11} \\ \varepsilon_{22} \\ \varepsilon_{12} \end{Bmatrix} = \begin{bmatrix} S_{1111} & S_{1122} & S_{1112} \\ S_{1122} & S_{2222} & S_{2212} \\ S_{1112} & S_{2212} & S_{1212} \end{bmatrix} \begin{Bmatrix} \sigma_{11} \\ \sigma_{22} \\ 2\sigma_{12} \end{Bmatrix} \tag{3.1.16}$$

The tensile modulus of the coupons becomes:

$$\frac{1}{S_{1111}} \tag{3.1.17}$$

3.2 Energy Methods

The theoretical calculation for bend stiffness was solved through energy methods. The total potential energy within a structure is:

$$\Pi = U - W \tag{3.2.1}$$

where:

Π = Total potential energy
U = Internal potential energy
W = Work applied

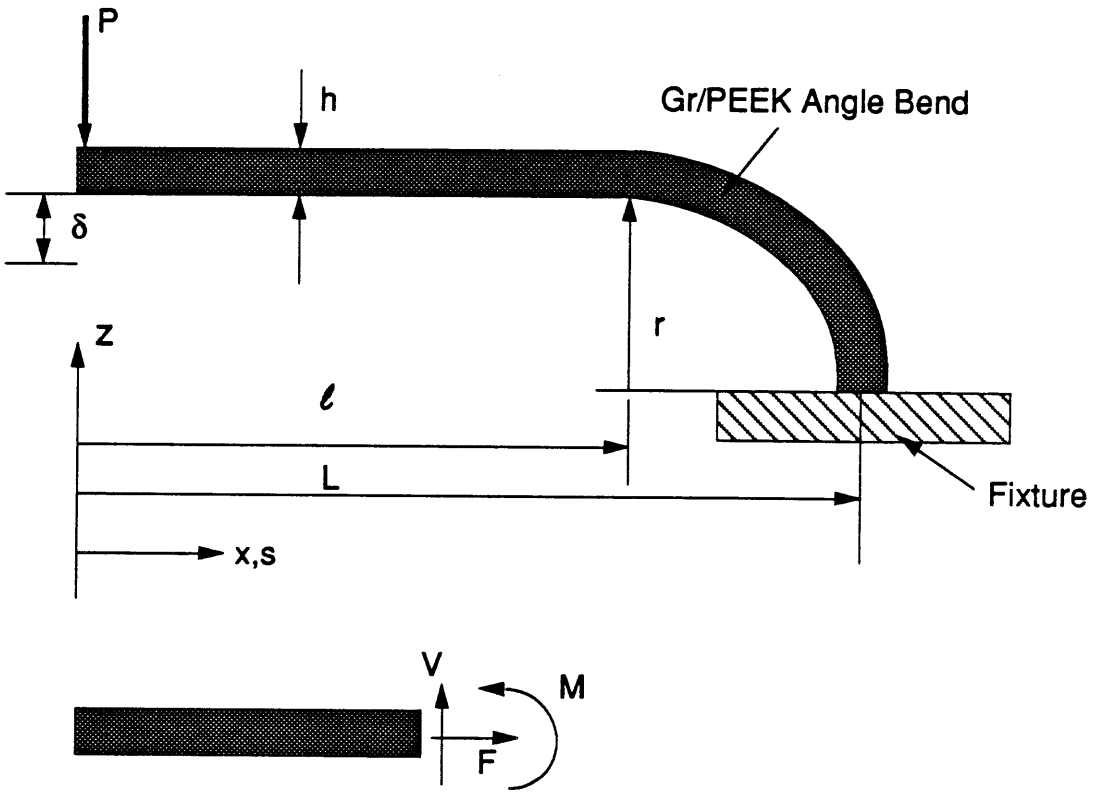

where:

F,V,M = Horizontal force, vertical force, moment
A = Cross sectional area
P = End load
δ = Deflection due to end load
s = Distance in beam
r = Radius of curvature
h = Thickness of bend specimen
ℓ = Length of straight section of bend specimen
L = Total horizontal length of bend specimen

Figure 3.3 Model for bend specimen stiffness.

This equation was reduced to the specific case of a bend with an end load:

$$U = \frac{1}{2}\int \frac{F^2}{AE_L} ds + \frac{1}{2}\int \frac{M^2}{E_L I} ds + \frac{1}{2}\int \frac{V^2}{A}\left(\frac{5}{6}G_{xz}\right)^{-1} ds \tag{3.2.2}$$

$$W = P\delta \tag{3.2.3}$$

$$\Pi = \frac{1}{2}\int \frac{F^2}{AE_L} ds + \frac{1}{2}\int \frac{M^2}{E_L I} ds + \frac{1}{2}\int \frac{V^2}{A}\left(\frac{5}{6}G_{xz}\right)^{-1} ds - P\delta \tag{3.2.4}$$

where:

G_{XZ} = Out-of-plane shear modulus of composite laminate
E_L = Tensile stiffness of composite laminate
I = Moment of inertia

Please see Figure 3.3, which is similar to Figure D-6 in reference [7]. The bend was modelled as a beam. In addition, the out-of-plane shear stiffness in the z direction was approximated by the in-plane shear stiffness:

$$G_{xz} \approx G_{xy} \tag{3.2.5}$$

F, V and M have been determined in reference [7] and are listed here. They were separated into the straight section and the curved section of the beam.

For $0 \le s \le \ell$:

$$\begin{aligned} F_s &= 0 \\ V_s &= P \\ M_s &= -Ps \end{aligned} \tag{3.2.6}$$

For $\ell \leq s \leq L$:

$$\begin{aligned} F_b &= -P\sin\theta \\ V_b &= P\cos\theta \\ M_b &= -P(\ell + r\sin\theta) \end{aligned} \tag{3.2.7}$$

These values were then inserted into equation 3.2.2 to find the internal potential energy of the system.

For the straight section: $0 \leq s \leq \ell$

$$\begin{aligned} \frac{1}{2}\int_0^{\ell} \frac{F^2}{AE_L}\,ds &= 0 \\ \frac{1}{2}\int_0^{\ell} \frac{V^2}{A}\left(\frac{5}{6}G_{xz}\right)^{-1}ds &= \frac{1}{2}\frac{P^2\ell}{A}\left[\frac{5}{6}G_{xz}\right]^{-1} \\ \frac{1}{2}\int_0^{\ell} \frac{M^2}{E_L I}\,ds &= \frac{1}{2}\frac{P^2}{E_L I}\frac{\ell^3}{3} \end{aligned} \tag{3.2.8}$$

For the bent section: $\ell \leq s \leq L$

$$\begin{aligned} \frac{1}{2}\int_{\ell}^{L} \frac{F^2}{AE_L}\,ds &= \frac{1}{2}\frac{P^2 r}{AE_L}\frac{\pi}{4} \\ \frac{1}{2}\int_{\ell}^{L} \frac{V^2}{A}\left(\frac{5}{6}G_{xz}\right)^{-1}ds &= \frac{1}{2}\frac{P^2 r}{A}\left(\frac{5}{6}G_{xz}\right)^{-1}\frac{\pi}{4} \\ \frac{1}{2}\int_{\ell}^{L} \frac{M^2}{E_L I}\,ds &= \frac{1}{2}\frac{P^2 r}{E_L I}\left[\frac{\ell^2\pi}{2} + 2\ell r + \frac{r^2\pi}{4}\right] \end{aligned} \tag{3.2.9}$$

The energy expression becomes:

$$\Pi = \frac{\pi}{8}\frac{P^2 r}{AE_L} + \frac{P^2}{2A}\left[\frac{5}{6}G_{xz}\right]^{-1}\left(\ell + \frac{r\pi}{4}\right) + \frac{P^2\ell^3}{6E_L I} + \frac{1}{2}\frac{P^2 r}{E_L I}\left[\frac{\ell^2\pi}{2} + 2\ell r + \frac{r^2\pi}{4}\right] - P\delta \qquad (3.2.10)$$

Applying the principle of minimum complementary energy,

$$\frac{\partial \Pi}{\partial P} = 0 \qquad (3.2.11)$$

the final equation reduces to:

$$P = K\delta \qquad (3.2.12)$$

where K, the stiffness of a bend, is:

$$K = \left[\frac{\pi}{4}\frac{r}{AE_L} + \frac{1}{A}\left(\frac{5}{6}G_{xz}\right)^{-1}\left(\ell + \frac{r\pi}{4}\right) + \frac{\ell^3}{3E_L I} + \frac{r}{E_L I}\left(\frac{\ell^2\pi}{2} + 2\ell r + \frac{r^2\pi}{4}\right)\right]^{-1} \qquad (3.2.13)$$

Chapter 4
MECHANICAL TESTING

4.1 Test Matrix

The test matrix consisted of two types of specimens and six different laminate types. The tensile coupons and bends were tested for stiffness. Please see Table 4.1 for a summary.

Table 4.1 Test Matrix.

Specimen	Layup	No. of Specimens	Plies
Tensile Coupon	100/0/0	4	20
Tensile Coupon	70/20/10	2	20
Tensile Coupon	50/40/10	2	20
Tensile Coupon	30/60/10	4	20
Tensile Coupon	0/100/0	3	20
Tensile Coupon	0/0/100	5	10
Bend	100/0/0	4	10

The number of specimens for each laminate was not ideal because of material loss caused by the manufacturing process.

4.2 Tensile Coupons

Figure 2.9 illustrates a tensile coupon. The tensile coupons were tested in a MTS machine that could apply a maximum load of 311 kN (70,000 lbs). The tests were conducted in load control. The loading rate was the following: 1) 636 N/s (143 lbs/s) for the 100/0/0's, 70/20/10's, and 50/40/10's, 2) 316 N/s (71 lbs/s) for the 30/60/10's, 3) 128 N/s (29 lbs/s) for the 0/100/0's, and 4) 62 N/s (14 lbs/s) for the 0/0/100's. The loading rates were set through the console. The top part of the coupon was gripped by the MTS machine on the glass tabs. The gripping pressure was between 5.5-11.0 MPa (800-1600 psi). A plastic right angle was pressed against the side of the coupon to insure that it was loaded correctly in the machine. The strain gage wires were attached to the strain gage box. The strain gages were then zeroed through the strain gage amplifier. A shunt resistor was used to properly calibrate the gages. The bottom part of the coupon was then gripped. A computer program was run that loaded the coupon, through the MTS machine, in tension and recorded the stress-strain data. Data was recorded every .5 seconds. The applied load was executed by the actuator on the lower part of the machine that gripped the bottom tabs. The top of the machine that gripped the specimen, called the crosshead, was stationary and measured the applied load. The recorded data consisted of the applied load, in lbs, and the 4 strain gage readings in μstrain. Three of those reading were from the rosette, while the fourth was from the single gage on the opposite surface of the coupon. The maximum amount of μstrain that could be measured was 20,470. Please see Figure 4.1 and Appendix E. Appendix E contains pictures of the machines used to conduct the coupon tests.

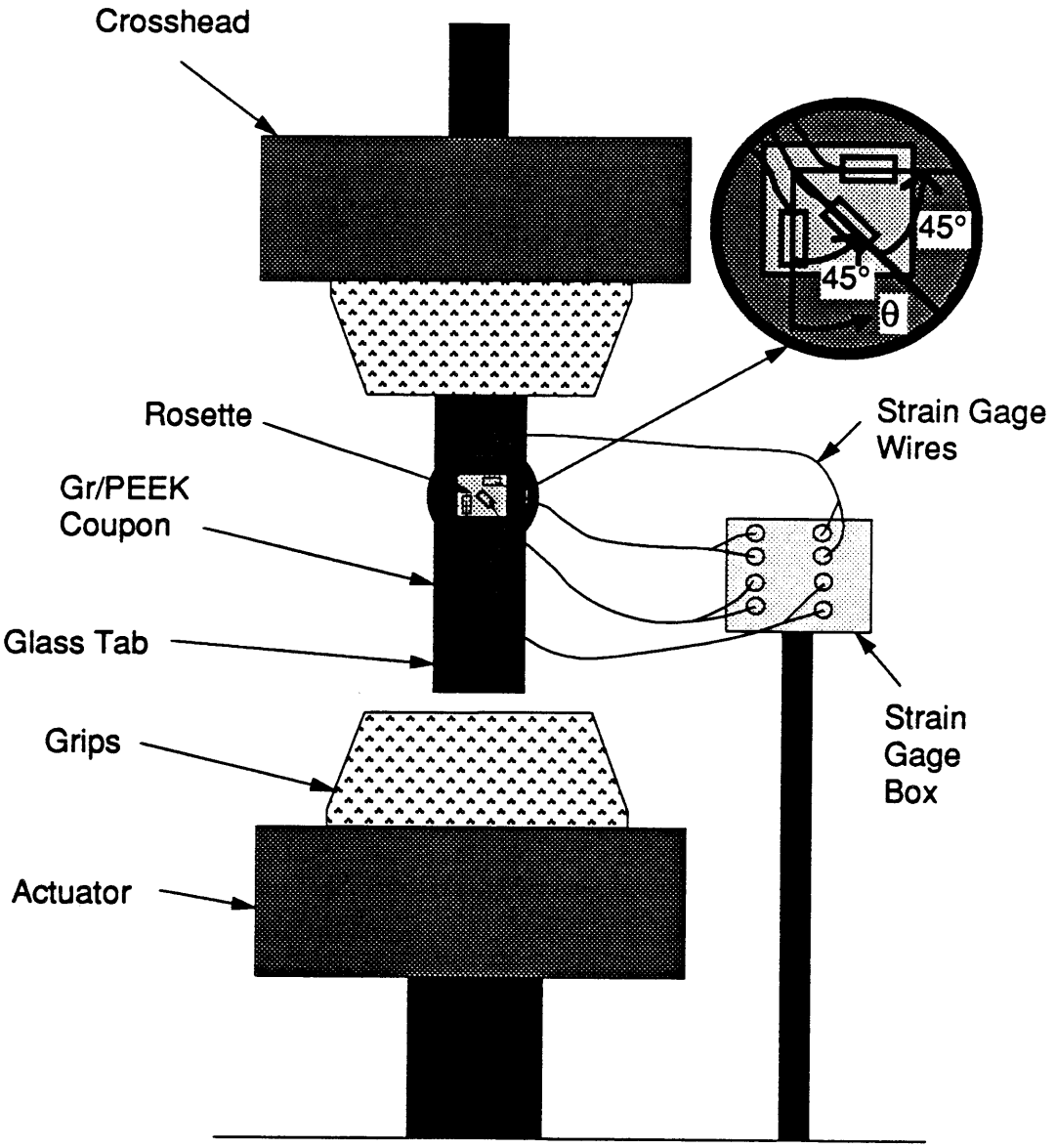

Figure 4.1 MTS testing machine.

4.3 Right Angle Bends

Figure 2.13 illustrates a typical bend specimen. The right angle bends were tested by bracing them against a strong back, a structure that consisted of parallel I beams. Please see Figure 4.2 and Appendix F for an illustration and picture of the bend test. Bolts were inserted into the two holes in the bend and through three metal spacers. One spacer had dimensions 64 mm (2.5 in) by 127 mm (5 in) by 13 mm (.5 in). The other two spacers had dimensions 64 mm (2.5 in) by 127 mm (5 in) by 5 mm (.19 in). The spacers were used so that the bolts would not pultrude into the strongback, thereby insuring the ability to tighten the bolts. The bolts went through the spacing between the I beams in the strongback and into the holes of an iron plate. Tightening the bolts braced the bend specimen to the strongback.

A piano wire was inserted into the aluminum slit on the upper, outer surface of the bend's long side. The length of the piano wire was 305 mm (12 in) folded over. An aluminum rod with a plate was attached to the piano wire. The piano wire, aluminum rod and weights applied the end load.

Initially, the weight of the aluminum rod was determined. Weights were placed on the rod's plate in intervals of 4.448 N (1 lb) up to 44.48 N (10 lbs). The displacement was measured after each 4.448 N (1 lb) increment through a dial gage. The dial gage had an accuracy of .0254 mm (.001 in) and was magnetically braced to the strongback during testing. The dial was put in compression so that it could measure the displacement as the specimen deflected downward due to the weight. An initial dial reading was recorded before any weight was applied to the bend.

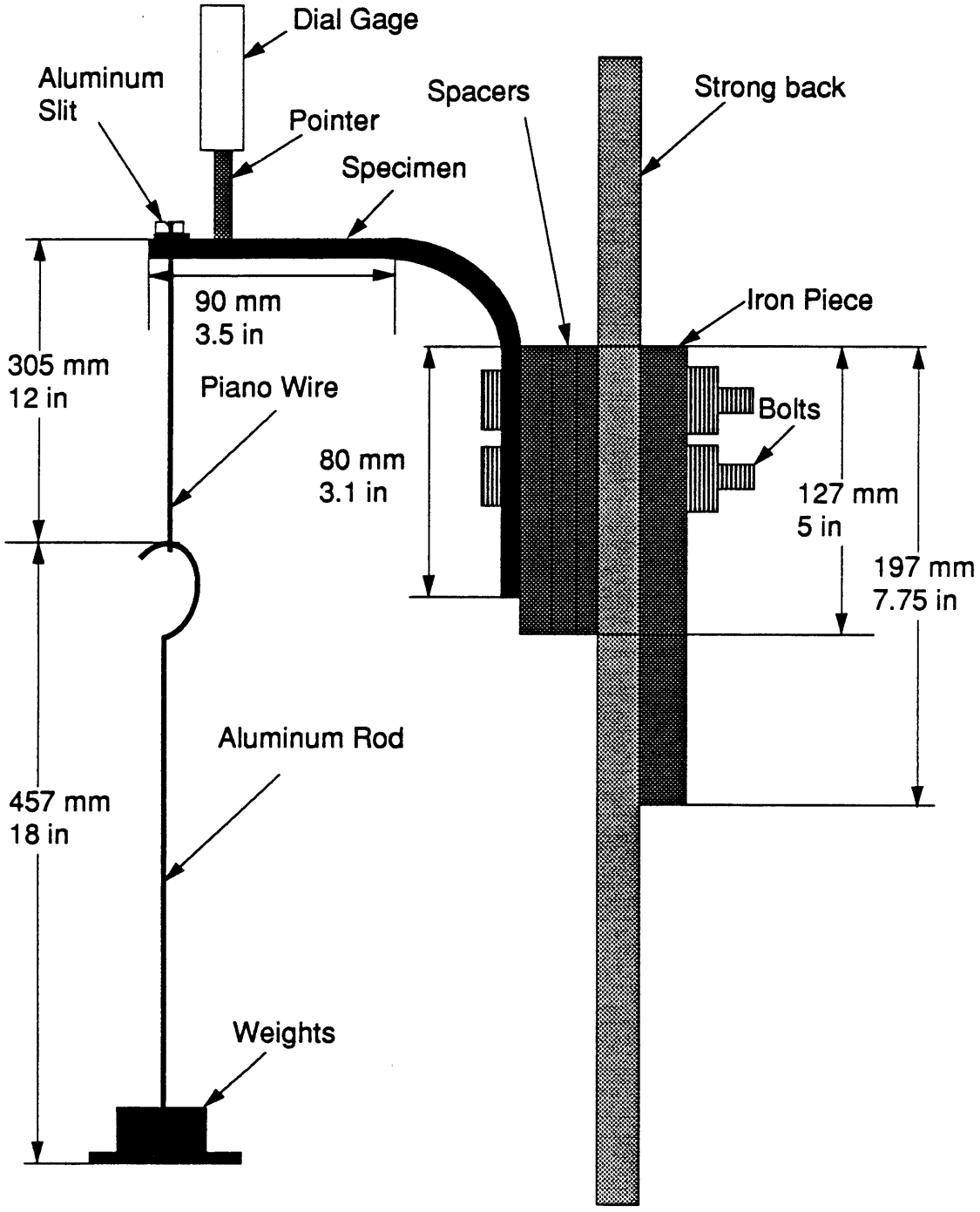

Figure 4.2 Test setup for bend specimens.

Chapter 5
RESULTS

The results are divided into four sections dealing with the four different processes employed to produce the four types of specimens.

5.1 Small Plates

5.1.1 Visual Observation

Plates P100/0/0-1, P100/0/0-4, P100/0/0-5 and P100/0/0-6 were similar in appearance. The bottom side, resting against the caul plate, was perfectly flat, while the other side, resting against the vacuum bag, had small but noticeable waviness. Visual observation of the surface was limited due to the Kapton that coated the bottom and top surfaces after processing. Despite the presence of the Kapton, the appearance of the small plates projected good consolidation due to the solid feel when handling them and the blending of the plies at the edge.

P100/0/0-2 was different than the other small plates, because the heat significantly burned the Kapton, causing a vacuum leak. Dense wrinkling occurred near the corner where the vacuum bag rended. Most of the Kapton that would normally cover the specimen was burned off within the wrinkled area. The wrinkling caused large differences in thickness of the specimen.

P100/0/0-7 was similar to plates P100/0/0-1, P100/0/0-4, P100/0/0-5 and P100/0/0-6, except that F-57 was used to remove the Kapton after processing. No surface burning was present. Once again, the surface against the caul

plate was flat, while the other surface against the vacuum bag had small but noticeable waviness. Good consolidation was apparent due to the solid feel and blending of the plies at the edges.

Please refer to Appendix B for pictures of the small plates. Specimen P100/0/0-3 was used for stiff diaphragm forming.

5.1.2 Microscopic Evaluation of Edges

A piece of each small plate was cut, 6.35 mm (.25 in) from an edge in the fiber direction, and evaluated under a microscope. For a picture of a typical edge, please see Appendix G. The edges of all the small plates, P100/0/0-1 thru P100/0/0-2 and P100/0/0-4 thru P100/0/0-7, were similar. The edges were characterized by a light, continuous silver color. No voids or delaminations were apparent.

5.1.3 Consolidation Distance

Consolidation distance was defined by the distance that the plies blended together during consolidation. This distance was a good indication of the part quality. If too much consolidation occurs, resin poor areas may develop. If too little consolidation is present, the bond between the plies may be poor. A good consolidation distance is approximately 63% of the thickness before manufacturing [3]. The ply thickness before consolidation was .254 mm (.01 in). Table 5.1 lists the specimen, the thickness before processing, the thickness after processing, and the consolidation distance as a percentage.

Table 5.1 Consolidation distance for the small plates.

Specimen	Average Initial Thickness (mm)	Average Final Thickness (mm)	Consolidation Distance (%)
P100/0/0-1	2.54	1.43	43.8
P100/0/0-2	2.54	1.74	31.6
P100/0/0-4	2.54	1.38	45.8
P100/0/0-5	2.54	1.37	46.1
P100/0/0-6	2.54	1.37	45.9
P100/0/0-7	2.54	1.31	48.4
		Average	43.6
		Coefficient of Variation	6.2%

The large thickness for specimen P100/0/0-2 was due to wrinkling which was caused by a loss in vacuum.

5.2 Tensile Coupons

5.2.1 Visual Observation

As a reminder, the tensile coupons were cut from and are equivalent to the large plates. The tensile coupons had several visible manufacturing flaws. The most visible flaw was minor surface burning, resulting in a resin poor surface. The surface burning was minor enough to warrant testing, but large enough to record. Resin poor surfaces were apparent in

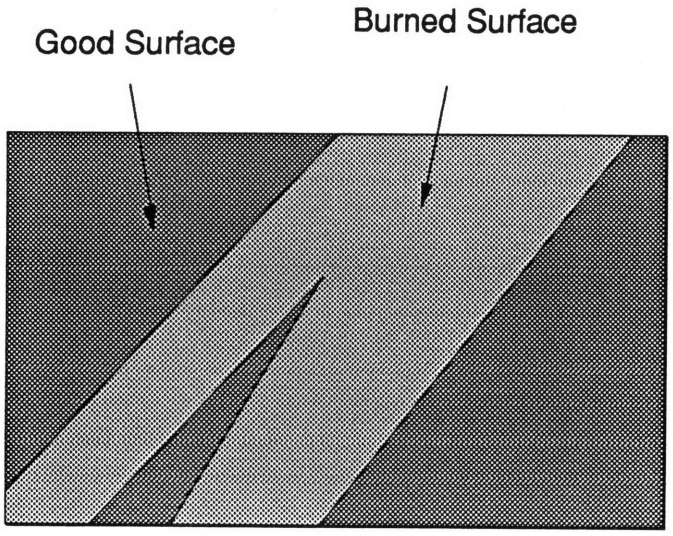

Figure 5.1 Illustration of burned surface on T30/60/10-15.

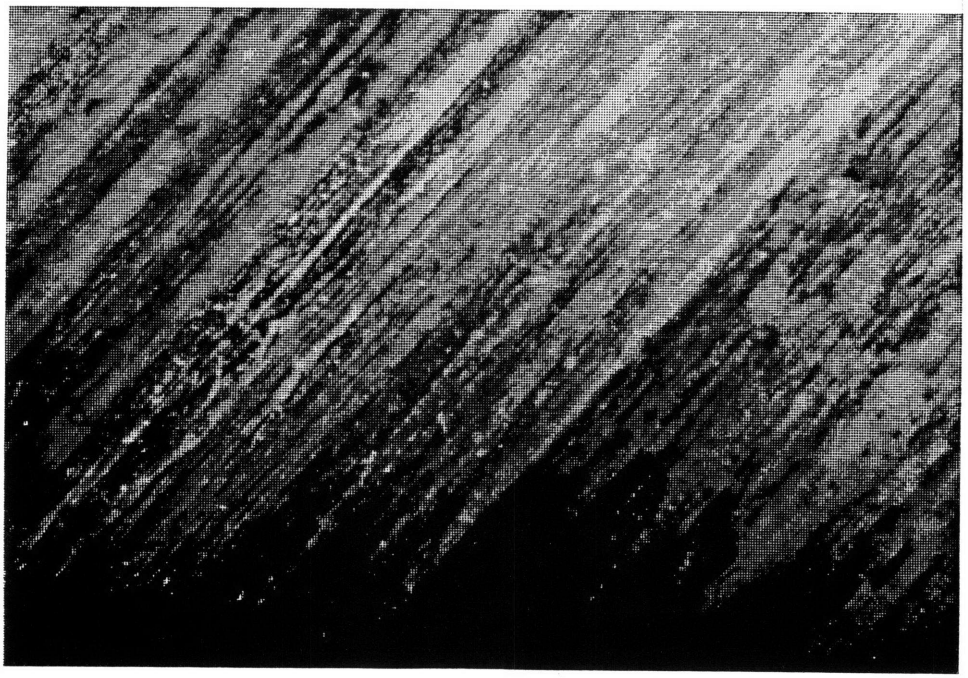

Figure J2 Picture of resin poor surface (burning) of T30/60/10-15.

tensile coupons T100/0/0-10, T100/0/0-11, T100/0/0-12, T30/60/10-13, T30/60/10-14, T30/60/10-15 and T50/40/10-17. Appendix C has pictures of the tensile coupons after manufacturing (before mechanical testing), while Appendix J has pictures of a good surface and a resin poor surface. Figure 5.1 illustrates the picture in Figure J2.

For all the coupons, the bottom surface was more smooth and flat as compared to the top surface. The bottom surface pressed against the caul plate during consolidation while the top surface pressed against the thin steel shims. Although the bottom surface was similar in all the specimens, the top surface varied in quality. A good surface was smooth without resin poor areas, a glossy black color, flat and with a "soft touch". The 0/0/100 coupons had the best surface quality, followed by the 0/100/0, 30/60/10 and 50/40/10 coupons. The 100/0/0 coupons had the worst top surface quality. The 100/0/0 coupons' top surface contained some dense waves and was a flat black color with a rough, hard touch. The dense waves were not similar to the slight waviness in the top surface of the small plates. Most of the coupons, except the 0/0/100's, had initial bending along the length. This was probably caused by the bent caul plate during processing. All the coupons appeared to possess good consolidation due to the solid feel when handling them.

5.2.2 Microscopic Evaluation of Edges

The edges of the tensile coupons were observed with the aid of a microscope. Appendix I has pictures of the edges of each type of coupon. The most prominent feature was the different shade of gray between the 0° plies and the ±45° and 90° plies. The ±45° and 90° plies were very similar in

color. Figures I1 and I2, pictures of specimen T0/100/0-2 and T0/0/100-6, reveal the particular shade of gray for the ±45° and 90° plies, while Figure I3 reveals the shade of gray associated with the 0° plies. The color of the ±45° and 90° ply edges was a light, continuous shade of gray, while the color of the 0° ply edges was a dark, non-continuous shade of gray. Figures I4-I6, pictures of the edges of specimens T30/60/10-15, T50/40/10-18, and T70/20/10-19, expose the difference in colors between the 0° plies and the 45° and 90° plies. Figures 5.2-5.4 illustrate these pictures.

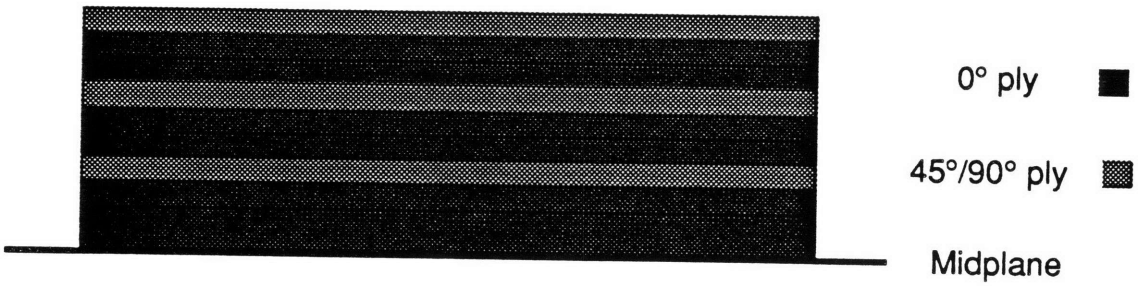

Figure 5.2 Illustration of T70/20/10-19 edge.

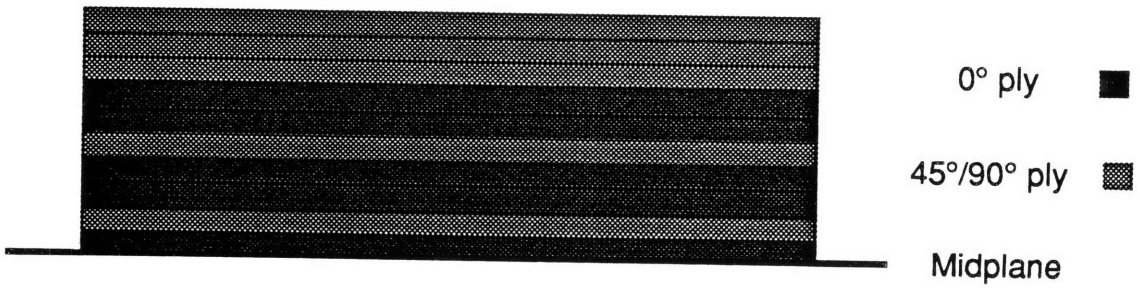

Figure 5.3 Illustration of T50/40/10-18 edge.

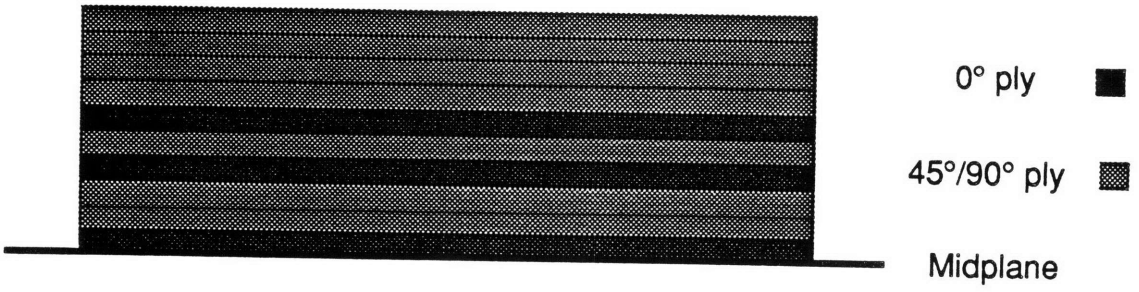

Figure 5.4 Illustration of T30/60/10-15 edge.

Indents, similar in appearance to pressing a ball point pen into cardboard, were present in the edges of some coupons. Figure J3 is a picture revealing the indents and Figure 5.5 illustrates the picture.

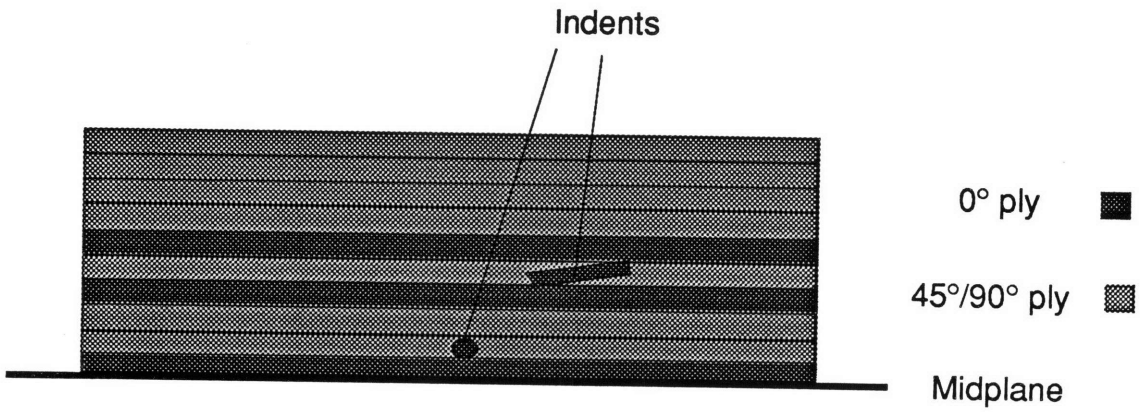

Figure 5.5 Illustration of indents within edge T30/60/10-13.

The size of the indents was usually a ply thickness or less and a length of approximately 3 ply thicknesses or less. The depth of the indents was unknown. The 100/0/0 and 70/20/10 coupons had no indents on the edges. The 50/40/10, 30/60/10, and 0/100/0 coupons had an average of 2, 2, and 4 indents on their edges, respectively. The 0/0/100 coupons had no indents on the edges except for one specimen, which had only one indent.

Other than the indents, the coupons appeared to have good consolidation as observed under a microscope. The plies were bonded together with no observable delaminations.

5.2.3 Consolidation Distance

The consolidation distance for the tensile coupons is listed in Table

5.2. The thickness of each coupon was calculated by averaging the six thickness measurements described in the manufacturing section. The consolidation distance was found by measuring the thickness of a pre-consolidated ply, multiplying by the appropriate number of plies for the particular specimen, and then comparing to the measured specimen thickness after processing. The initial ply thickness was .254 mm (.01 in). The reduction in width due to consolidation should give an indication of ply to ply bonding quality and the amount of autoclave pressure that is optimal for Gr/PEEK parts.

5.2.4 Mechanical Testing

The results of the coupon tests are tabulated in Table 5.3-5.8. Table 5.9 lists the load, stress, and strain for the two endpoints which contained the interval that determined the stiffness for each coupon. Graphs of stress vs. strain for the coupons can be found in Appendix H. Appendix C contains pictures of the coupons before and after testing.

The stiffness was calculated based on strains in the principal directions. The initial offset for each strain gage was set to zero. The shear strain, ε_{AC}, corresponding to the axes of the horizontal and vertical gages on the rosette was calculated using equation 5.2.1 [18].

$$\varepsilon_B = \frac{\varepsilon_A + \varepsilon_C}{2} + \varepsilon_{AC} \tag{5.2.1}$$

Please see Figures 3.1 and 4.1. This shear strain was used to find θ_P, the amount of rotation necessary for the rosette axes to be the principal axes, i.e. the axes where shear strain equals zero using equation 5.2.2 [18].

$$\varepsilon_{12} = \frac{\varepsilon_C - \varepsilon_A}{2} \sin 2\theta + \varepsilon_{AC} \cos 2\theta \tag{5.2.2}$$

Table 5.2 Consolidation distance for the tensile coupons.

Specimen	Average Initial Thickness (mm)	Average Final Thickness (mm)	Consolidation Distance (%)
T100/0/0-9	5.08	2.88	43.3
T100/0/0-10	5.08	2.94	42.2
T100/0/0-11	5.08	2.82	44.4
T100/0/0-12	5.08	2.78	45.3
T70/20/10-19	5.08	2.68	47.2
T70/20/10-20	5.08	2.73	46.3
T50/40/10-17	5.08	2.95	42.0
T50/40/10-18	5.08	2.87	43.4
T30/60/10-13	5.08	2.87	43.5
T30/60/10-14	5.08	2.85	43.8
T30/60/10-15	5.08	2.82	44.5
T30/60/10-16	5.08	2.80	44.9
T0/100/0-1	5.08	2.72	46.5
T0/100/0-2	5.08	2.86	43.7
T0/100/0-3	5.08	2.79	45.1
T0/0/100-4	2.54	1.35	46.7
T0/0/100-5	2.54	1.35	46.8
T0/0/100-6	2.54	1.40	45.0
T0/0/100-7	2.54	1.46	42.5
T0/0/100-8	2.54	1.36	46.3
		Average	44.7%
		Coefficient of Variation	3.6%

Rearranging equation 5.2.2 to solve for θ_P yields the following expression from which θ_P can be easily calculated.

$$\tan 2\theta_P = \frac{2\varepsilon_{AC}}{\varepsilon_A - \varepsilon_C} \tag{5.2.3}$$

Substituting $\theta=\theta_P$, the calculated shear strain in the rosette axis system, ε_{AC}, and the longitudinal and transverse strain readings from the rosette into equations 5.2.4 and 5.2.5, the principal strains, ε_{11} and ε_{22}, were determined.

$$\varepsilon_{11} = \frac{\varepsilon_A + \varepsilon_C}{2} + \frac{\varepsilon_A - \varepsilon_C}{2}\cos 2\theta_P + \varepsilon_{AC}\sin 2\theta_P \tag{5.2.4}$$

$$\varepsilon_{22} = \frac{\varepsilon_A + \varepsilon_C}{2} - \frac{\varepsilon_A - \varepsilon_C}{2}\cos 2\theta_P - \varepsilon_{AC}\sin 2\theta_P \tag{5.2.5}$$

For an ideal layup, testing procedure and strain gage application, θ_P should be zero for the stacking sequences used. Transforming the strains into principal strains eliminates the error in the application of the rosette and helps to make the coupon test more precise. Even though the use of the rosette did not eliminate the error in layup and the placement of the coupon in the MTS machine, it was a small step for greater precision in the mechanical testing. θ_P is listed in Tables 5.3-5.8 to give an idea of the "error" in the layup, testing procedure and rosette application for the tensile coupons. θ_P is listed as the average of the θ_P for the 30th and 70th data point. θ_P could vary by a few degrees from one data point to the next. The stiffness for each coupon was done by a linear curve fit between the 30th

Table 5.3 Results of mechanical tests for 100/0/0 coupons.

Specimen	Stiffness	Linear Curve Fit "Goodness"	Failure		θ_P
	E_{11} (GPa)	R	Stress (MPa)	μStrain	degrees
T100/0/0-9	130	.999	------	------	2
T100/0/0-10	139	.999	------	------	7
T100/0/0-11	123	.999	------	------	3
T100/0/0-12	125	.999	------	------	-7
Average	129	------	------	------	1
Coefficient of Variation	5.5%	------	------	------	------

Table 5.4 Results of mechanical tests for 70/20/10 coupons.

Specimen	Stiffness	Linear Curve Fit "Goodness"	Failure		θ_P
	E_{11} (GPa)	R	Stress (MPa)	μStrain	degrees
T70/20/10-19	107	.999	1656	14530	0
T70/20/10-20	103	1.000	1582	14401	0
Average	105	------	1619	14466	0
Coefficient of Variation	2.7%	------	3.2%	0.6%	0

Table 5.5 Results of mechanical tests for 50/40/10 coupons.

Specimen	Stiffness	Linear Curve Fit "Goodness"	Failure		θ_P
	E_{11} (GPa)	R	Stress (MPa)	μStrain	degrees
T50/40/10-19	70	.999	1033	14180	-1
T50/40/10-20	74	.999	1126	14264	-4
Average	72	------	1080	14222	-3
Coefficient of Variation	3.9%	------	6.1%	0.4%	------

Table 5.6 Results of mechanical tests for 30/60/10 coupons.

Specimen	Stiffness	Linear Curve Fit "Goodness"	Failure		θ_P
	E_{11} (GPa)	R	Stress (MPa)	μStrain	degrees
T30/60/10-13	51	.999	773	10274	-3
T30/60/10-14	53	.999	752	13850	1
T30/60/10-15	54	.999	815	15271	0
T30/60/10-16	53	.999	805	14601	-1
Average	53	------	786	13499	-1
Coefficient of Variation	2.4%	------	3.7%	16.5%	------

Table 5.7 Results of mechanical tests for 0/100/0 coupons.

Specimen	Stiffness	Linear Curve Fit "Goodness"	Failure		θ_P
	E_{11} (GPa)	R	Stress (MPa)	μStrain	degrees
T0/100/0-1	18	.999	367	------	-2
T0/100/0-2	17	.997	264	------	1
T0/100/0-3	18	.997	296	------	-3
Average	18	------	309	------	-1
Coefficient of Variation	3.3%	------	17.1%	------	------

Table 5.8 Results of mechanical tests for 0/0/100 coupons.

Specimen	Stiffness	Linear Curve Fit "Goodness"	Failure		θ_P
	E_{11} (GPa)	R	Stress (MPa)	μStrain	degrees
T0/0/100-4	------	------	------	------	------
T0/0/100-5	12	.992	78	7573	1
T0/60/10-6	10	.999	44	4138	0
T0/60/10-7	9	.997	38	3859	2
T0/0/100-8	10	.998	62	6390	-2
Average	10	------	56	5490	0
Coefficient of Variation	12.3%	------	32.7%	32.6%	------

Table 5.9 Beginning and ending data used to determine the stiffness of each tensile coupon.

Specimen	30th Data Point			70th Data Point		
	Load (kN)	Stress (MPa)	μStrain	Load (kN)	Stress (MPa)	μStrain
T100/0/0-9	10	56	361	22	130	921
T100/0/0-10	10	59	349	22	134	912
T100/0/0-11	10	61	491	22	140	1135
T100/0/0-12	10	61	463	22	142	1112
T70/20/10-19	10	69	590	22	162	1440
T70/20/10-20	10	74	640	22	169	1560
T50/40/10-17	10	59	750	22	136	1870
T50/40/10-18	10	65	814	22	152	1981
T30/60/10-16	5	28	510	11	68	1250
T30/60/10-15	5	29	510	11	68	1230
T30/60/10-14	5	29	490	11	67	1200
T30/60/10-13	2	13	261	5	30	580
T0/100/0-1	2	13	650	4	31	1622
T0/100/0-2	2	11	570	4	25	1411
T0/100/0-3	2	11	583	4	26	1425
T0/0/100-5	1	7	310	2	19	1272
T0/0/100-6	1	15	1000	2	33	2925
T0/0/100-7	1	12	1001	2	29	2885
T0/0/100-8	1	13	1163	2	30	2971

and 70th data point for each test. Each test had a nominal 600 data points; and the chosen interval was in the linear region for all the tests. Table 5.9 lists the endpoints of the intervals. Tables 5.3-5.8 list the value of "R", the "goodness" of the curve fit, for an idea of the linearity of the interval that determined the stiffness. A perfect linear relationship was R equal to 1. The graphs in Appendix H contain stress vs. the principal longitudinal and transverse strains transformed from the rosette strain readings, and the non-principal longitudinal strain reading from the single strain gage on the opposite surface of the coupon. For the graphs in Appendix H, ε_{11} and ε_{22} are the principal strains calculated from the rosettes, while ε_{11}-2 is the strain reading from the single strain gage.

From Tables 5.3-5.8, the ply mechanical properties for Gr/PEEK can be determined by using the method outlined in Chapter 3 and are listed in Table 5.10.

Table 5.10 Ply constants for Gr/PEEK.

Statistic	E_L (GPa)	E_T (GPa)	ν_{LT}	G_{LT} (GPa)
Average	129	10	.35	5
Coefficient of Variation	5.5%	12.3%	34.0%	15.3%

Table 5.11 lists the ply mechanical properties of Gr/PEEK cited in other references.

Table 5.11 Gr/PEEK ply constants from other references.

Reference	E_L (GPa)	E_T (GPa)	ν_{LT}	G_{LT} (GPa)
Present	129	10	.35	5
Ref [17]	142	9.6	.25	6
Ref [9]	131	9.54	------	------
Ref [6]	134-141	8.90-10.35	------	5.1-6.3
Ref [5]	134	9.45	.28	5.4

Table 5.12 [E] Matrix for the laminate families.

Laminate	E_{1111} (GPa)	E_{2222} (GPa)	E_{1122} (GPa)	E_{1212} (GPa)
100/0/0	130.2	10.1	3.5	5.0
70/20/10	100.5	28.5	9.20	10.7
50/40/10	82.9	34.8	14.9	16.3
30/60/10	65.2	41.2	20.5	22.0
0/100/0	41.9	41.9	31.9	33.3
0/0/100	10.1	130.2	3.5	5.0

Table 5.13 [S] Matrix for the laminate families.

Laminate	S_{1111} (1/GPa)	S_{2222} (1/GPa)	S_{1122} (1/GPa)	S_{1212} (1/GPa)
100/0/0	.0078	.1000	-.0027	.2000
70/20/10	.0102	.0362	-.0033	.0938
50/40/10	.0131	.0311	-.0056	.0613
30/60/10	.0182	.0288	-.0091	.0455
0/100/0	.0568	.0568	-.0432	.0300
0/0/100	.1000	.0078	-.0027	.2000

The stiffness and compliance matrices, [E] and [S], can be calculated for each laminate family using the ply constants and the procedure outlined in Chapter 3. Table 5.12 and 5.13 list the [E] and [S] matrices.

From the S_{1111} term, the strain can be calculated from an applied, or known, stress. The calculations for the theoretical stress strain curves were done with the stress known instead of the strain known, because the testing was done with an applied, known stress and a measured strain. The predictability was assessed by plotting the theoretical, or predicted, stiffnesses of the 70/20/10, 50/40/10 and 30/60/10 coupons to their corresponding predicted stiffnesses. Please see Figures 5.6-5.8. 100/0/0, 0/100/0 and 0/0/100 coupons were not plotted, since they were used to derive the S_{1111} term. The comparison of theoretical to experimental stiffnesses is listed in Table 5.14.

Table 5.14 Comparison of analytical to experimental stiffness for 70/20/10, 50/40/10 and 30/60/10 tensile coupons.

Coupon Type	Theoretical Stiffness $1/S_{1111}$ (GPa)	Experimental Stiffness E_{11} (GPa)	% Difference
70/20/10	98	105	-7.1
50/40/10	76	72	5.2
30/60/10	55	53	3.6

Some phenomena occurred during testing that should be noted. Failure of the 0/0/100 laminates was characterized by multiple, clean breaks across the width of the specimens. The cooling rate of the coupons

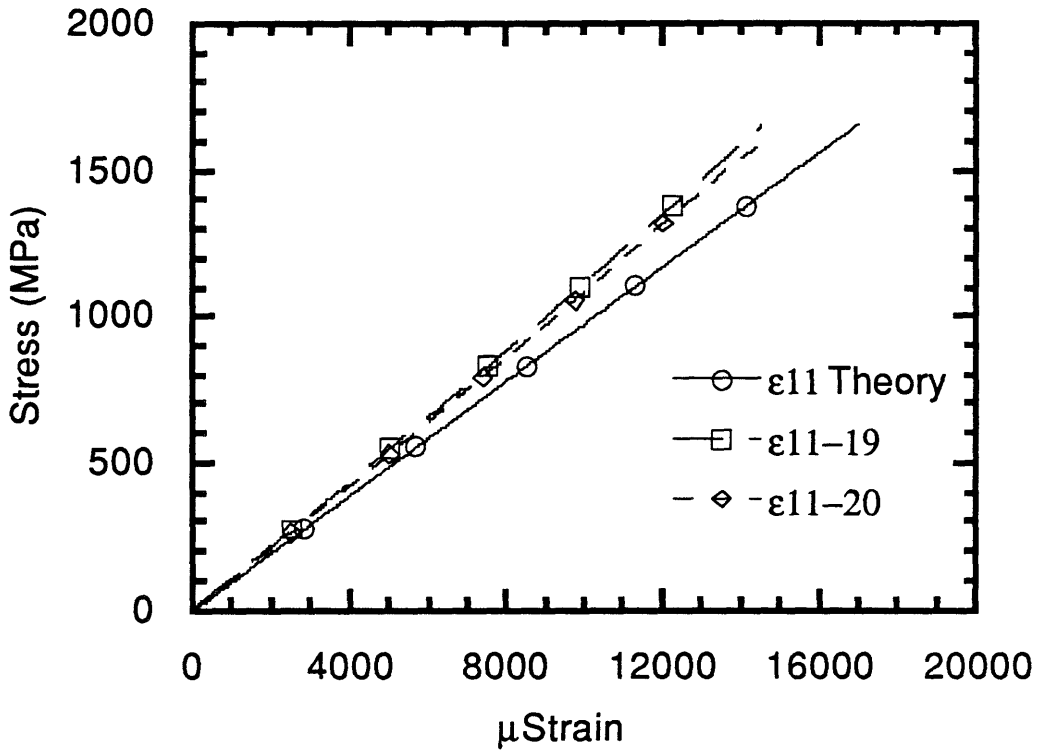

Figure 5.6 Comparison of analytical and experimental strain to failure for the T70/20/10-19 and T70/20/10-20 coupons using Classical Laminated Plate Theory. The experimental strains are principal strains. The symbols only mark the corresponding line and are not data points or calculations.

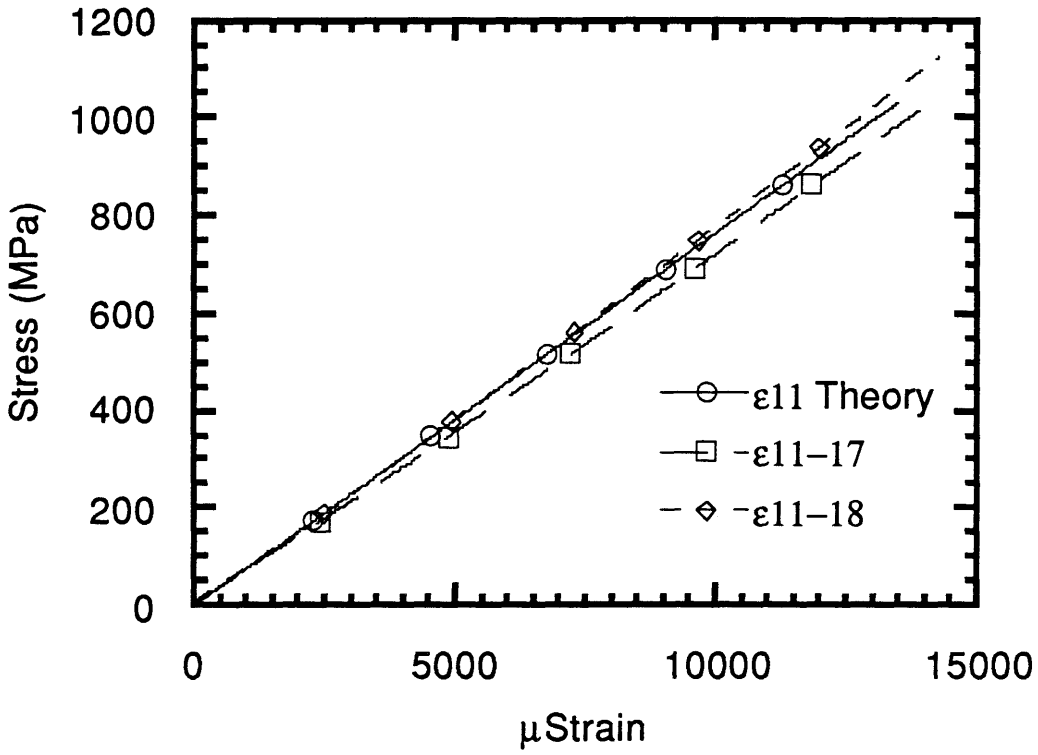

Figure 5.7 Comparison of analytical and experimental strain to failure for the T50/40/10-17 and T50/40/10-18 coupons using Classical Laminated Plate Theory. The experimental strains are principal strains. The symbols only mark the corresponding line and are not data points or calculations.

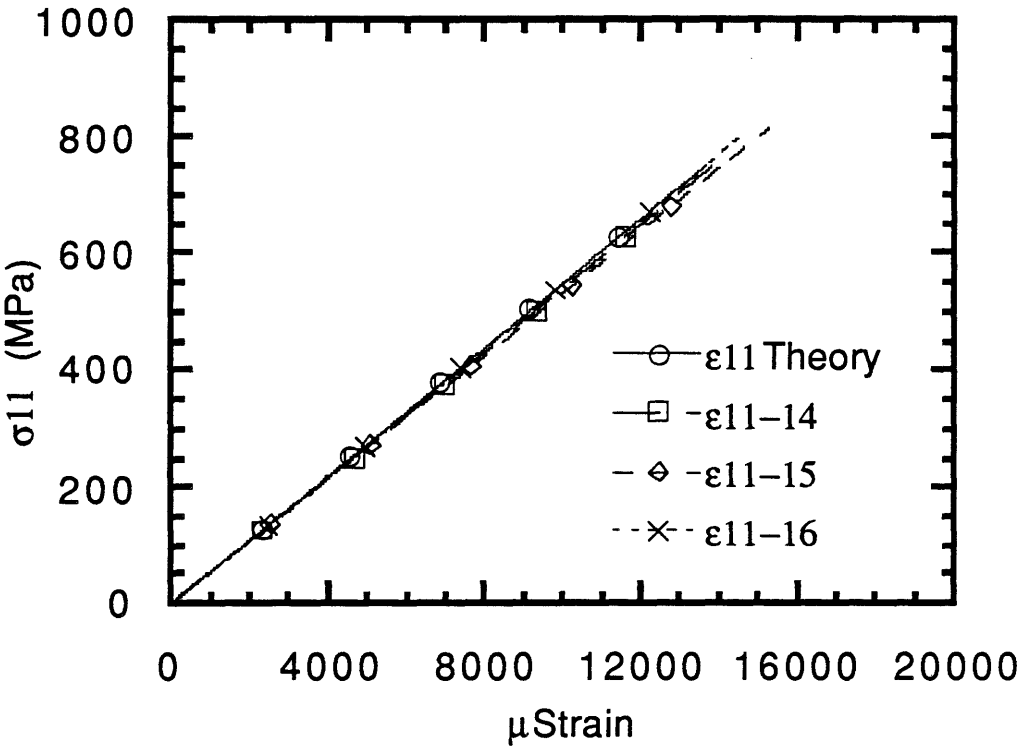

Figure 5.8 Comparison of analytical and experimental strain to failure for the T30/60/10-14, T30/60/10-15, and T30/60/10-16 coupons using Classical Laminated Plate Theory. The experimental strains are principal strains. The symbols only mark the corresponding line and are not data points or calculations.

was nominally 3°C/min (5°F/min), creating a high crystalline matrix of approximately 40% by weight [5]. The crystalline nature of the matrix might be the cause of the linear stress-strain curve for the 0/0/100 coupon tests which were dominated by the thermoplastic matrix PEEK. One would expect some region of non-linearity in a tensile test that was dominated by a thermoplastic matrix. The failure stress varied significantly from one tensile coupon to another.

The 100/0/0 laminates failed because of adhesive shear failure. The adhesive bonded the glass tabs to the Gr/PEEK coupon. Multiple splitting occurred parallel to the fibers after adhesive shear failure; and no splitting occurred transverse to the fibers. As a result, failure stress and strain for the 100/0/0 tensile coupons were not obtained. Table 5.15 lists the gripping pressure and the load applied by the machine when the FM-123 adhesive failed in shear.

The 0/100/0 coupons were significantly plastic. The 0/100/0 behavior possessed non-linearity in contrast to all the other laminates. They deformed similar to a rubber band being stretched. There was visible thinning of these coupons after failure. Table 5.16 lists the percent reduction in width at the midsection due to testing for the 0/100/0 specimens. The strain gage could not read the large strains near failure.

From inspection of the graphs in Appendix H, the longitudinal rosette strain gage and the single gage sometimes differed from one another. Even though the single gage was not in the principal axis system, the difference between the two gages was large enough to create the possibility of bending-stretching coupling. Small errors in layup would be the most likely cause if bending-stretching coupling was present.

Table 5.15 Shear failure of FM-123 adhesive.

Specimen	Gripping Pressure (MPa)	Failure Load (kN)
T100/0/0-9	6.9	240
T100/0/0-10	6.9	231
T100/0/0-11	10.3	265
T100/0/0-12	10.3	281

Table 5.16 Reduction of width during testing of 0/100/0 tensile coupons at the midsection.

Specimen	Initial Width (mm)	Final Width (mm)	% Change
0/100/0-1	52.30	42.64	18.47
0/100/0-2	60.55	53.11	12.29
0/100/0-3	58.83	49.93	15.13

5.3 Right Angle Bends from Layup in Part Form

5.3.1 Visual Observation

Appendix D contains a picture of each bend specimen. Despite the presence of Kapton on both the inner and outer surfaces of the right angle bends, two phenomena were apparent. The top surface, which pressed against the Kapton vacuum bag, had a slight waviness similar to the small plates. The bottom surface, which pressed against the iron bend, was completely flat. The second phenomena was the presence of a wrinkle that

extended through the entire width of the bend specimen at the 90° curvature. This wrinkle was not present before processing. As consolidation occurred, the vacuum bag pressed the specimen, reducing its length. The extra length was probably absorbed within the bend, causing the wrinkle. The nominal dimensions of the wrinkle were 5 mm at the base, 2 mm from the top edge of the surface of the bend, and extending along the width. The wrinkle typically contained or affected 8 of the 10 plies. Spaces between the plies within the wrinkle were visible without the use of a microscope. Please see Appendix K for a picture of the wrinkle. The edges surrounding the two holes that were drilled in each specimen by the diamond drill had no visible delaminations or irregularities.

5.3.2 Microscopic Evaluation of Edges

Appendix K contains pictures of a typical bend edge and wrinkle. From picture K2, the wrinkle is large as compared to the thickness of the specimen. A significant number of plies were affected by the wrinkle, including large delaminations. The wrinkle occurred in all four bend specimens. Other than the wrinkle, the bend edges contained no delaminations or irregularities.

5.3.3 Consolidation Distance

The thickness before processing is compared to the thickness after processing in Table 5.17. The thickness measurement was obtained by averaging the six thickness measurements described in the manufacturing section for bend specimens. The nominal ply thickness for APC-2 before processing was .254 mm (.01 in). Multiplying the ply thickness by the

appropriate number of plies gave the initial thickness, while the final thickness was measured after manufacturing. The % difference between the initial and final thickness was the consolidation distance. The reduction in thickness due to consolidation should help to reveal the quality of the ply bonding in the laminates and the optimal autoclave pressure during processing.

5.3.4 Mechanical Testing

Figure 5.9 plots end shear stress vs. displacement. The end shear stress was used instead of an end load because each specimen had a different cross-sectional area. Figure 5.10 is a graph of theoretical stiffness and the experimental stiffness. The stiffness varied for each specimen because the theory used post-manufacturing geometrical dimensions. Table 5.18 lists the theoretical and experimental stiffnesses for each bend.

Table 5.17 Consolidation distance for the bend specimens.

Specimen	Average Initial Thickness (mm)	Average Final Thickness (mm)	Consolidation Distance (%)
B100/0/0-1	2.54	1.41	44.7
B100/0/0-2	2.54	1.44	43.5
B100/0/0-3	2.54	1.42	44.2
B100/0/0-4	2.54	1.38	45.8
		Average	44.5%
		Coefficient of Variation	2.2%

Table 5.18 Comparison of theoretical to experimental bend stiffness.

Specimen	K Theory (N/m)	K Experiment (N/m)	% difference
B100/0/0-1	2622	1506	-42.6
B100/0/0-2	2859	2295	-19.7
B100/0/0-3	2230	2933	31.5
B100/0/0-4	2693	3413	26.7
Average w/ B1	2601	2536	-4.1
Average w/o B1	2594	2880	12.8
Coefficient of Variation w/B1	------	32.6%	------
Coefficient of Variation w/o B1	------	19.5%	------

Three observations during testing should be mentioned. After unloading, the specimens did not return to their original zero point. The specimens were permanently deformed by loading into the non-linear region. Table 5.19 lists the results.

Specimen B100/0/0-1 was originally tested in the MTS machine far into the non-linear region; consequently, the results for B100/0/0-1 listed in the tables and graphs come from a pre-deformed specimen and are treated differently than the other initially undeformed specimens. The MTS machine was not used because it could not measure the small loads associated with the bends, i.e. 44 N (10 lbs).

Table 5.19 New zero points after testing as compared to the maximum deflection.

Specimen	Maximum Deflection (mm)	Change in zero point (mm)	% of maximum deflection
B100/0/0-1	37.84	7.93	20.9
B100/0/0-2	25.88	2.72	10.5
B100/0/0-3	17.19	1.61	9.3
B100/0/0-4	16.12	1.93	12.0

The third observation was the difficulty in measuring the displacement. After the weights had stopped movement, the displacement would increase but its rate of increase would decrease over time. A measurement would be made after two to three minutes. The displacement would have stopped or be increasing very slowly at this time. This movement occurred after approximately 22.24 N (5 lbs) was applied; the displacement stopped quickly under 22.24 (N).

5.4 Right Angle Bends from Stiff Diaphragm Forming

Appendix L1 contains a picture of small plate P100/0/0-3 after the single attempt at stiff diaphragm thermoforming. The picture reveals a burned small plate. The heat blanket burned through the Kapton and deformed the plate. In addition, the Kapton could not push against the pre-consolidated plate to form a bend since it was rended. Originally, P100/0/0-3 looked similar to small plates P100/0/0-1, P100/0/0-4, P100/0/0-5, and P100/0/0-6 in Appendix B.

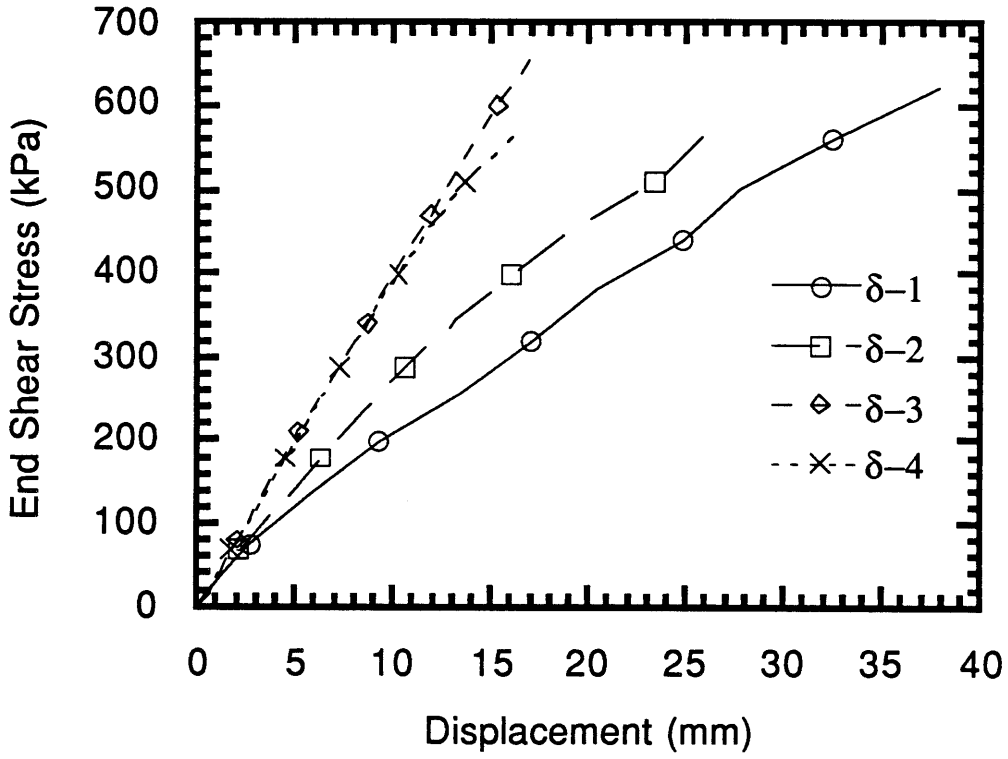

Figure 5.9 Graph of the end shear stress due to an end load vs. displacement for bend specimens B100/0/0-1, B100/0/0-2, B100/0/0-3, and B100/0/0-4.

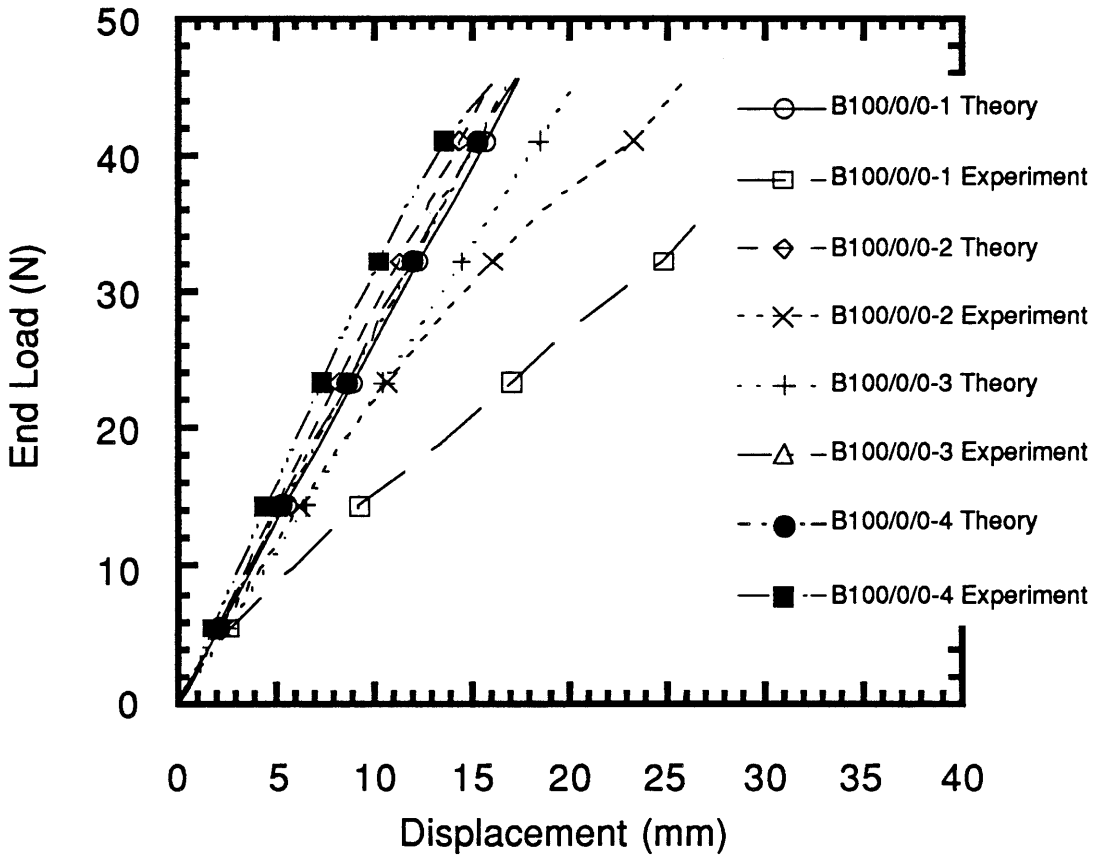

Figure 5.10 Load vs. displacement illustrating comparison of analytical and experimental stiffness for bend specimens B100/0/0-1, B100/0/0-2, B100/0/0-3, and B100/0/0-4.

Chapter 6
DISCUSSION

6.1 Small Plates

6.1.1 Quality

The quality of the small plates was the best of the four types of specimens manufactured. Even though the first 6 plates, P100/0/0-1, P100/0/0-2, P100/0/0-3, P100/0/0-4, P100/0/0-5, and P100/0/0-6, had Kapton adhering to both surfaces, the application of F-57 on P100/0/0-7 removed the Kapton. P100/0/0-7 showed no sign of burning or lack of consolidation, despite the fact that the temperature gradient ΔT was larger than the processing window of 360°C (680°F) to 427°C (800°F). At the same time, P100/0/0-2 was significantly burned at one of its corners. The Kapton had burned off and a dense winkling occurred where the bag had rended. Although the existence of a processing window was unknown at this time, in retrospect, it was unlikely that plate P100/0/0-2 was processed in this window. Considering the results of P100/0/0-7 and P100/0/0-2, the processing window was determined by probability, not absolutes. If a specimen was consolidated outside the processing window, a high probability existed that it would burn or not consolidate properly. Despite the high probability, sometimes a specimen consolidated outside the processing window did not possess burning or a lack of consolidation. Minor surface burning on the other plates, P100/0/0-1,3,4,5,6, could not be determined due to the presence of the Kapton. Although the top surface had a little waviness, technology developed in the manufacturing of the

large plates could solve the problem. The use of the metal shim eliminated the slight waviness in the large plates. The low consolidation distance, 44% as opposed to 63%, could probably be corrected by increasing the autoclave pressure to 1.2 MPa (175 psi) from .34 MPa (50 psi). A microscopic evaluation revealed no problems with the edges. Overall, the small plates had good quality; and the minor quality problems they did have could be corrected.

6.2 Large Plates (Tensile Coupons)

6.2.1 Quality

The quality of the tensile coupons was poor. Surface burning was apparent in 7 of the 20 specimens. Surface burning or lack of consolidation caused a rejection of 41% of the consolidated Gr/PEEK. The high temperature gradient, which did not fall in the processing window just as in the small plates, affected the large plates significantly more than the small plates. In other words, the consequences of not keeping the in-plane temperatures of the large plates within the processing window were very apparent, as opposed to the case of the small plates. The processing window was between a maximum temperature of 427°C (800°F), the point at which the probability of the Kapton and Gr/PEEK burning was high, and the minimum temperature of 360°C (680°F), the point at which the probability of not consolidating the Gr/PEEK plies was high.

In addition, there was initial bending before testing, probably due to the bent caul plate during processing. The top surface varied in quality from coupon to coupon. In some coupons, significant waviness resulted,

but not of the same type as in the small plates. The edges of some non-unidirectional laminates had indents within the edges, although the majority of the edge surface area for all the coupons appeared properly consolidated. These indents indicated a possibility of a high void content within the matrix. Once again, the consolidation distance was approximately 43%, which was lower than the expected value of 63%. This was not a significant problem, since the autoclave pressure can be adjusted higher than 50 psi (345 kPa). The slight waviness of the top surface was eliminated by the steel shims. There seems to be a correlation between the amount of waviness and the bending stiffness of the material that pushes against the surface of the composite during processing. The bottom surfaces of all the specimens, including the small plates, the large plates and the bends, had good bottom surfaces. The shims, which had more bending stiffness than the Kapton but less than the caul plate, produced more level top surfaces than the small plates, but less level top surfaces than the bottom surfaces which pressed against the caul plate. No Kapton was present on the surfaces due to the use of several coats of F-57 on both surfaces of the large plates during processing.

In general, the quality of the large plates was poor, because the problems could not be corrected easily.

6.2.2 Structural Integrity

Even though the quality of the large plates was poor, the structural integrity, as defined by stiffness after manufacturing, compared well with other references. The average E_L from the other references was 136 GPa, as compared to 129 GPa for the present investigation, a 5% difference. The

E_T and G_{LT}, the transverse and shear stiffness, were almost exact, with the average from the other references being 10 GPa and 5.7 GPa as compared to 10 GPa and 5 GPa for the present investigation. Despite the poor quality of the tensile coupons, the structural integrity was good. Even though quality is closely associated with structural integrity, structural integrity is the bottom line when it comes to accepting or rejecting a part. Structural integrity addresses the problems of whether the part can do what it was designed to do. Quality may affect the mechanical properties of the composite part, but it might not affect the critical property that determines whether the part can do its designed job. If a part has good structural integrity but not quality, the part should not be rejected if the criteria is mechanical performance.

6.2.3 Predictability

The ability to predict the tensile stiffness of the 70/20/10, 50/40/10, and 30/60/10 coupons using Classical Laminated Plate Theory was good. From inspection of Table 5.14 and Figures 5.6-5.8, the theoretical stiffness was close to the experimental stiffness, even near failure. The difference was less than 10%. This analytical approach was accurate to failure due to the linear to failure stress-strain curves of the particular coupons plotted. However, this solution procedure would not accurately predict the stiffness near failure of the 0/100/0 coupons, due to their non-linear stress-strain relationship from initial loading to final failure.

6.3 Right Angle Bend Specimens with Final Part Layup

6.3.1 Quality

The quality of the right angle bends was poor due to the presence of a large wrinkle in the curvature of the bend. The wrinkle contained the majority of plies and extended the entire width of the specimens. Major delaminations between the plies were observable within the wrinkle. A wrinkle occurred in each specimen.

Besides the wrinkle, the bend specimens had similar quality features as those of small plates P100/0/0-1, 4, 5 and 6. Kapton adhered to both surfaces. A little waviness existed on the top surface, while the bottom surface was level. A microscopic evaluation revealed no irregularities except within the area of the wrinkle. The consolidation distance was 45%, less than the expected 63%.

Overall, the quality problems that were similar to the small plates could be eliminated by the technology gained in the study. However, the cause of the wrinkle is still not well understood. Since the technology developed throughout the study did not address or eliminate the wrinkle, the quality of the bend specimens was poor due to the wrinkle. In other words, the wrinkle might be a hard problem to solve.

6.3.2 Predictability

Despite the presence of a wrinkle, predictability of the structural integrity of the bend specimens was good. By inspection of Table 5.17, the average theoretical stiffness predicted the experimental stiffness within

12.8%. Comparing the theory to the experiment on an individual basis does not reveal accuracy because of the large coefficient of variation among the experimental stiffnesses. Although the bends had minor differences in their post-manufacturing geometry, the nominal dimensions were equal and therefore made it reasonable to compare and average the theoretical and analytical stiffnesses of the bends. Since the experimental stiffness was close to the theoretical stiffness on average, the bends had good predictability of the structural integrity as defined by stiffness to an end load. The large coefficient of variation for the experimental stiffnesses was probably related to the presence of the wrinkle at the curvature of each bend.

6.4 Right Angle Bend Specimens with Thermoforming

Stiff diaphragm thermoforming was attempted once unsuccessfully. Little time was set aside for developing this manufacturing procedure due to the problems associated with processing the other specimens. Therefore, no real conclusions can be made with respect to stiff diaphragm thermoforming. However, some problems that prevented successful processing can be listed for future reference.

The first problem was the heat blanket and Kapton combination. When producing the bends with the layup of the plies in final part form, the blanket rested on the top surface of the Kapton vacuum bag at 471°C (880°F) for 80 minutes without any problems. When thermoforming, however, the vacuum bag did rend when the blanket was set at 471°C (880°F) for 40 minutes. The Kapton vacuum bag must stay in good shape, because it

pushes down on the consolidated but pliable Gr/PEEK flat plate to form a bend in addition to maintaining a good vacuum.

The second problem was the high temperature vacuum tape. Even though it was possible to form the Kapton vacuum bag, the stiff diaphragm, to the awkward shape of the assembly, such that the process could work, the vacuum bag did not stick to the high temperature vacuum tape good enough for vacuum sealing. The high temperature vacuum tape did not have enough tack. The stiff diaphragm fit the assembly by bunching up the Kapton along the edges with extra vacuum tape.

6.5 The Manufacturing Processes

The three manufacturing processes which made the small plates, large plates, and bends all used a heat blanket to reach the high temperature of 393°C (740°F). The critical factors in all of the processing was the heat blanket and the level of insulation.

6.5.1 Quality and Repeatability

One important feature for successful processing was insulation that reduced the in-plane thermal gradient and retained the heat from the cool autoclave. Thermal gradients in excess of 67°C (120°F) can cause significant difficulties when consolidating Gr/PEEK. A processing window was discovered which revealed a high probability for burning or lack of consolidation outside a certain temperature range. If the temperature rose above 427°C (800°F) on the Kapton vacuum bagging, then a high probability existed that the Kapton vacuum bag might burn, thus creating a loss of

vacuum and dense wrinkling and burning within the laminate. If the processing temperature was below 360°C (680°F), then a high probability existed that consolidation would not occur. The heat blanket and consolidation assembly should be insulated to avoid these gradients. In addition, due to the inherent nature of the blanket, an insulator was also required to spread out the heat from under the electrical wires to the area under the stitching. Creating a partial oven within an autoclave by surrounding the entire assembly with an insulator was an important step to processing Gr/PEEK specimens that had enough quality to warrant mechanical testing.

From inspection of Tables 2.4, 2.6 and 2.9, the in-plane temperature gradient for the small plates, large plates and bends was 72°C (130°F), 84°C (151°F), and 77°C (139°C), respectively. Note the correlation between the level of insulation and the temperature gradient. The insulation was best for the small plates, since the big insulator could be wrapped around the 2 dimensional assembly. The bend assembly was similar to the small plate assembly, except for the addition of one more spatial dimension due to the height of the iron mold. There was more possibility of heat leaking out of the system due to the increased volume and awkwardness of the assembly. The large plates had the worst insulation and the largest temperature gradient. The insulation did not surround the edges of the caul plate. In addition, the insulator had to be spread out over the large assembly. The insulator was wrapped around itself for the small plates and bends. Almost every time a specimen was processed, a high probability existed that unsuccessful consolidation would result. For the particular manufacturing procedures used, the 3 processes involving a heat blanket had poor quality due to the large temperature gradient that created a high

probability for unsuccessful consolidation. However, at the same time, specimens were formed with quality good enough to warrant mechanical testing. The heat blanket process could form Gr/PEEK parts, but not very well. From an implicit understanding of other references, the maximum ΔT was 11°C (20°F), far below the ΔT present in the processes used for this investigation.

The repeatability of the process was poor as well. From inspection of Tables 2.4, 2.6, and 2.9, the coefficient of variation for the temperature gradients for the small plates, large plates and bends was 31%, 16% and 35%. These values are large. When using these processes, one did not know what to expect. A risk was taken every time a specimen was consolidated.

6.5.2 Longevity of the Heat Blanket

The longevity of the heat blanket was poor and a significant constraint on the investigation. The small heat blanket had a lifetime of 25 thermal cycles. The first large heat blanket lasted 1 cycle due to the fire. The second large heat blanket showed degradation of the fiberglass covering after approximately 4 heating cycles. For whatever reason, the track record of the heat blankets was very poor. Mass production of Gr/PEEK specimens, which was desired for this study, could not be done due to the short heat blanket life span.

Initially, the fiberglass surrounding the blanket hardens due to the thermal cycling. Cracks developed within the fiberglass, leaving the insulated heating wires visible. However, the blanket still operated effectively in the presence of cracks and rips in the fiberglass. Thermal cycling also degraded the stitching that clamped the large lead wires to the

blanket. After a number of heating cycles, the stitching no longer clamped the lead wires in place, which meant the connection between the large lead wires and the tiny heating wires could easily break, causing an open circuit and final heat blanket failure. The connection of the lead wires to the heating wires was the weak link in the heat blankets and the cause of failure for the small heat blanket.

6.5.3 Practicality

For the particular manufacturing procedures employed in the study, using a heat blanket in an unheated but pressurized autoclave to process Gr/PEEK composite parts was impractical due to the poor quality, poor repeatability, and poor longevity. However, this type of process might become practical if different manufacturing procedures are used, such as increasing the level of insulation around the assembly. Even the low cost of the heat blanket process, which is the main advantage of this process, comes into question. In the long run, the cost of all the heat blankets purchased, the wasted time, and the wasted material due to burning and lack of consolidation might be higher than another process that is more expensive initially.

6.5.4 Comments on the Fire

The procedure that resulted in a fire was simulated except for the heat blanket and release agent. Although a large heat blanket was used to process the large plates with the same engineering features, it was not the exact same one as in the fire. In other words, the first large blanket might

have had a manufacturing flaw. It was possible a short circuit or other electrical malfunction occurred during consolidation, resulting in a fire. Only the blanket had the power to inflict the complete destruction of the assembly. A possible but unlikely reason was the Frekote 700 release agent. Since F-57 was used as a release agent to avoid a possible repeat of a fire, uncertainty existed if the the Frekote 700 was the cause. However, Frekote 700 was used in reference [16] to manufacture Gr/PEEK specimens at a temperature of 393°C (740°F), which was above the fire flash point of 382°C (720°F).

6.5.5 Thermal Strains and Mechanical Stress

From the experience of the ply buckling in Chapter 2, mechanical stresses caused by thermally induced strains are significant, even below the consolidation temperature. Every good consolidated laminate, except unidirectional laminates, are pre-stressed due to the difference in the coefficient of thermal expansion from ply to ply. The reason why no ply buckling exists is because the surface of each ply is clamped onto the surface of an adjacent ply by the matrix. This surface clamping did not occur in test #18 described in Chapter 2. If the stress-strain curve is linear, the pre-stressed condition does not affect the stiffness and does not enter into the analytical analysis for stiffness. However, the thermal pre-stressed condition might affect the strength of the laminate.

Chapter 7
CONCLUSIONS AND RECOMMENDATIONS

Gr/PEEK specimens were made by using a heat blanket in an unheated, pressurized autoclave. Small plates, large plates and bends were formed by surrounding the composite assemblies in an insulator during consolidation. The effects of manufacturing were investigated through the following criteria: visual observation, microscopic evaluation of the edges, consolidation distance and mechanical testing. This criteria was used to determine the quality, structural integrity and predictability of the structural integrity of the specimens after manufacturing. In addition, the quality, repeatability, longevity and practicality of the manufacturing process itself was also examined. The stiffness of the tensile coupons and bends were analytically determined by Classical Laminated Plate Theory and energy methods. From this work, the following conclusions have been drawn:

1. For the particular manufacturing procedures used in this study, the heat blanket process could form Gr/PEEK parts, although not very well.

2. The quality, repeatability and longevity of the process make the process impractical for the unique manufacturing procedures used to make the specimens. However, if the insulation around the assembly during consolidation is improved, the increase in quality and repeatability may make the process practical.

3. When using the heat blanket in an unheated autoclave, an insulator must surround the system, creating an oven to reduce the gradient heating and retain the heat from the cool autoclave environment.

4. The large plates (tensile coupons) had good structural integrity as defined by tensile stiffness.

5. The predictability of the structural integrity for the large plates (tensile coupons) and bends was good.

6. The large plates and bends had poor quality, while the small plates had good quality.

7. The degree of surface smoothness on a Gr/PEEK specimen seemed to be related to the bending stiffness of the material it pressed against during consolidation.

8. The fire was caused by the heat blanket or Frekote 700, but most likely a manufacturing flaw in the heat blanket.

9. A pressure of .34 MPa (50 psi) produced specimens that had a consolidation distance of 43%, less than the expected value of approximately 63%. A pressure of .34 MPa is too low a pressure to produce specimens with the expected consolidation distance. A pressure of 1.4 MPa (200 psi) is used by other references.

10. Thermal induced strains are important to consider, even below the consolidation temperature.

11. Several coats of F-57 worked well as a release agent in place of Frekote 700.

Based on the results of this work, the following recommendations are made for future work:

1. Purchase an autoclave capable of 399°C (750°F) and a pressure of 1.4 MPa (200 psi).

2. Build an economical small oven (<$10,000) that can be inserted into the present autoclave and heat the Gr/PEEK to a uniform 393°C (740°F) while using the maximum pressure that the autoclave can apply to the Gr/PEEK (1.2 MPa or 175 psi).

3. Investigate the effects of manufacturing on buckling, strength and compressive stiffness of the laminate.

4. Manufacture bends and other parts using post-forming techniques.

5. Investigate the effects of heat and pressure during consolidation on the mechanical properties of Gr/PEEK.

REFERENCES

1. Brewer, J.C., "The Effect of Ply Thickness on the Free Edge Delamination of Graphite/Epoxy Laminates," S.M. Thesis, Department of Aeronautics and Astronautics, M.I.T, 1986.

2. Kardos, J.L., R. Dave, M.P. Dudukovic, "Voids in Composites," Manufacturing International, 1988.

3. Muzzy, J.D., "Processing of Advanced Thermoplastic Composites," Manufacturing International, 1988.

4. Gutowski, T.G., "A Resin Flow/Fiber Deformation Model for Composites", Sampe Quarterly, 1985.

5. Springer, George S., "Manufacturing Thermoplastic Matrix Composites," AFWAL-TR-88-4115, Wright Patterson Air Force Base, Ohio, 1988.

6. National Materials Advisory Board, "The Place for Thermoplastic Composites in Structural Components", 1987.

7. Soll, W., "Behavior of Advanced Thermoplastic Composites in Forming," S.M. Thesis, Mechanical Engineering Department, M.I.T., 1987.

REFERENCES (continued)

8. Mallon, P., C. O'Bradaigh, R. B. Pipes, "Thermoforming of Fiber Reinforced Thermoplastic Matrix Composites," Center for Composite Materials, University of Delaware, Report No. 87-57, 1987.

9. O'Bradaigh, C., P. Mallon, "Polymeric Diaphragm Forming of Continuous Fiber Reinforced Thermoplastics," Center for Composite Materials, University of Delaware, 1988.

10. Smiley, A., R. B. Pipes, "Diaphragm Forming of Carbon Fiber Reinforced Thermoplastic Composite Materials," Center for Composite Materials, University of Delaware, Report No. 88-11, 1988.

11. Hoggatt, J. T., S. Oken, E. E. House. "Advanced Fiber Reinforced Thermoplastic Structures", AFWAL-TR-80-3023, Wright Patterson Air Force Base, Ohio, 1980.

12. Brent, D.N., "Strength of Laminated Composite Bends," S.M. Thesis, Department of Aeronautics and Astronautics, M.I.T., 1987.

13. Chang, F, G. Springer, "The Strengths of Fiber Reinforced Composite Bends,"*Journal of Composite Materials*, Volume 20, 1986.

REFERENCES (continued)

14. Sun, C., S. Kelly, "Failure in Composite Angle Structures, Part I: Initial Failure," *Journal of Reinforced Plastics and Composites*, Volume 7, 1988.

15. Lagace, P., J. Brewer, C. Varnerin, TELAC Manufacturing Course, Technology Laboratory for Advanced Composites, MIT, 1988.

16. Horton, R., R. Whitehead et al., "Damage Tolerance of Composites," AFWAL-TR-87-3030, Wright-Patterson Air Force Base, Ohio, 1988.

17. Coquill, S., D. Adams, "Mechanical Properties of Several Neat Polymer Matrix Materials and Unidirectional Carbon Fiber-Reinforced Composites," NASA Contractor Report 181805, 1989.

18. Bisplinghoff, R., J. Mar, T. Pian, Statics of Deformable Solids, Addison-Wesley Publishing Co., 1965.

19. Metallic Materials and Elements for Aerospace Vehicle Structures, MIL-HDBK-5E, Volume I, 1986.

APPENDICES

Appendix A

Female Mold

This appendix contains figures and a description of the female mold, and an explanation of its intended role in making Gr/PEEK bends from Stiff Diaphragm Thermoforming. The female mold was never used in the investigation.

The female mold was designed for thermoforming Gr/PEEK consolidated flat plates. The bottom part of the "V" within the mold would be covered with fiberglass air breather followed by Kapton release film. These materials would be held in place by the screws around the edge of the "V". A flat, consolidated Gr/PEEK laminate would rest just inside the "V". After applying Kapton release film and fiberglass air breather, the Kapton vacuum bag would be applied. The vacuum bag would be "bunched" together at the vacuum tape to allow for it to follow the "V" during forming. Using an insulator on the top and bottom with cartridge heaters and heaters from the autoclave, the mold would rise to a temperature of 393°C (740°F). Vacuum and pressure would be applied. Since the plies would be already consolidated, a large pressure of 1.4 MPa (200 psi) would be unnecessary. A pressure of .34 MPa (50 psi) would probably be more appropriate. The heat, pressure and vacuum would push the vacuum bag against the pliable plate into the mold, creating a right angle bend.

This mold was not used due to the difficulty of heating within the autoclave and the aluminum material properties at this temperature. The mold was too big to have an insulated environment. In addition, a graph of strength vs. temperature for aluminum 6061, the mold metal, revealed that aluminum lost 90% of its strength at 399°C (750°F) relative to room temperature [19]. The use of aluminum at this temperature would be a risk, but not a high enough risk to rule it out.

The female mold was of dimensions 381 mm (15 in) long, 356 mm (14 in) wide, and 152 mm (6 in) thick. The mold was formed in sections, since there was a problem in finding a milling machine that could handle an aluminum block of this size.

Originally, the mold was solid aluminum and was cut in four sections. Each section was milled so that the faces were smooth and rectangular. Two end caps were formed, having dimensions 381 mm (15 in) long, 108 mm (4.25 in) wide and 152 mm (6 in) thick, by cutting along the length of the block. The middle section, which had dimensions 381 mm (15 in) long, 140 mm (5.5 in) wide and 152 mm (6 in) thick, was cut in half along the width. Please see Figures A1-A3. A 45° cut was milled on both parts of the middle section, beginning at 51 mm (2 in) from the bottom and extending to the top surface. This milling created a right angle when these two parts were put together. 13 mm (.5 in) holes were drilled for steel rods that held the mold together. Two were placed lengthwise, going under the "V"; and four went through the width, from one end cap, through the middle section, to the opposite end cap. To provide a vacuum seal up to the surface, indents of 3 mm (.125 in) thick and 13 mm (.5 in) wide were milled along the outside vertical surface of the middle section surrounding the "V"; another similar indent extended under the "V" parallel to the vertex. These cuts were filled with high temperature vacuum tape to seal the mold for vacuum.

Vacuum was applied by tapping a 13 mm (.5 in) pipe fitting in one of the endcaps, then drilling a hole through the endcap and into the middle section above the vacuum tape. The hole did not go through the other endcap. Small holes were drilled from the vertex of the "V" downward in the hole along the vertex. 22 holes were tapped on the mold's top surface that surrounded the "V"; and helicoils were inserted so that screws would hold the materials used in the forming process so that they would not move when the composite slid into the "V". A shim at the bottom would be

necessary, since the "V" was too sharp at the vertex and might break the fibers during processing.

Holes for the heating cartridges were drilled and reamed, 4 in each end of the middle section, and 2 in each endcap. The holes were 51 mm (2 in) deep and of diameter 10 mm (.375 in). These heating cartridges would be used to help heat the mold. The heating cartridges were 51 mm (2 in) long with a 10mm (.375 diameter), type F loads, 240 Volts, 500 Watts, 41 Watts/cm^2 (262 Watts/in^2), and catalog number CIR-20207 from Chromalox.

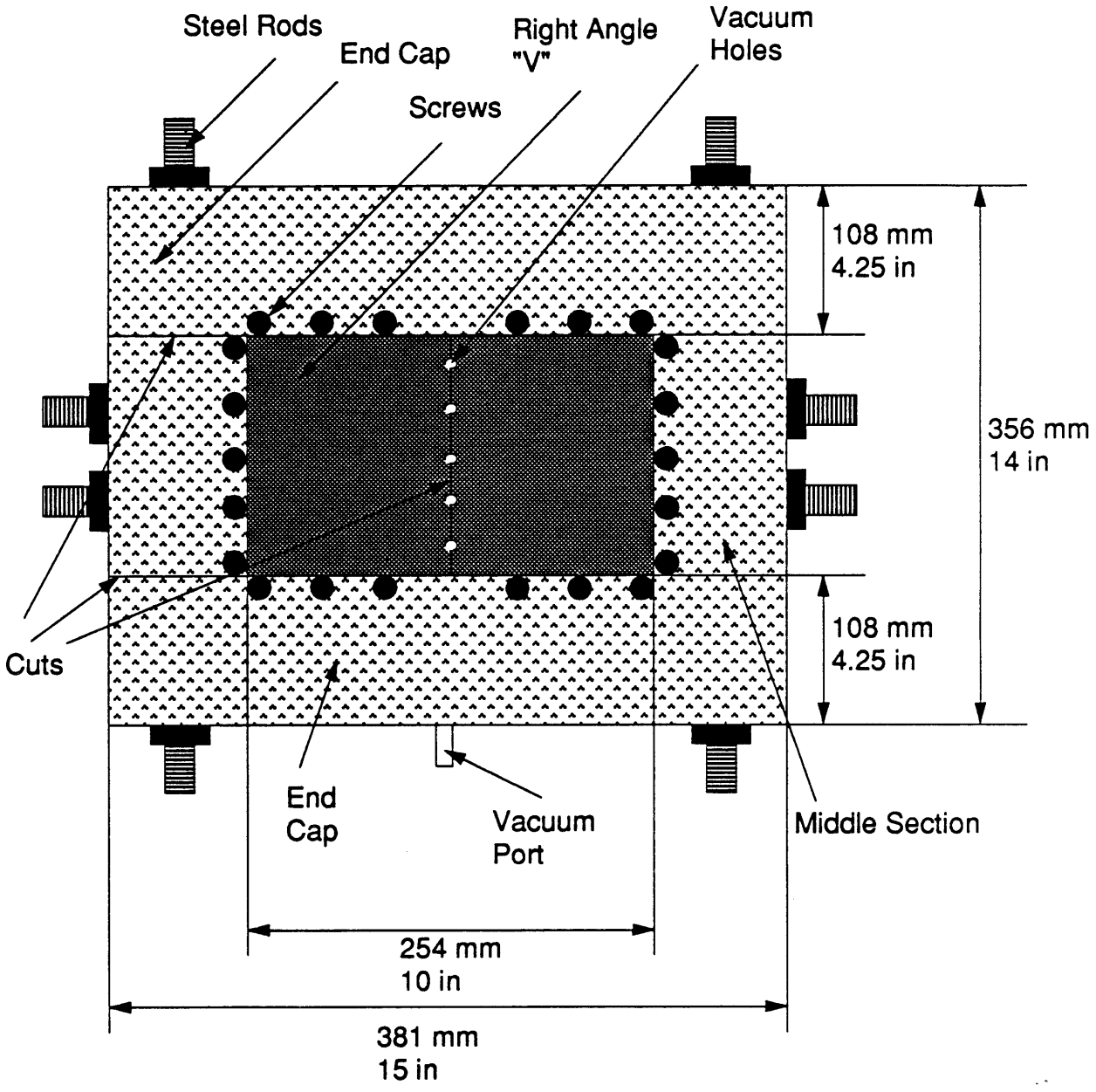

Figure A1 Top View of the female mold.

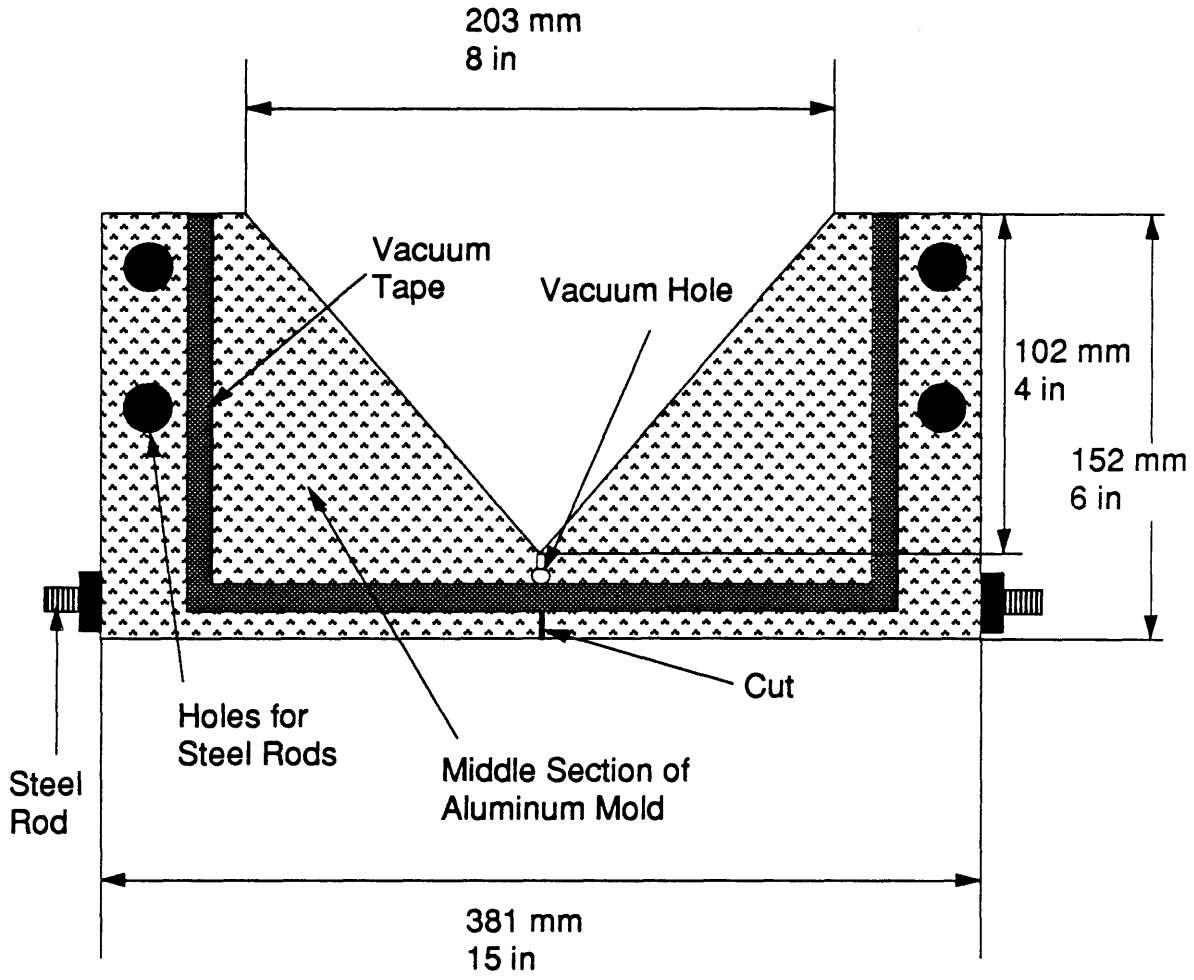

Figure A2 Side view of mold middle section.

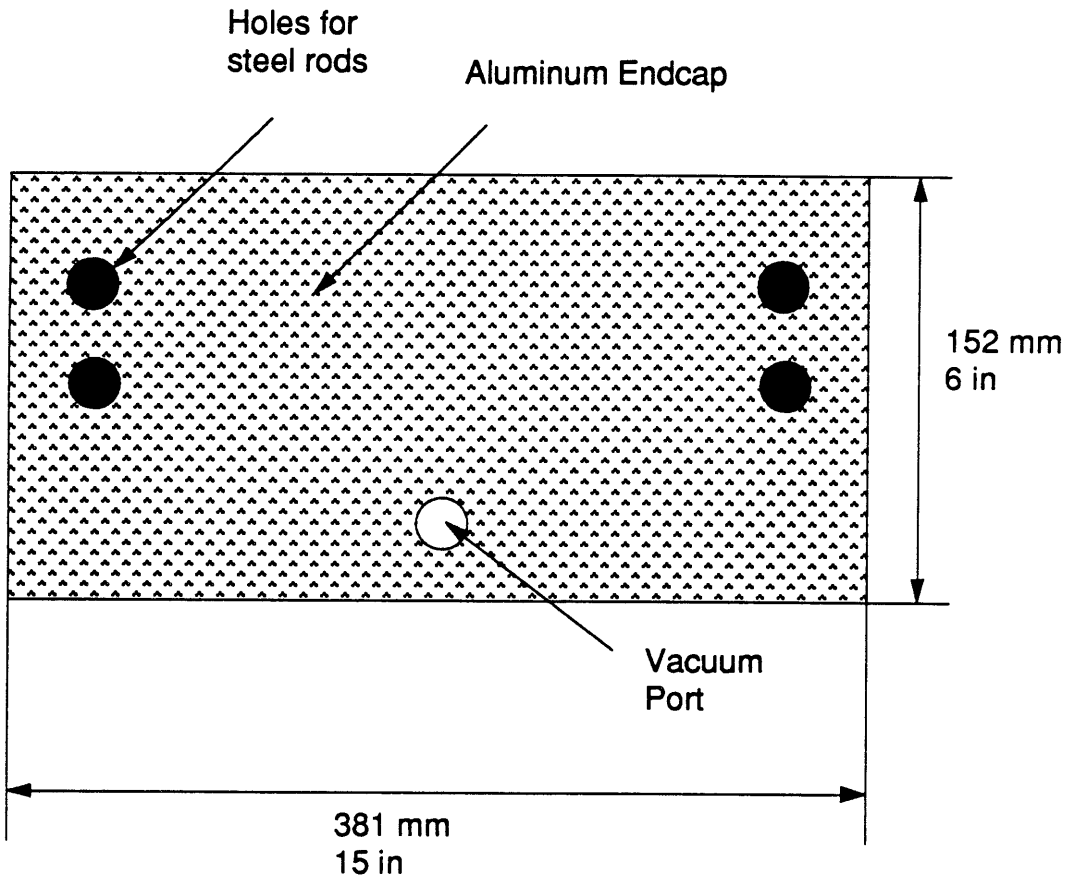

Figure A3 Side view of the endcap with the vacuum hole.

Appendix B

Pictures of Small Plates

This appendix contains pictures of the small plates after processing.

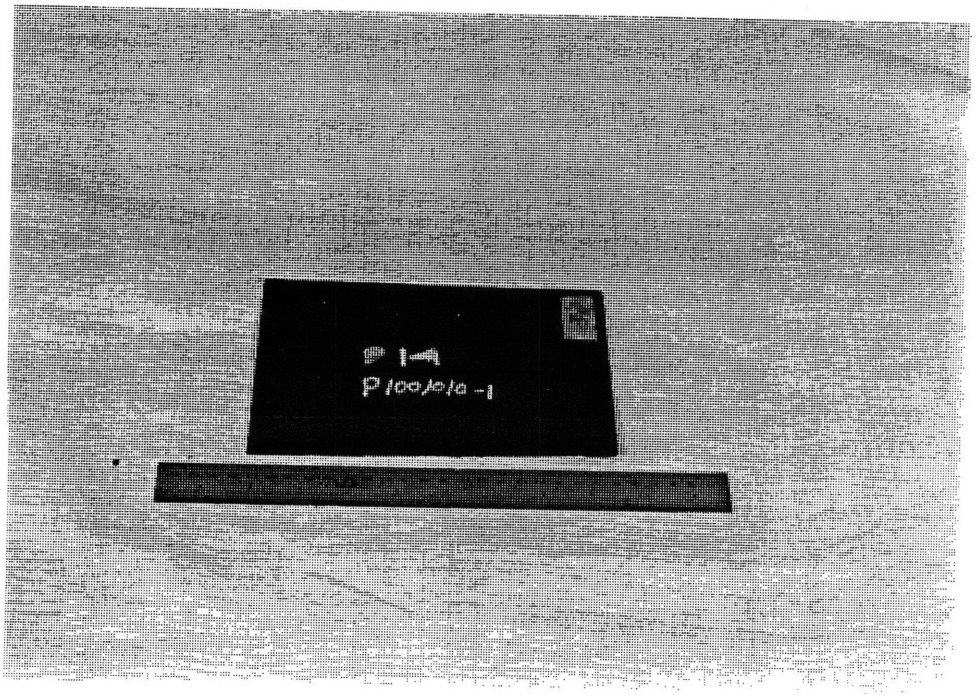

Figure B1 Picture of specimen P100/0/0-1.

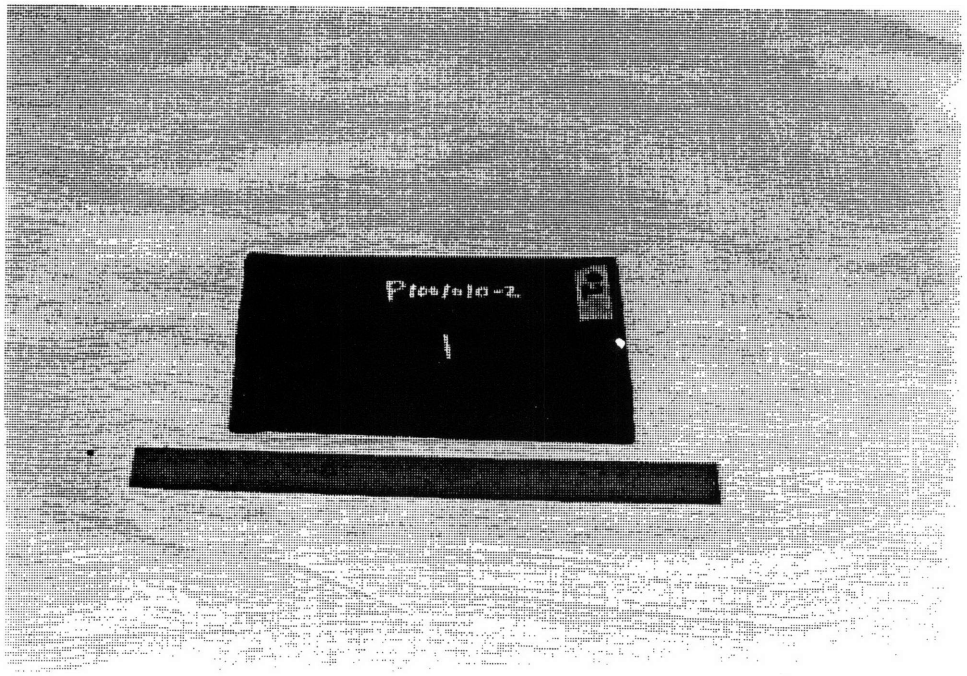

Figure B2 Picture of specimen P100/0/0-2.

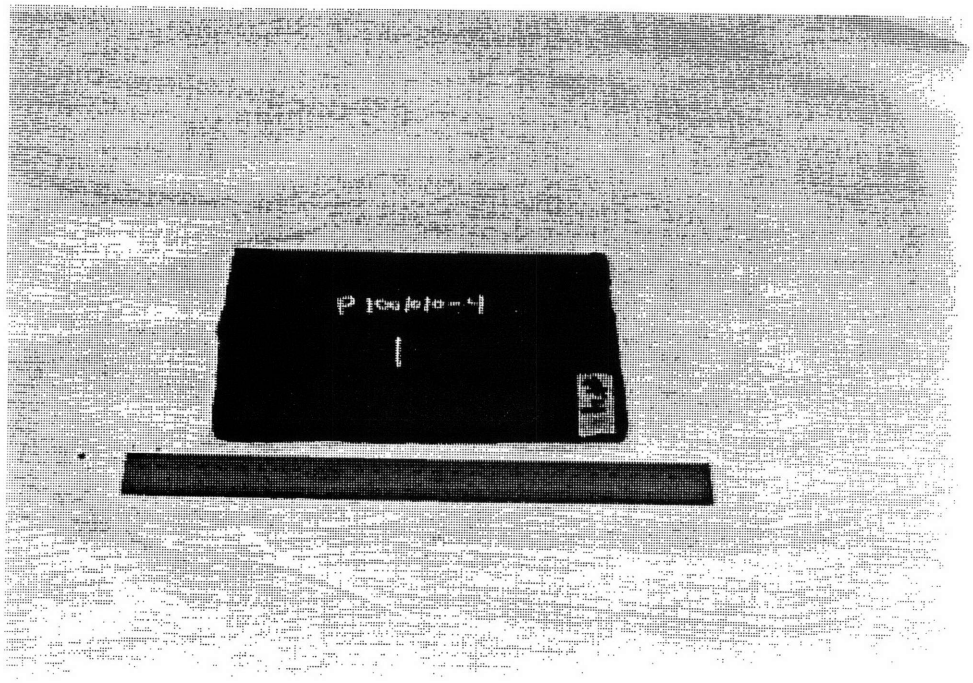

Figure B3 Picture of specimen P100/0/0-4.

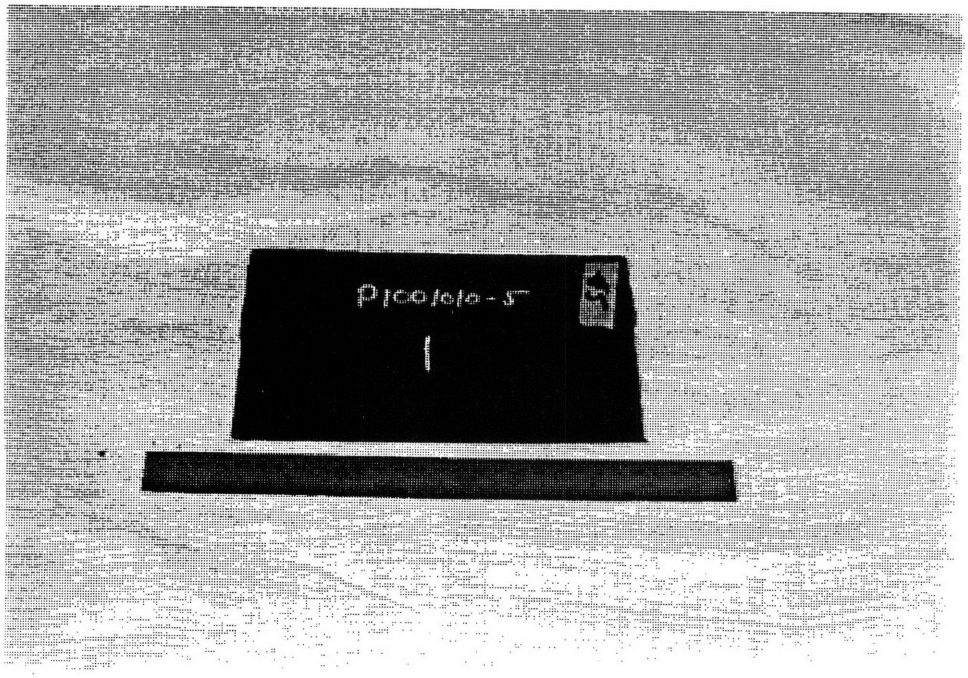

Figure B4 Picture of specimen P100/0/0-5.

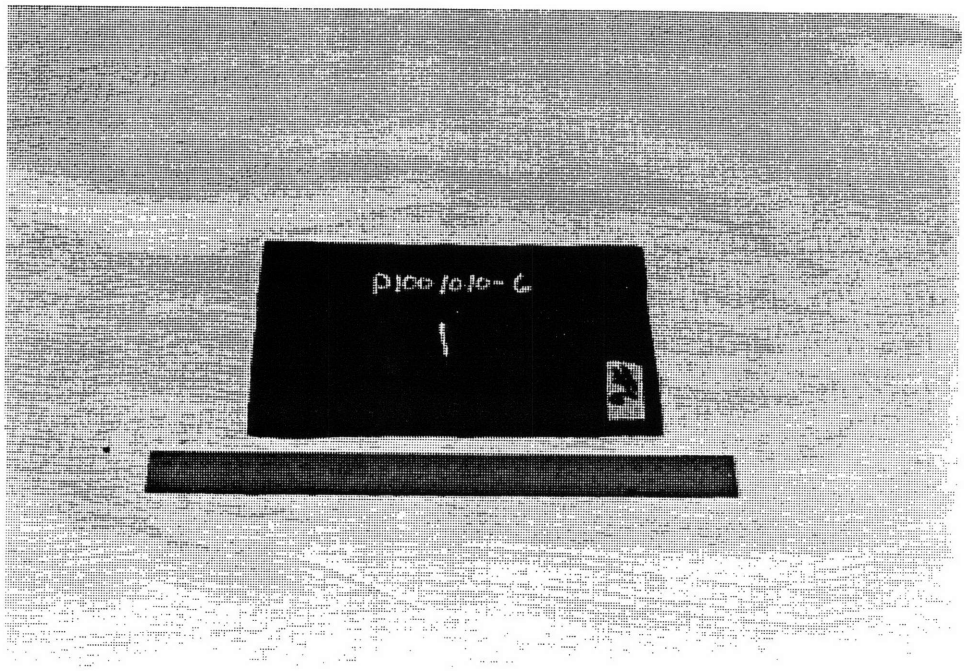

Figure B5 Picture of specimen P100/0/0-6.

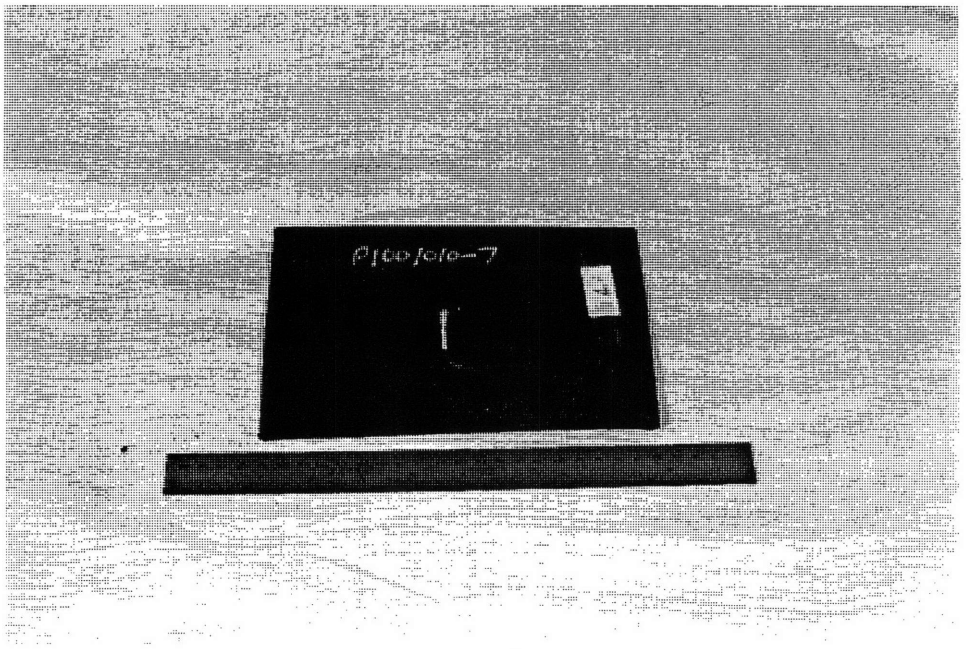

Figure B6 Picture of specimen P100/0/0-7.

Appendix C

Pictures of Tensile Coupons Before and After Testing

This appendix contains pictures of each coupon before and after testing. This includes: 1) 4 specimens of 100/0/0, 2) 2 specimens of 70/20/10, 3) 2 specimens of 50/40/10, 4) 4 specimens of 30/60/10, 5) 3 specimens of 0/100/10, and 6) 5 specimens of 0/0/100.

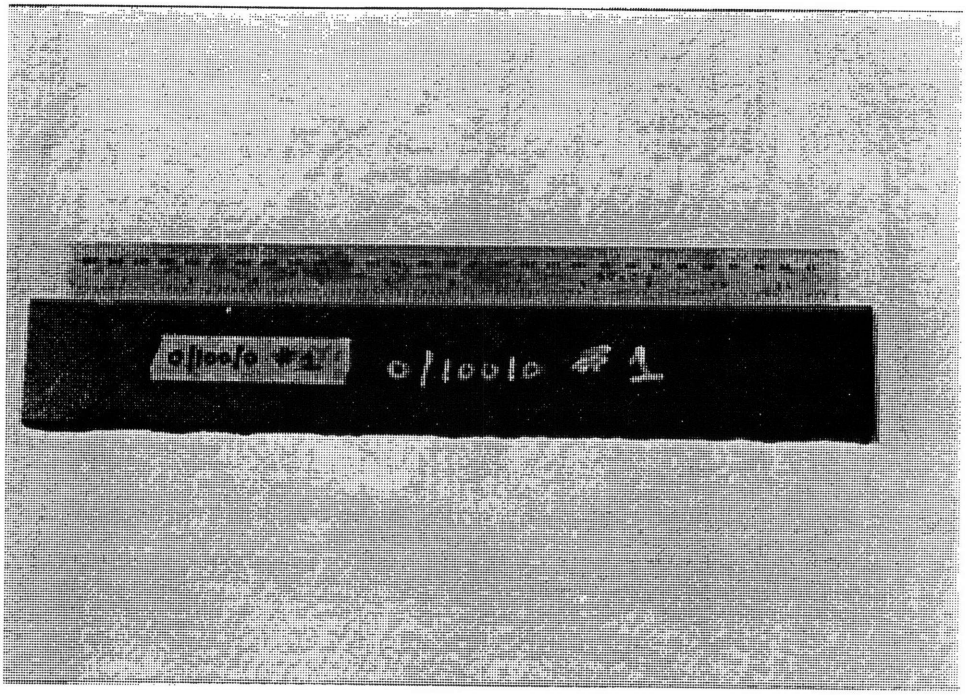

Figure C1 Picture of specimen T0/100/0-1 before testing.

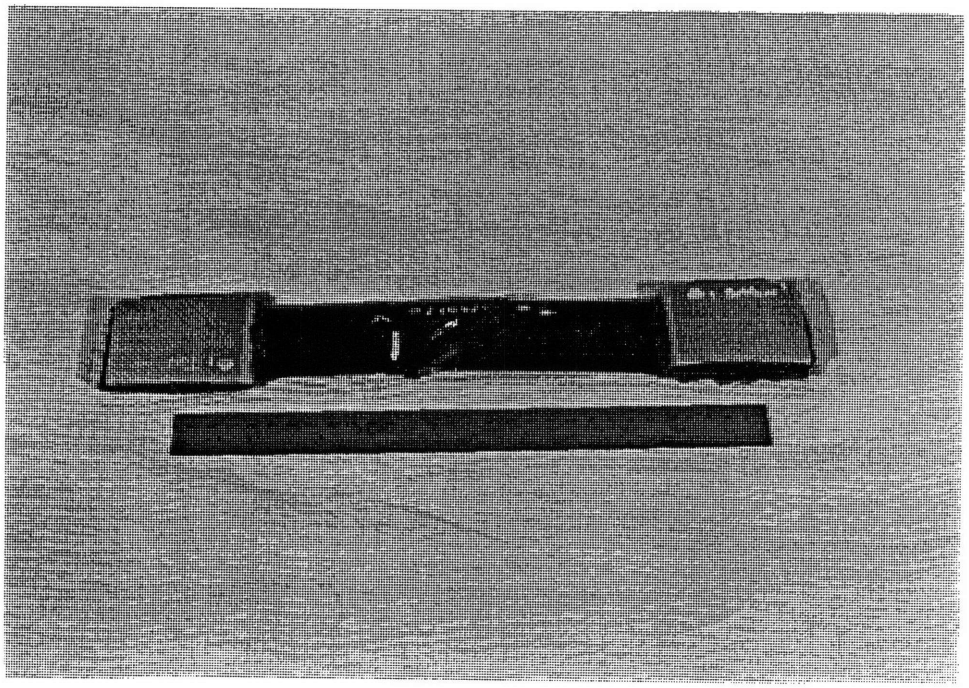

Figure C2 Picture of specimen T0/100/0-1 after testing.

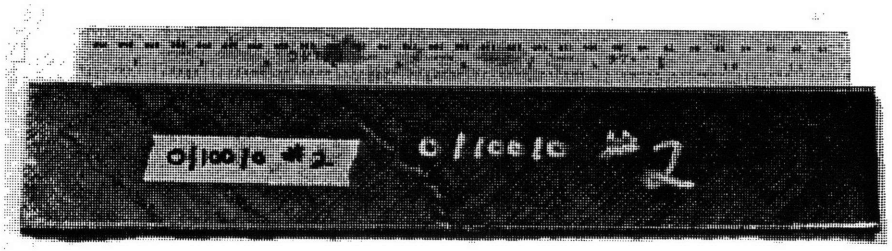

Figure C3 Picture of specimen T0/100/0-2 before testing.

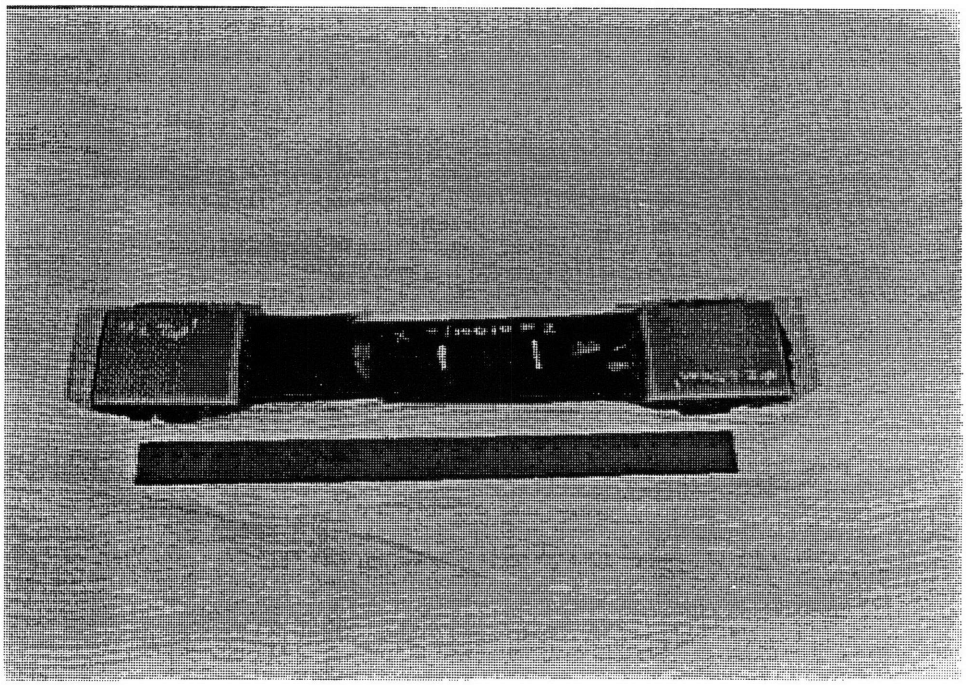

Figure C4 Picture of specimen T0/100/0-2 after testing.

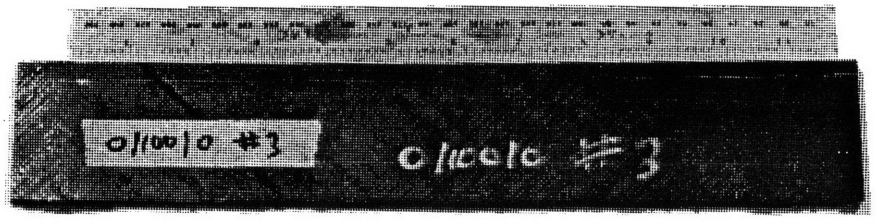

Figure C5 Picture of specimen T0/100/0-3 before testing.

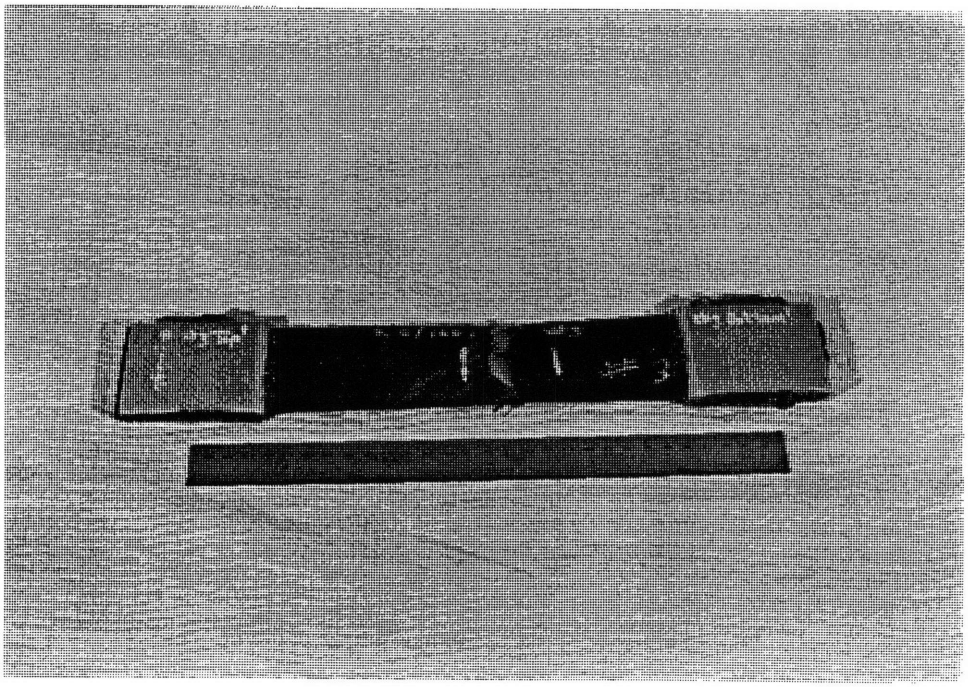

Figure C6 Picture of specimen T0/100/0-3 after testing.

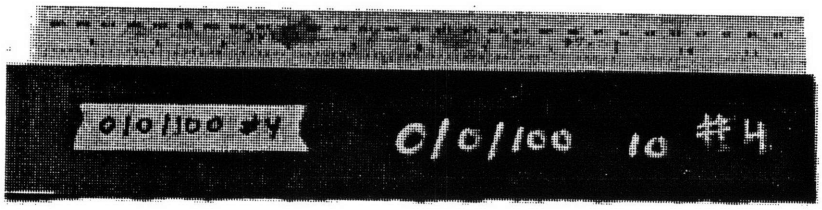

Figure C7 Picture of specimen T0/0/100-4 before testing.

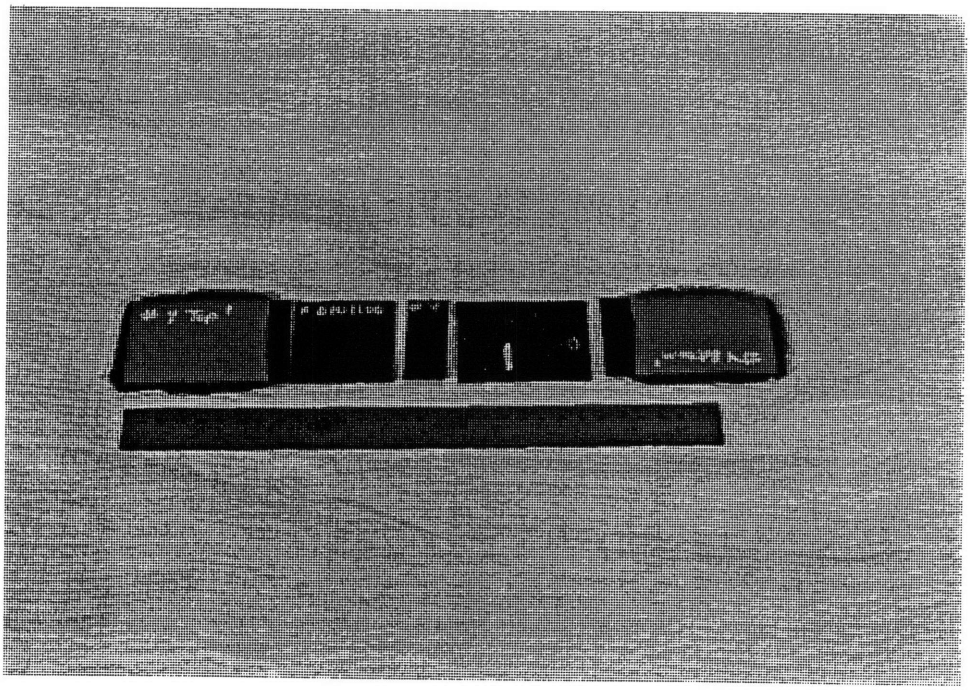

Figure C8 Picture of specimen T0/0/100-4 after testing.

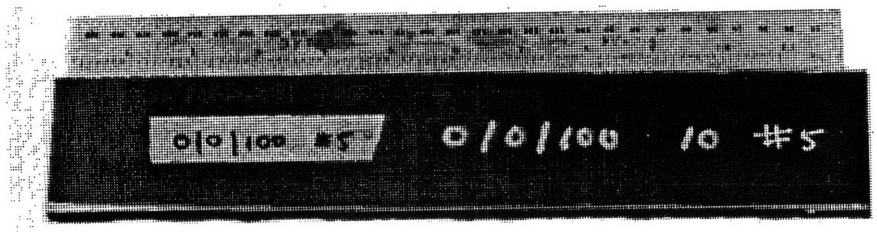

Figure C9 Picture of specimen T0/0/100-5 before testing.

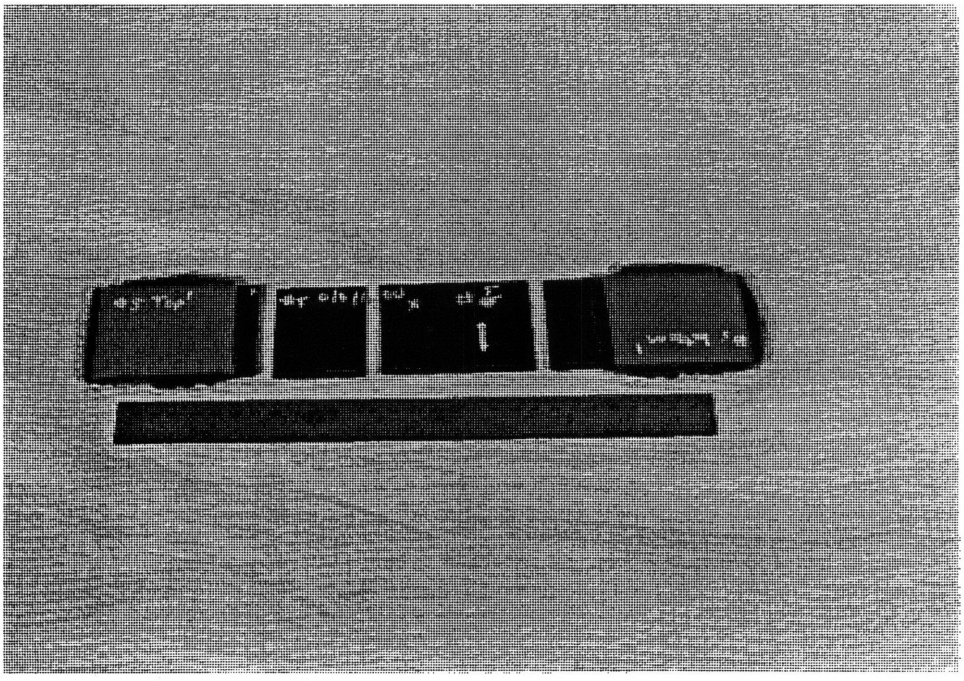

Figure C10 Picture of specimen T0/0/100-5 after testing.

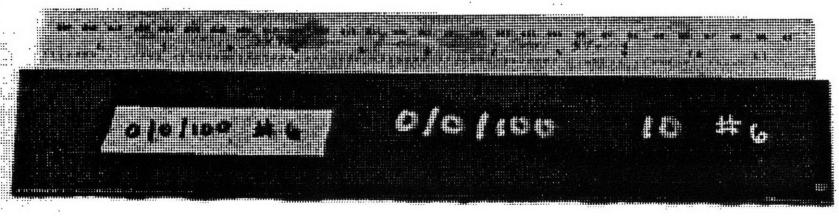

Figure C11 Picture of specimen T0/0/100-6 before testing.

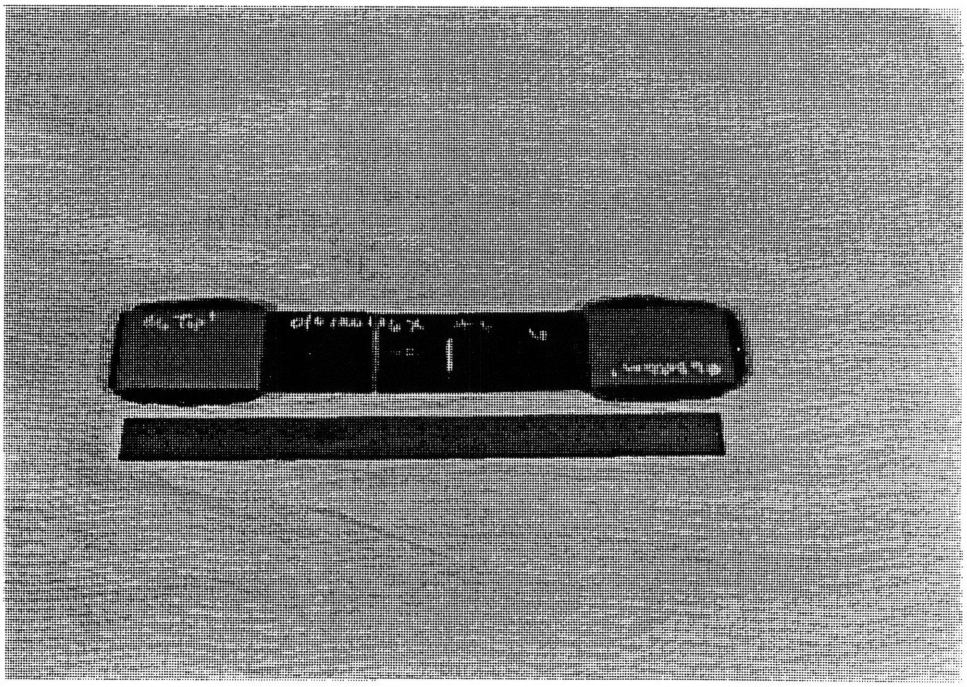

Figure C12 Picture of specimen T0/0/100-6 after testing.

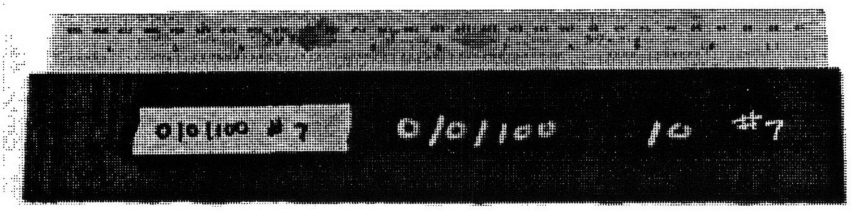

Figure C13 Picture of specimen T0/0/100-7 before testing.

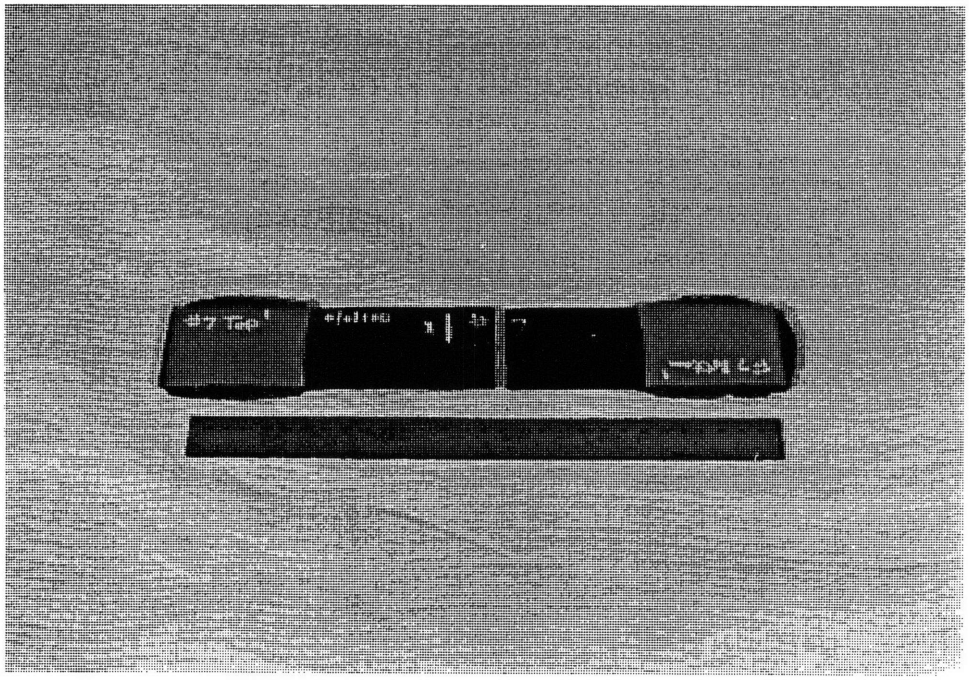

Figure C14 Picture of specimen T0/0/100-7 after testing.

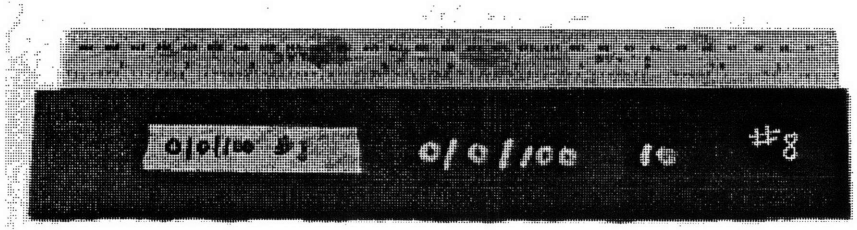

Figure C15 Picture of specimen T0/0/100-8 before testing.

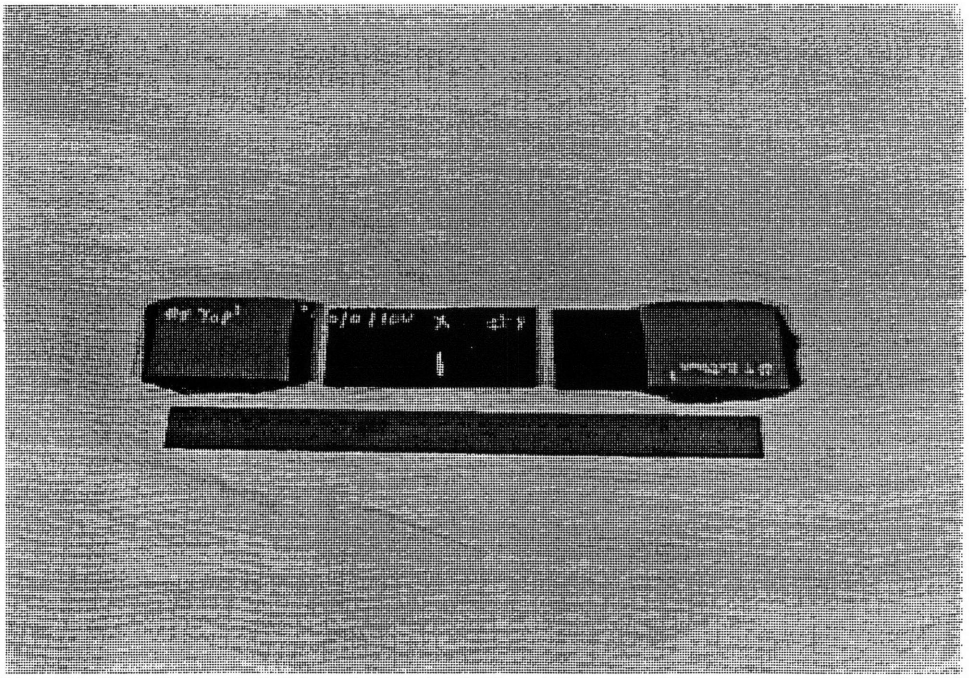

Figure C16 Picture of specimen T0/0/100-8 after testing.

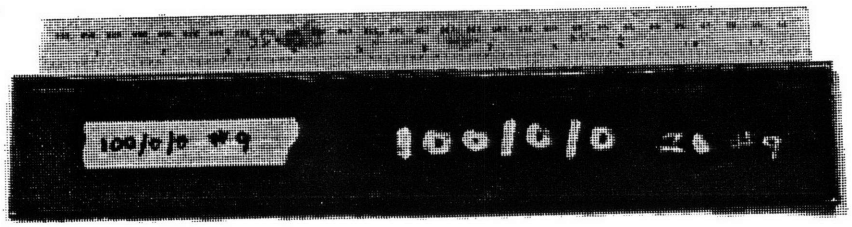

Figure C17 Picture of specimen T100/0/0-9 before testing.

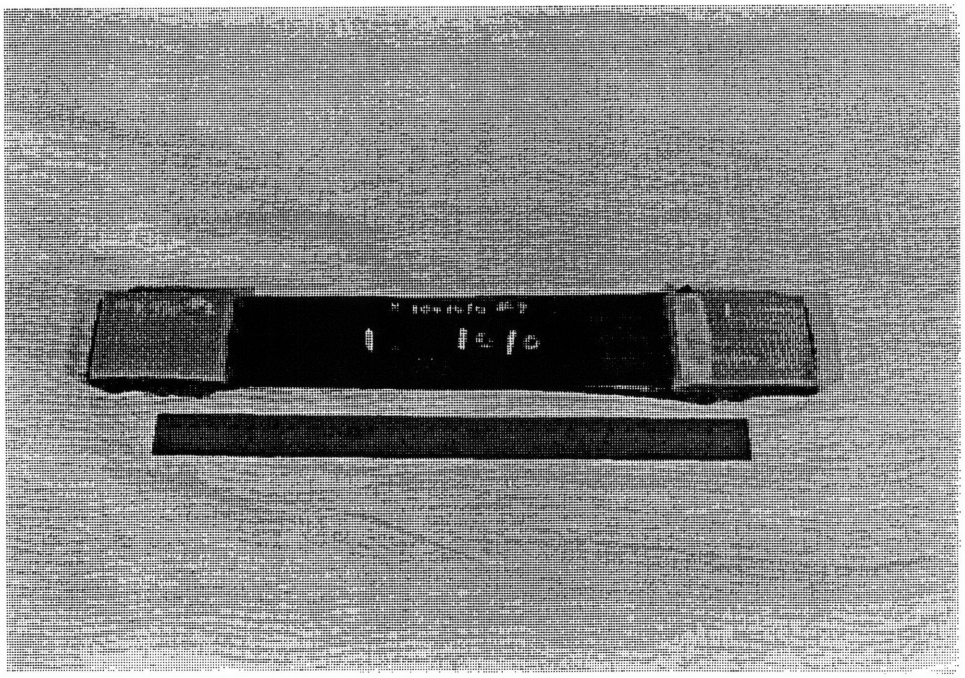

Figure C18 Picture of specimen T100/0/0-9 after testing.

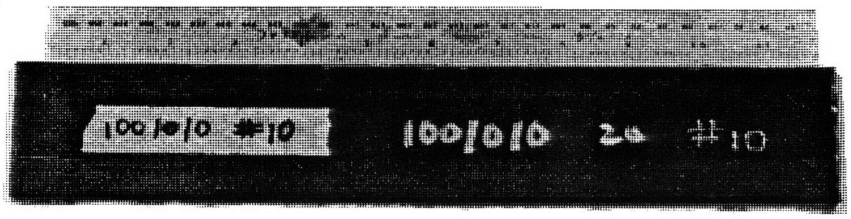

Figure C19 Picture of specimen T100/0/0-10 before testing.

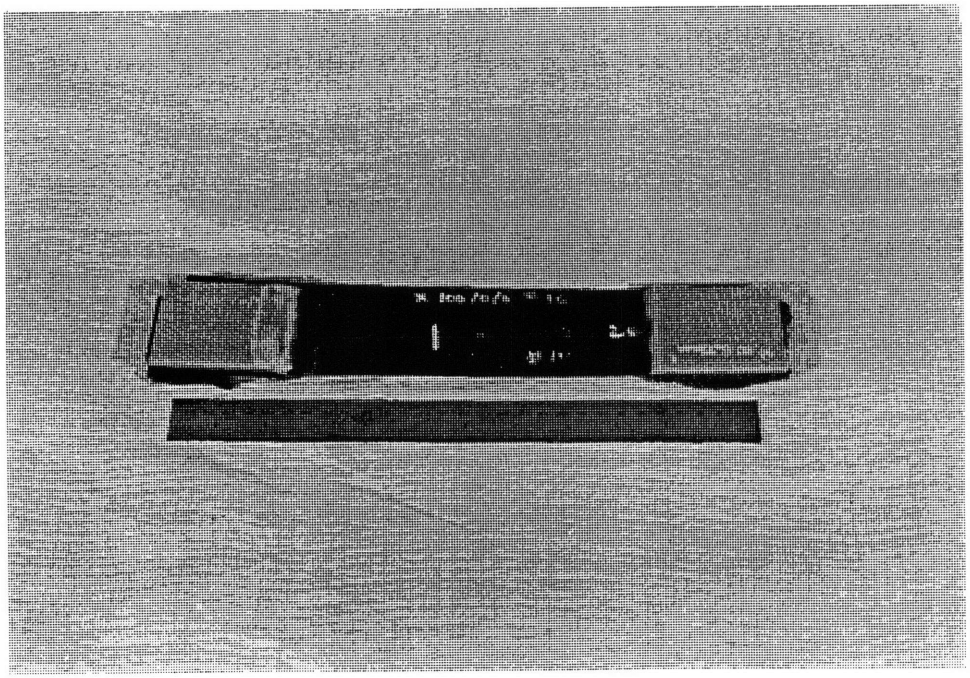

Figure C20 Picture of specimen T100/0/0-10 after testing.

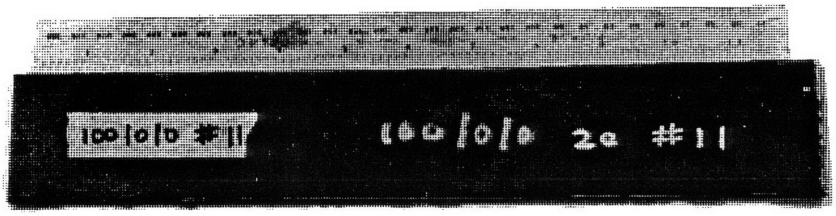

Figure C21 Picture of specimen T100/0/0-11 before testing.

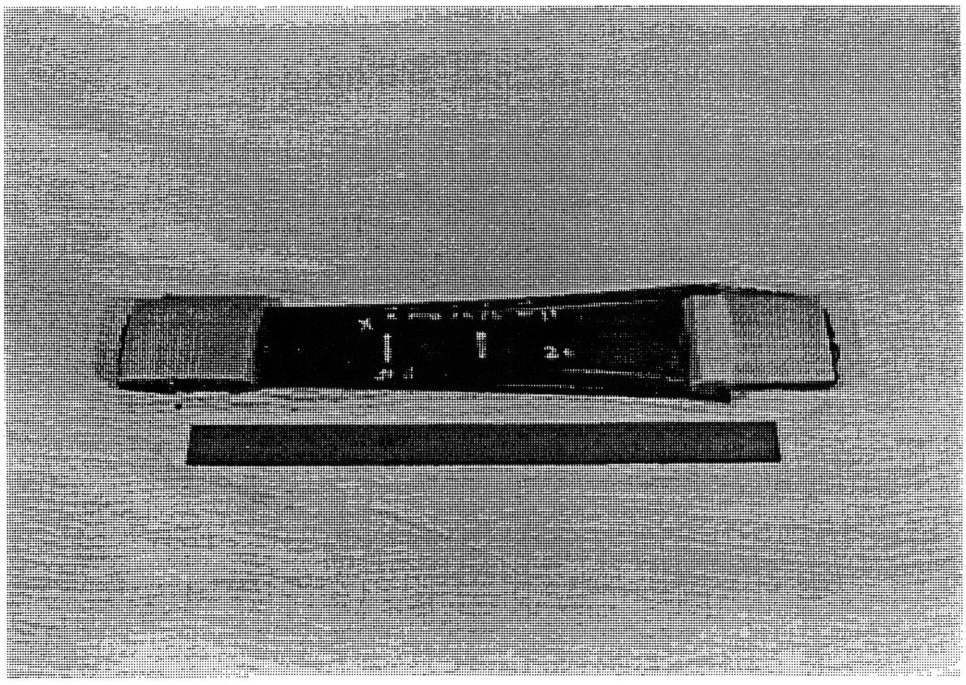

Figure C22 Picture of specimen T100/0/0-11 after testing.

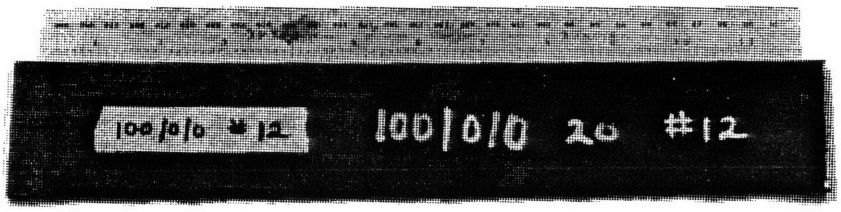

Figure C23 Picture of specimen T100/0/0-12 before testing.

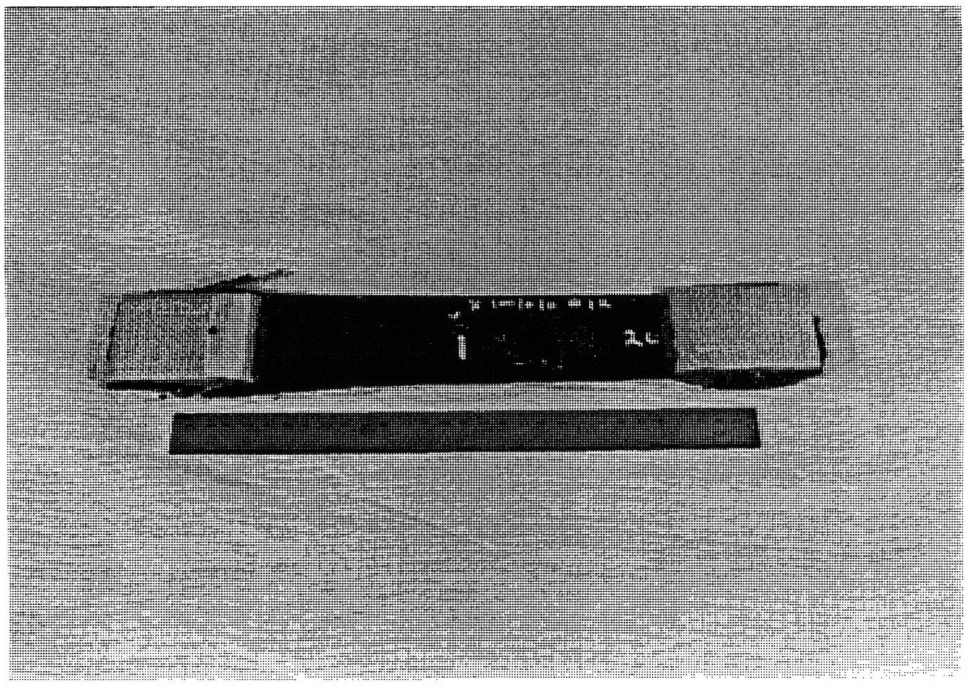

Figure C24 Picture of specimen T100/0/0-12 after testing.

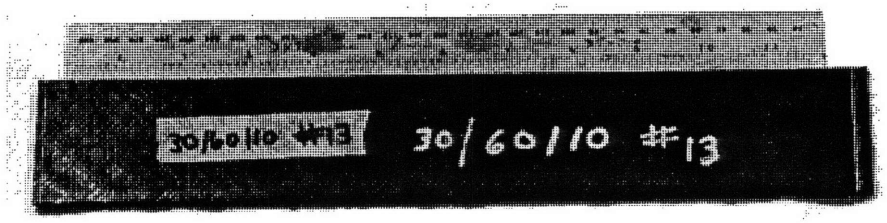

Figure C25 Picture of specimen T30/60/10-13 before testing.

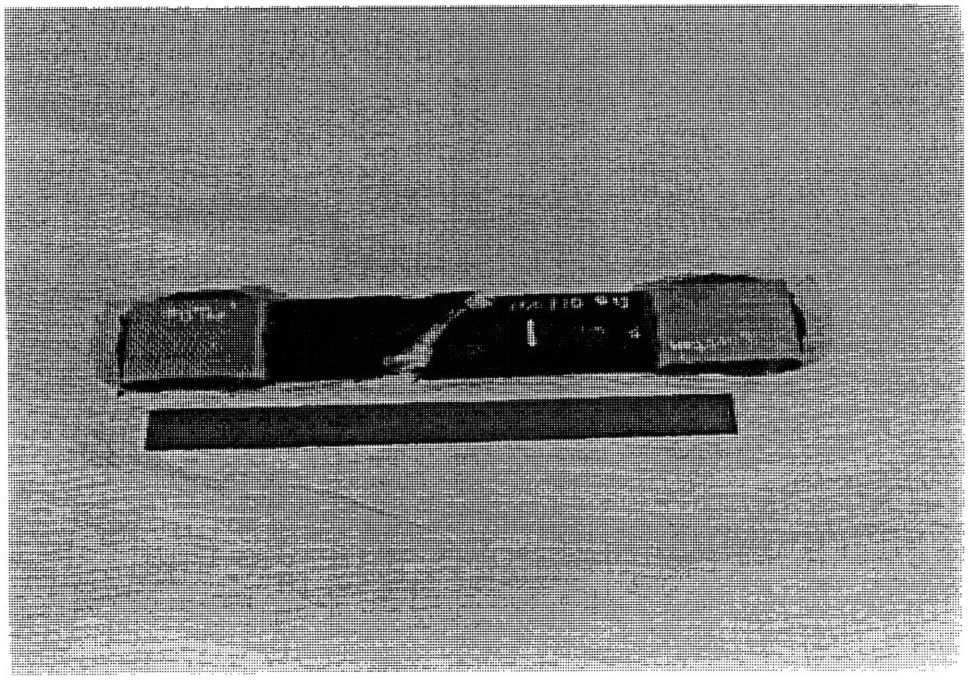

Figure C26 Picture of specimen T30/60/10-13 after testing.

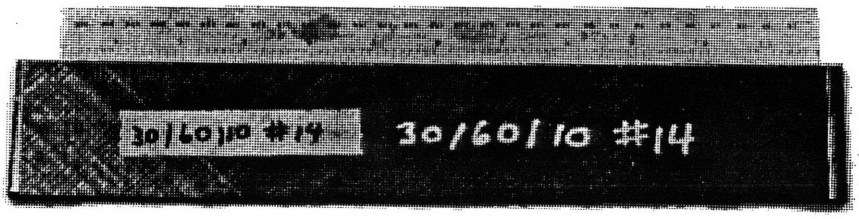

Figure C27 Picture of specimen T30/60/10-14 before testing.

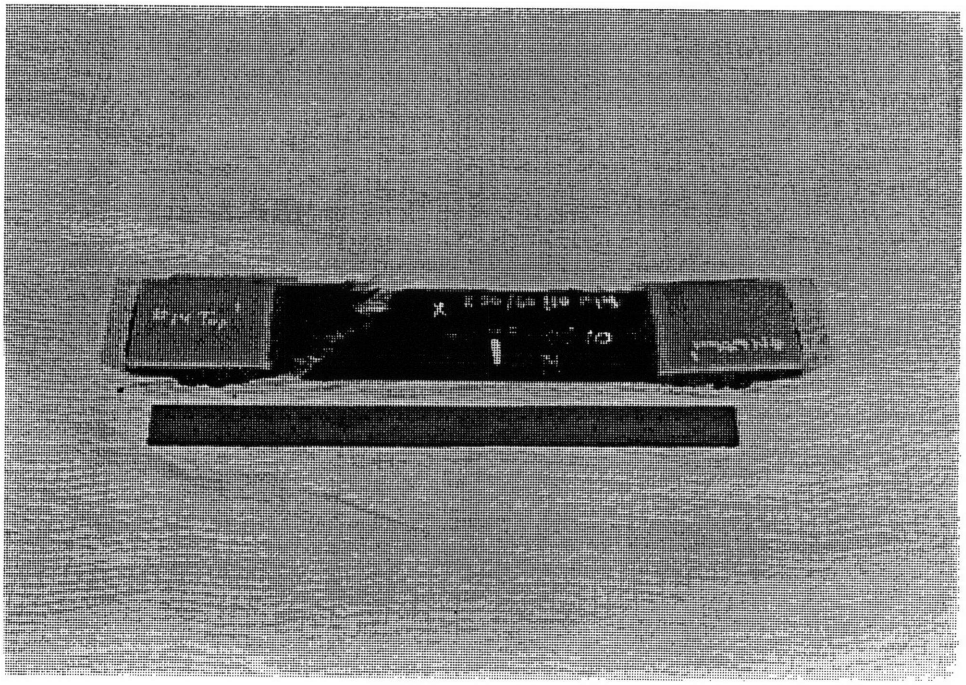

Figure C28 Picture of specimen T30/60/10-14 after testing.

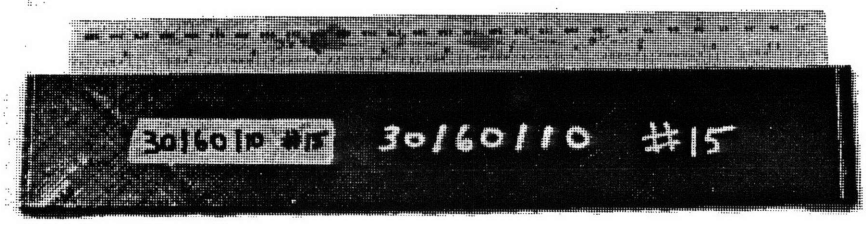

Figure C29 Picture of specimen T30/60/10-15 before testing.

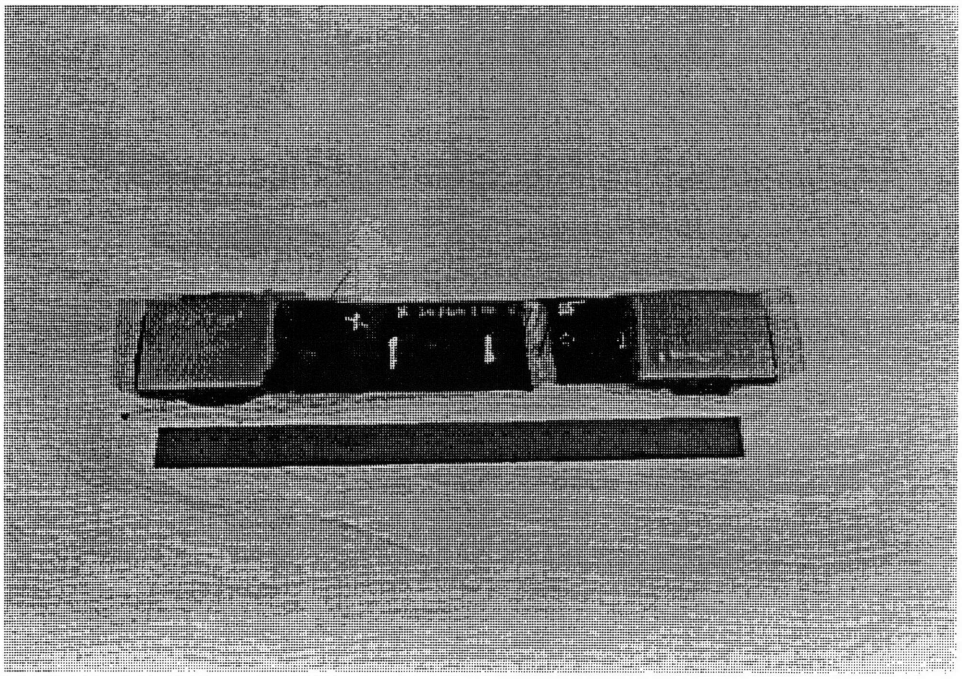

Figure C30 Picture of specimen T30/60/10-15 after testing.

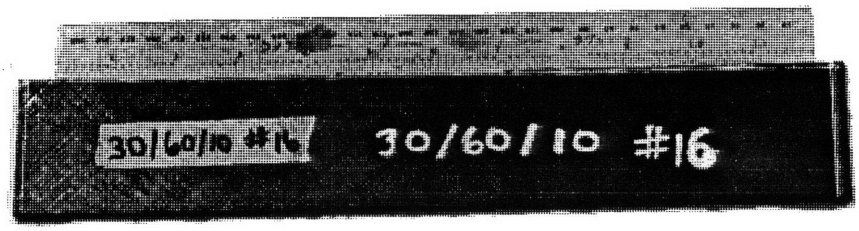

Figure C31 Picture of specimen T30/60/10-16 before testing.

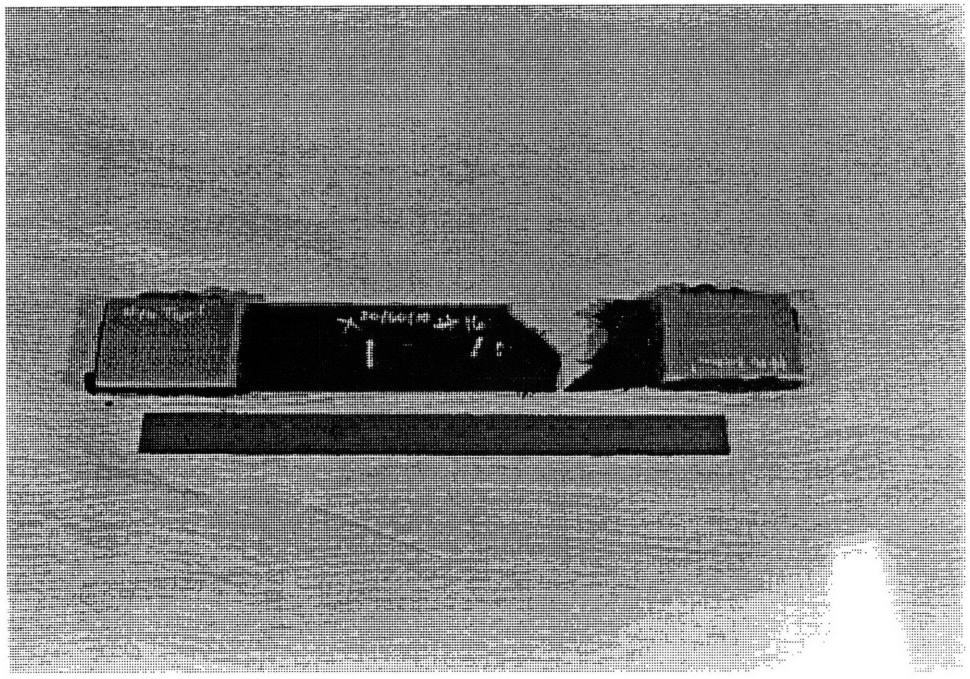

Figure C32 Picture of specimen T30/60/10-16 after testing.

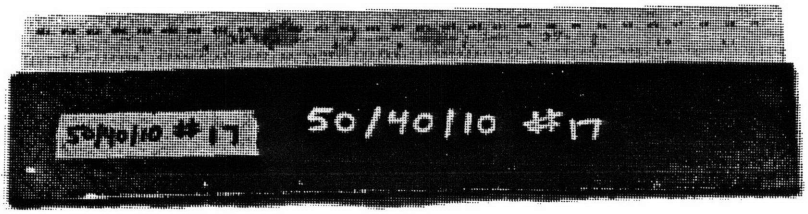

Figure C33 Picture of specimen T50/40/10-17 before testing.

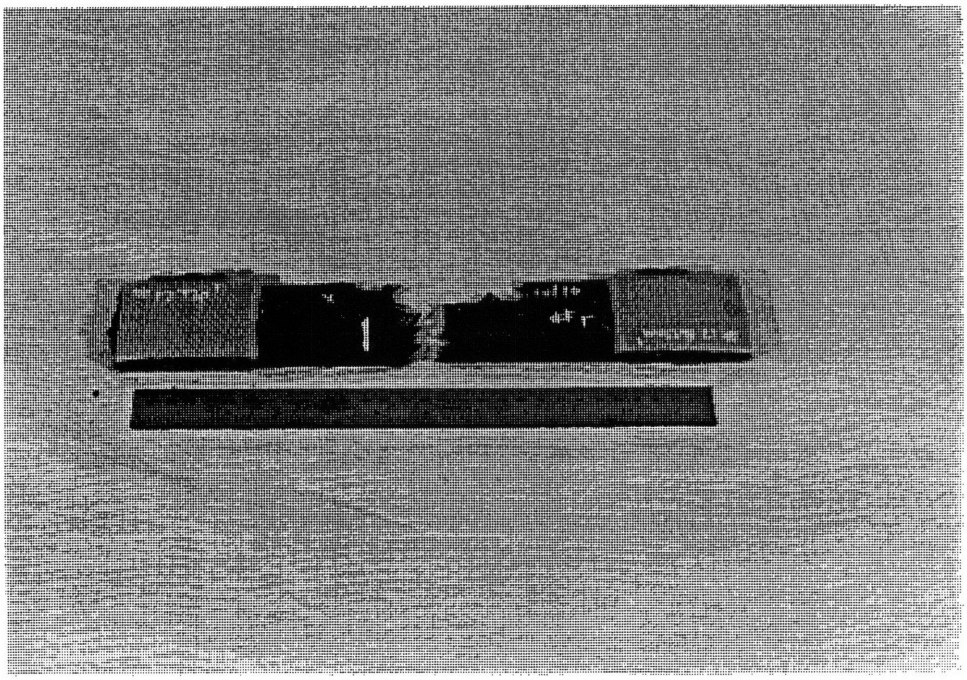

Figure C34 Picture of specimen T50/40/10-17 after testing.

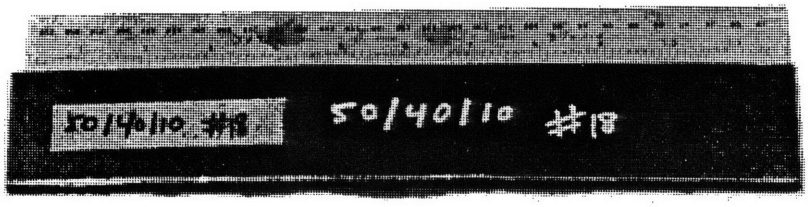

Figure C35 Picture of specimen T50/40/10-18 before testing.

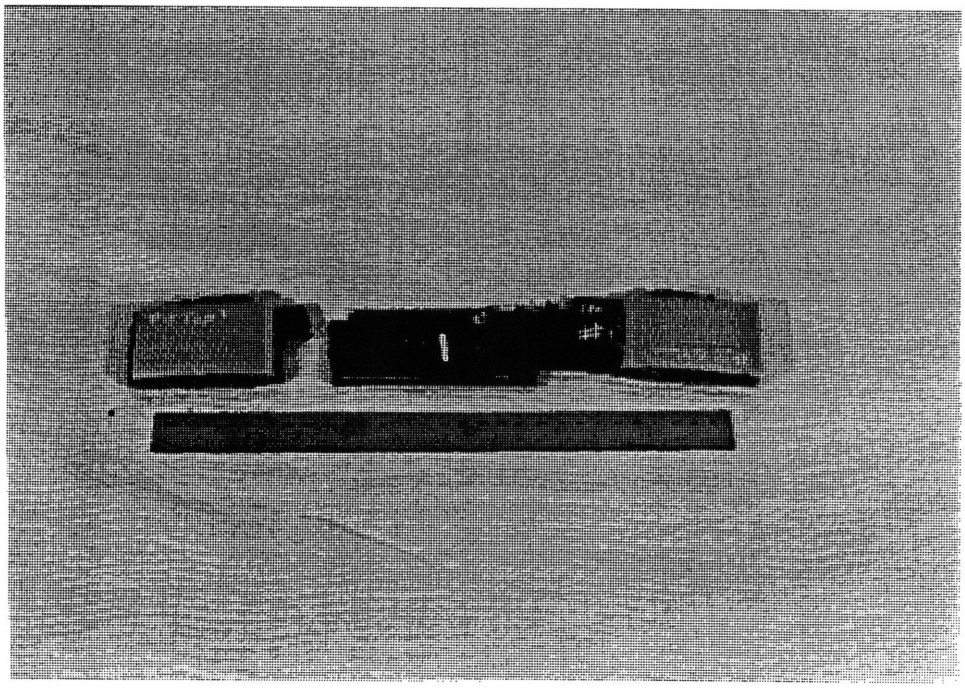

Figure C36 Picture of specimen T50/40/10-18 after testing.

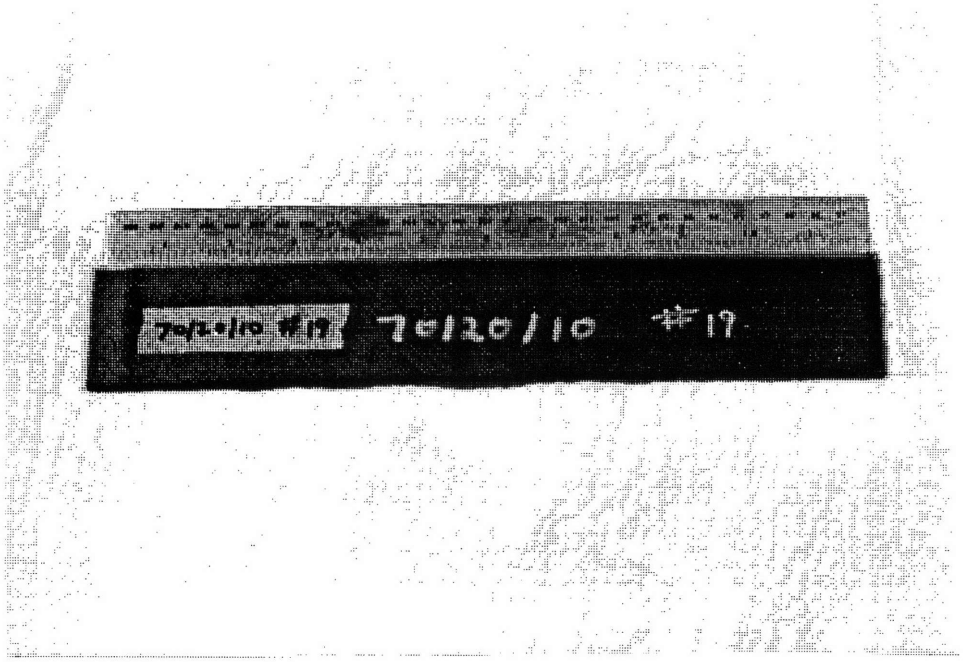

Figure C37 Picture of specimen T70/20/10-19 before testing.

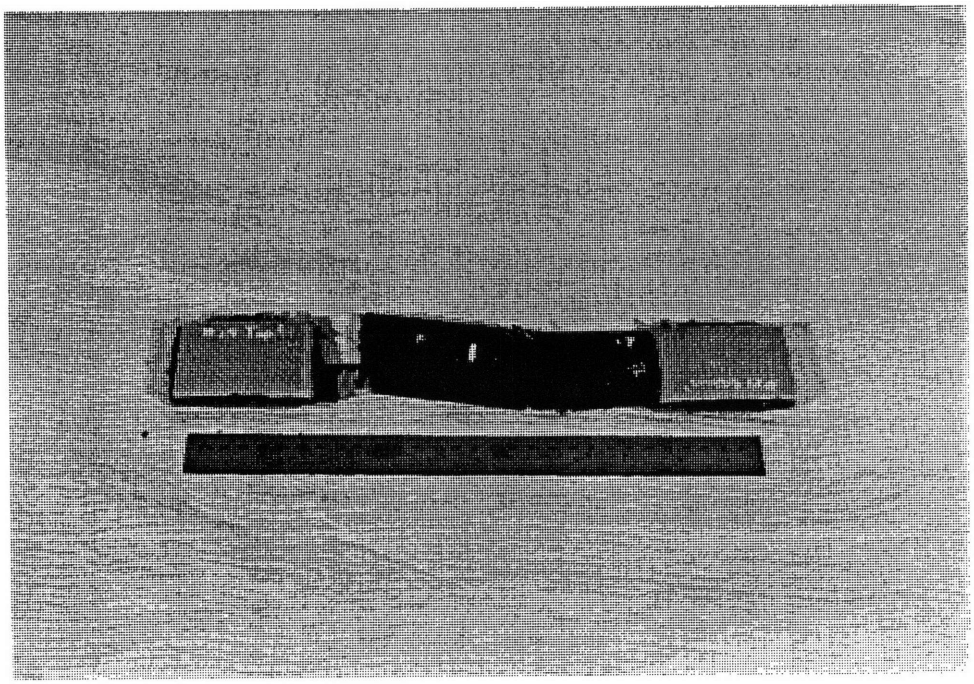

Figure C38 Picture of specimen T70/20/10-19 after testing.

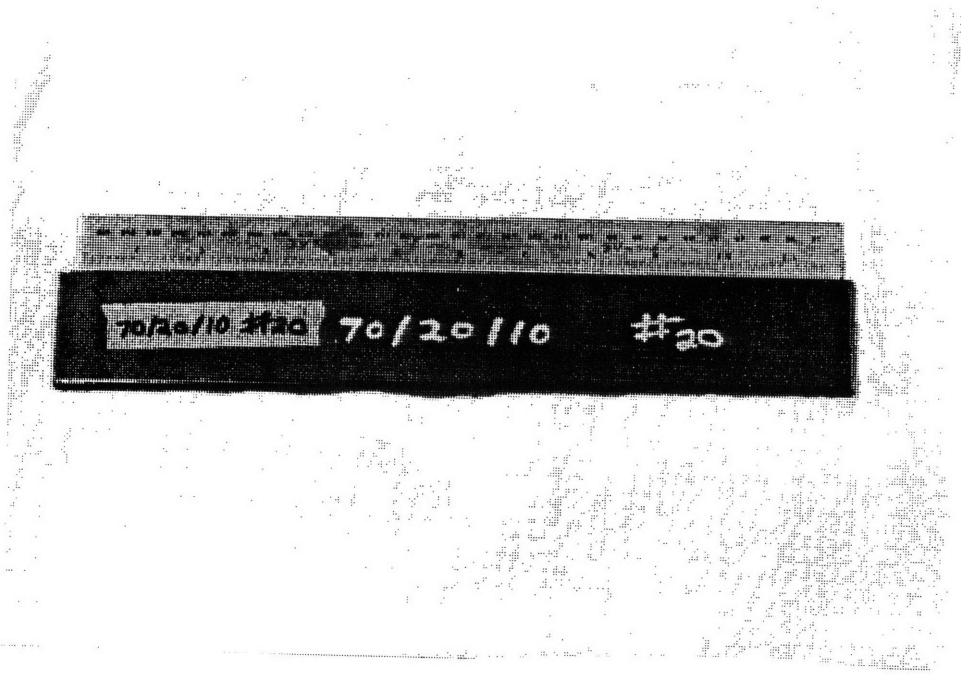

Figure C39 Picture of specimen T70/20/10-20 before testing.

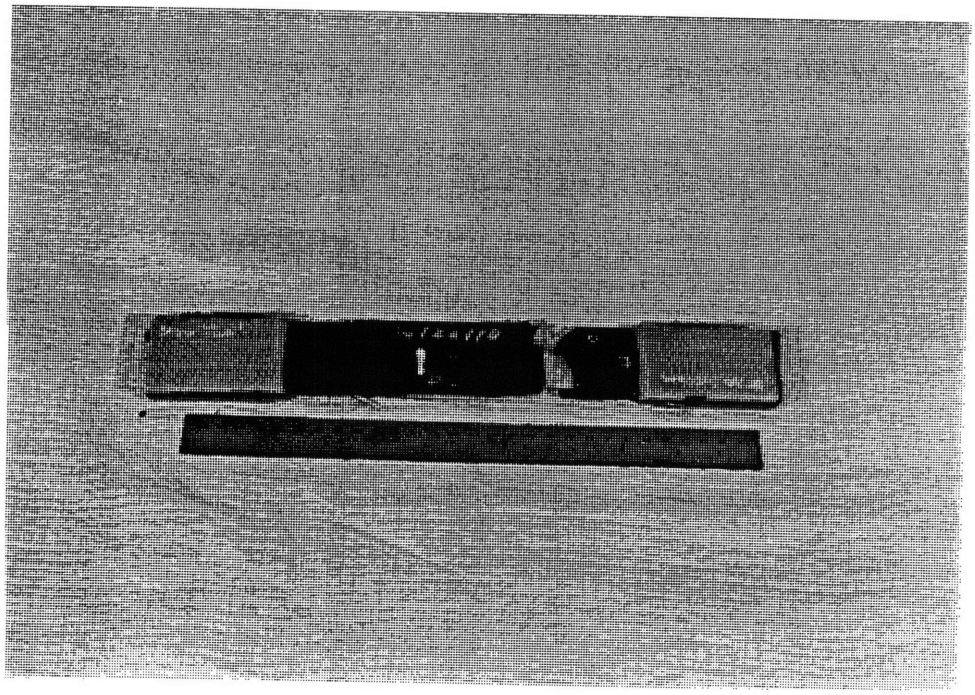

Figure C40 Picture of specimen T70/20/10-20 after testing.

Appendix D

Pictures of Bend Specimens

This Appendix contains pictures of the four bend specimens after manufacturing.

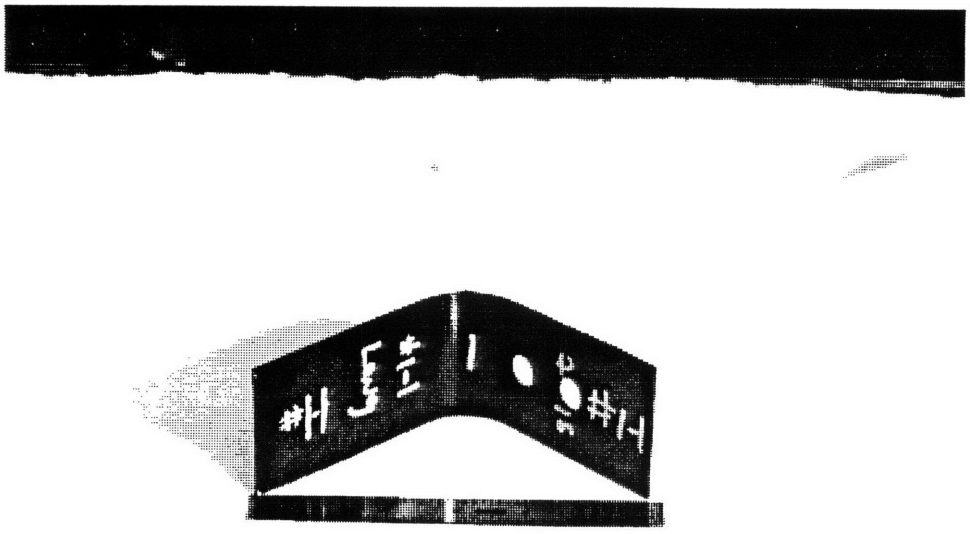

Figure D1 Picture of specimen B100/0/0-1.

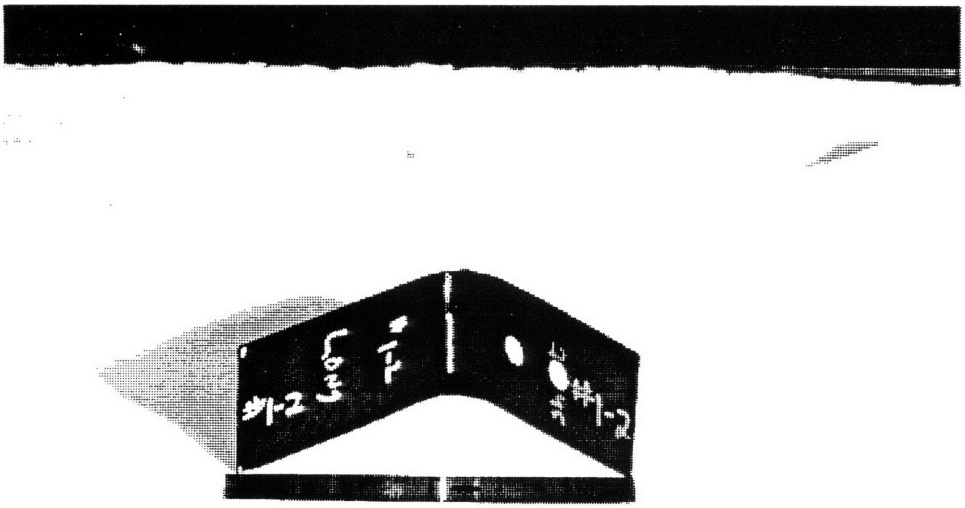

Figure D2 Picture of specimen B100/0/0-2.

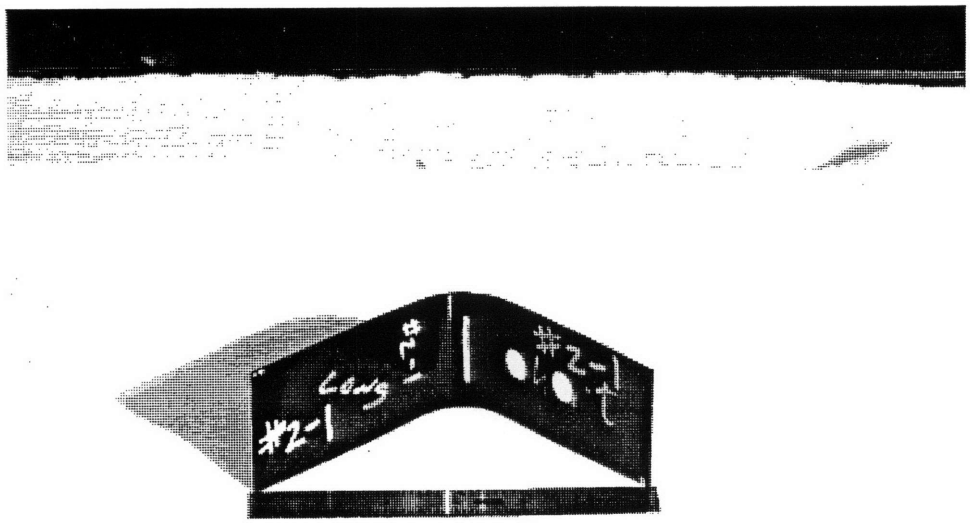

Figure D3 Picture of specimen B100/0/0-3.

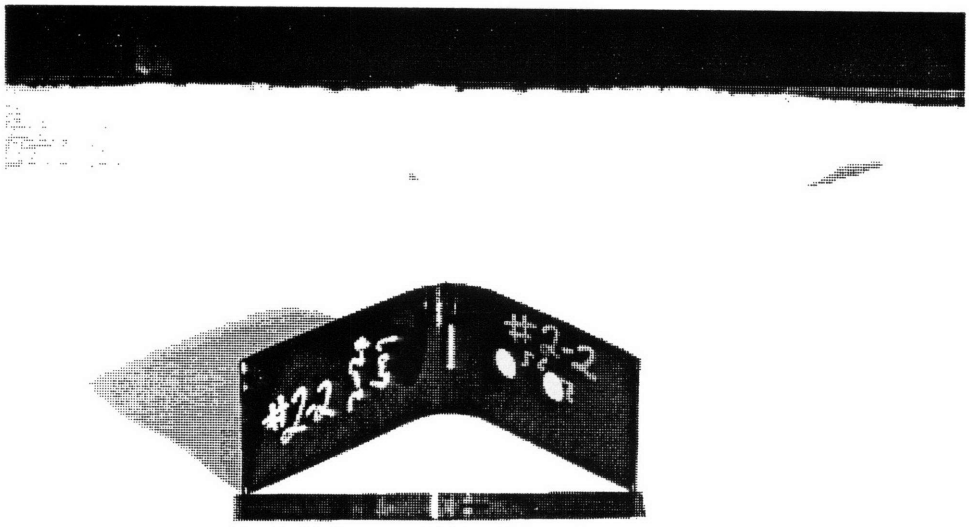

Figure D4 Picture of specimen B100/0/0-4.

Appendix E

Pictures of Testing Equipment for Tensile Coupons

This appendix contains pictures of the testing machines used for the tensile coupons. A picture is provided for the MTS testing machine, the console, the terminal, and the strain amplifier.

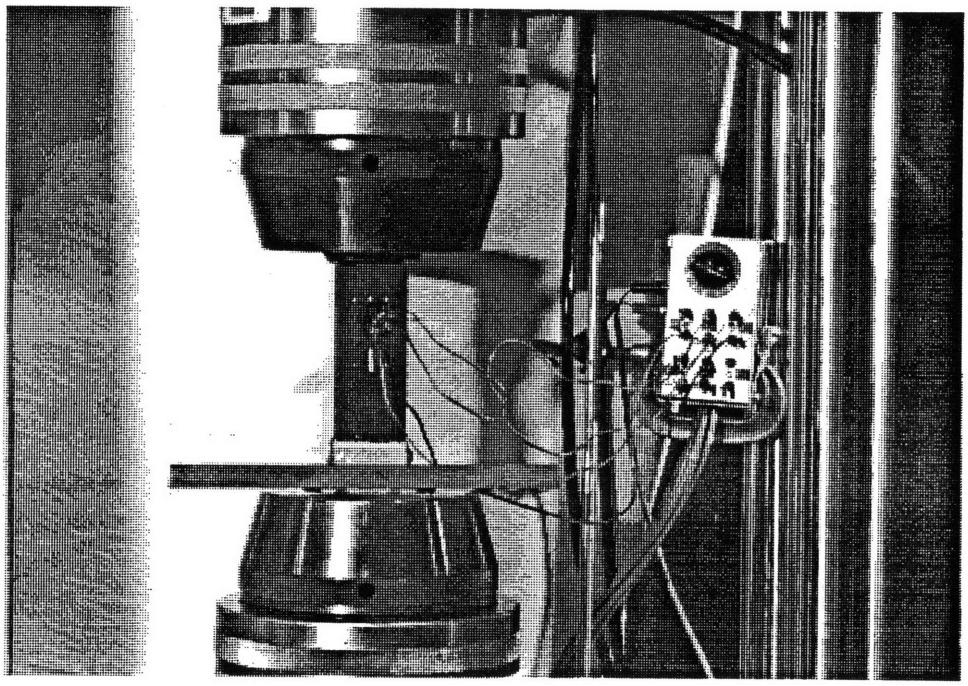

Figure E1 Picture of MTS testing machine.

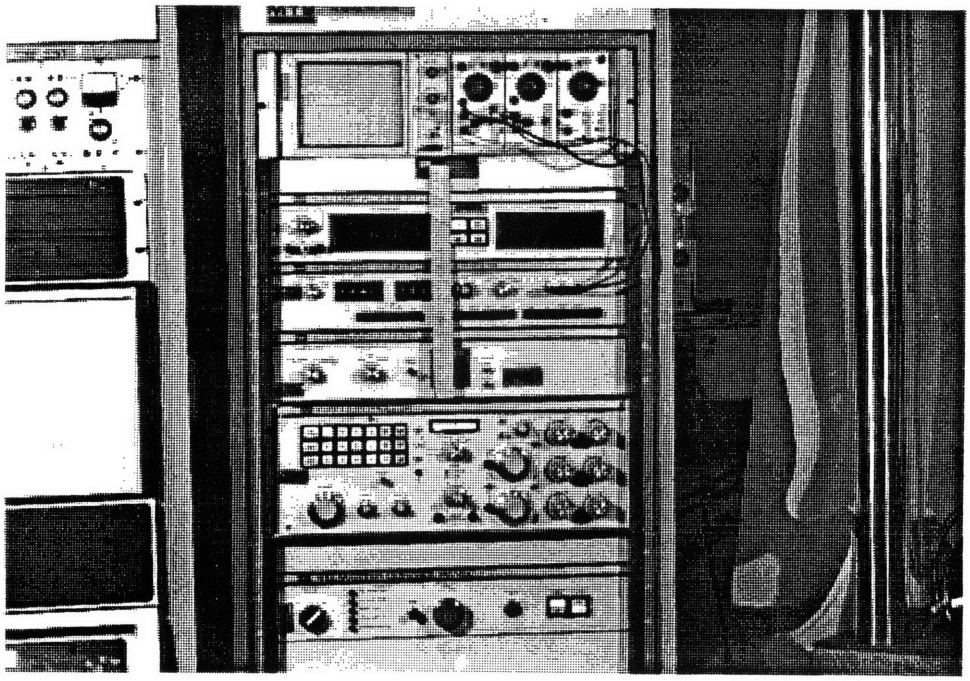

Figure E2 Picture of console for MTS machine.

Figure E3 Picture of terminal for MTS machine.

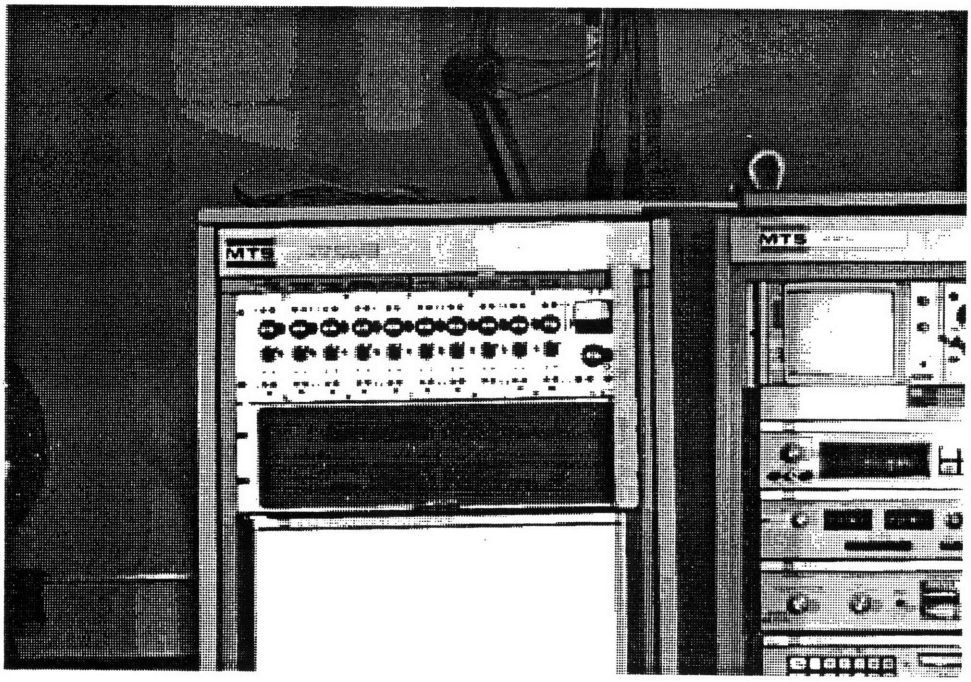

Figure E4 Picture of strain amplifier.

Appendix F

Picture of Bend Test Setup

This appendix contains a picture of the test setup used for the bend specimens.

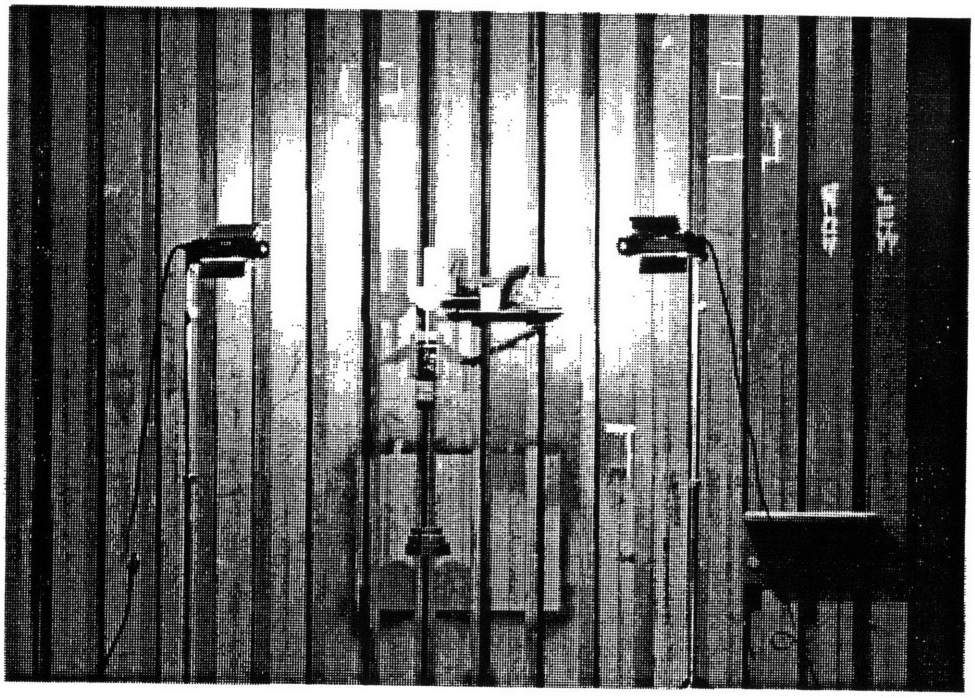

Figure F1 Picture of test setup for right angle bend specimens.

Appendix G

Picture of Small Plate Edge

This Appendix contains a typical picture of an edge of a small, unidirectional plate along the fiber direction.

Figure G1 Picture of a typical edge (P100/0/0-1) of the small plate specimens. The thickness of the specimen is 1.43 mm (.056 in) and the ruler increments are 1.59 mm (.063 in).

Appendix H

Stress-Strain Graphs for the Tensile Coupons

This Appendix contains the stress-strain graphs for all the tensile coupons for the four strain gages, three within the rosette and one standard gage on the other surface of the tensile coupon.

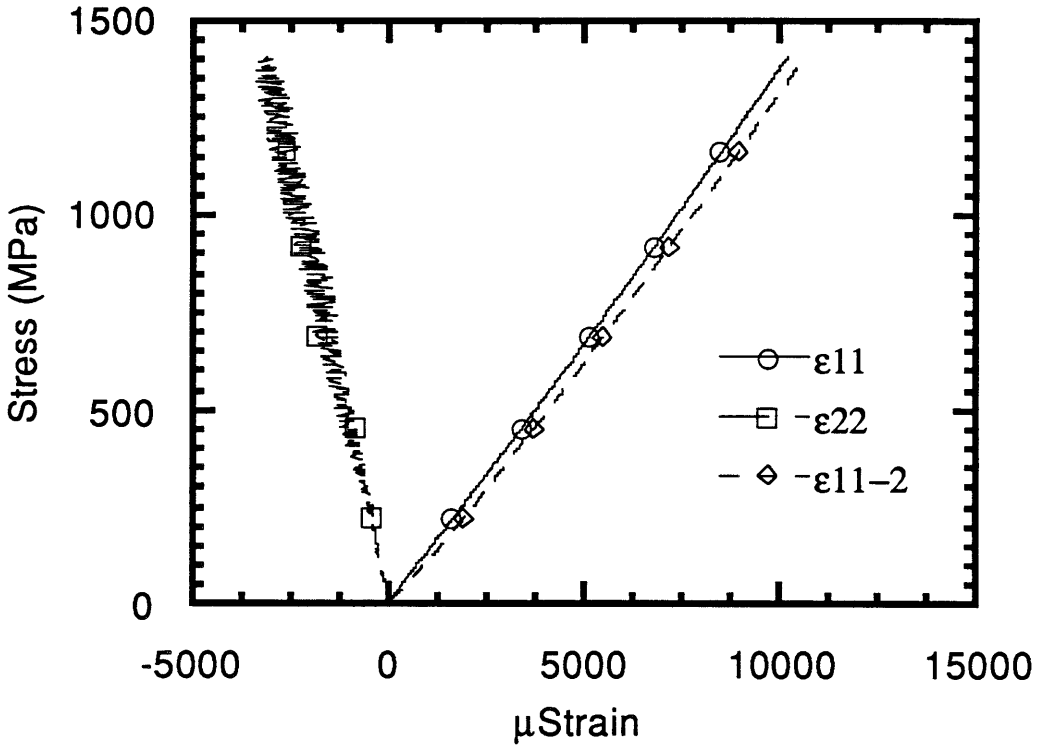

Figure H1 Stress vs. strain graph of specimen T100/0/0-9. The stress is the applied stress by the MTS machine. ε_{11} and ε_{22} are principal strains calculated from the rosette strain gage in the longitudnal and transverse axes of the coupon. ε_{11}-2 is the strain reading from the single gage on the other surface of the coupon and is not a principal strain. The symbols only identify the corresponding line; the symbols are not data points. The lines consist of only data points.

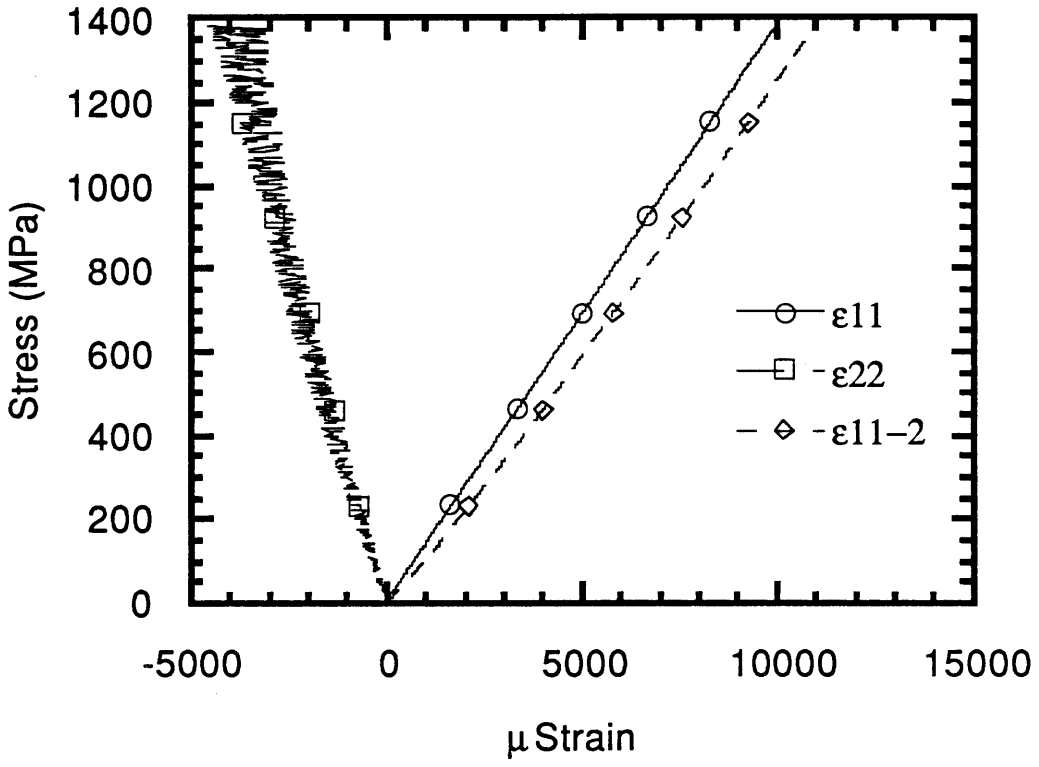

Figure H2 Stress vs. strain graph of specimen T100/0/0-10. The stress is the applied stress by the MTS machine. ε_{11} and ε_{22} are principal strains calculated from the rosette strain gage in the longitudnal and transverse axes of the coupon. ε_{11}-2 is the strain reading from the single gage on the other surface of the coupon and is not a principal strain. The symbols only identify the corresponding line; the symbols are not data points. The lines consist of only data points.

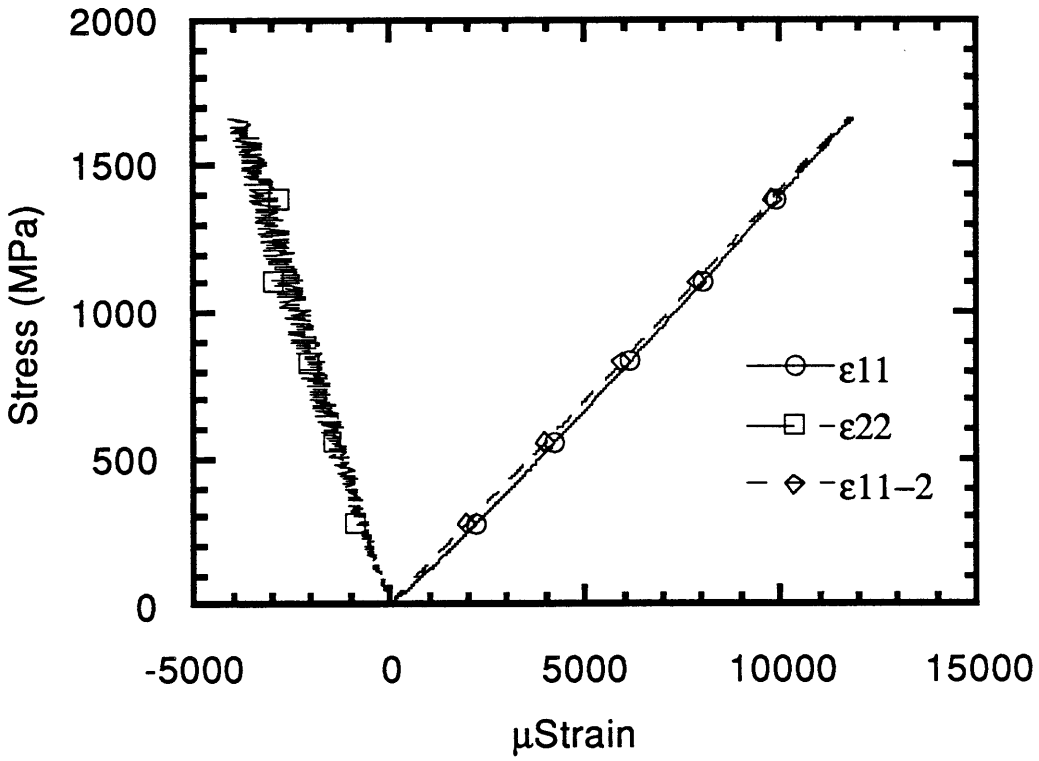

Figure H3 Stress vs. strain graph of specimen T100/0/0-11. The stress is the applied stress by the MTS machine. ε_{11} and ε_{22} are principal strains calculated from the rosette strain gage in the longitudnal and transverse axes of the coupon. ε_{11}-2 is the strain reading from the single gage on the other surface of the coupon and is not a principal strain. The symbols only identify the corresponding line; the symbols are not data points. The lines consist of only data points.

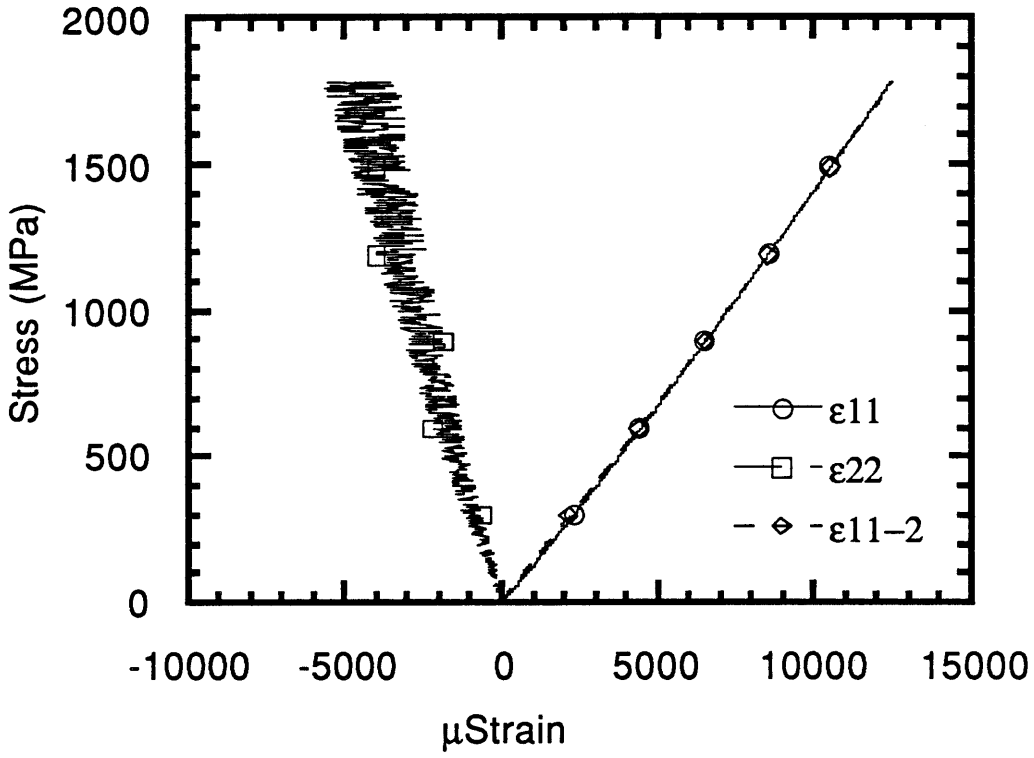

Figure H4 Stress vs. strain graph of specimen T100/0/0-12. The stress is the applied stress by the MTS machine. ε_{11} and ε_{22} are principal strains calculated from the rosette strain gage in the longitudnal and transverse axes of the coupon. ε_{11}-2 is the strain reading from the single gage on the other surface of the coupon and is not a principal strain. The symbols only identify the corresponding line; the symbols are not data points. The lines consist of only data points.

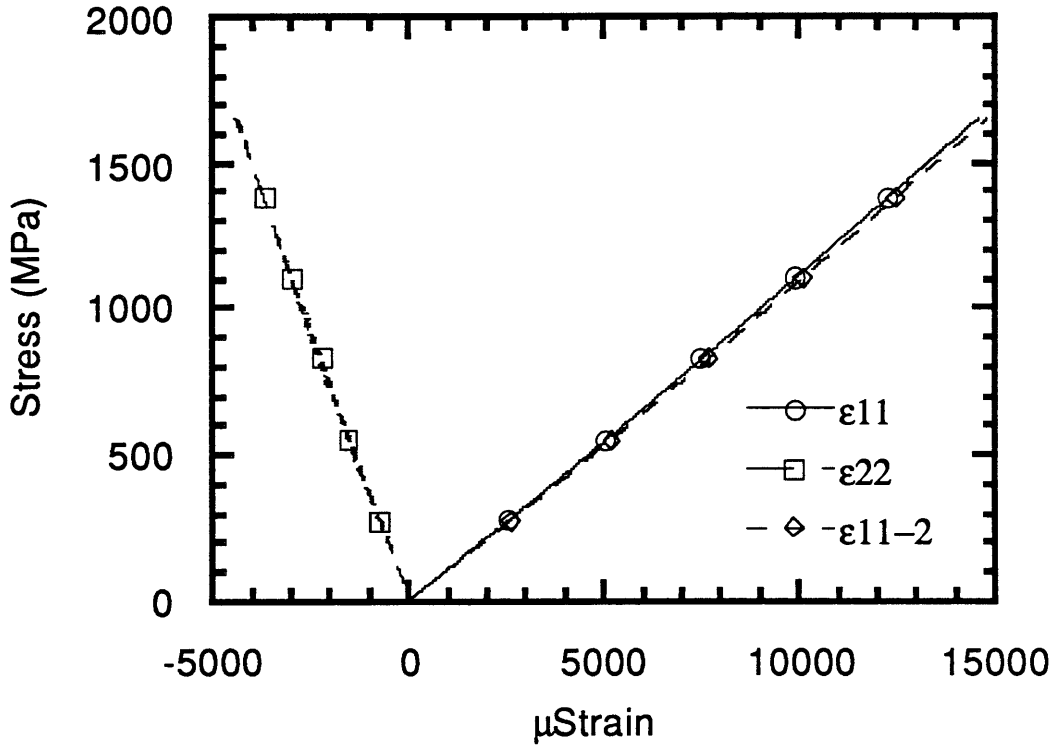

Figure H5 Stress vs. strain graph to failure of specimen T70/20/10-19. The stress is the applied stress by the MTS machine. ε_{11} and ε_{22} are principal strains calculated from the rosette strain gage in the longitudnal and transverse axes of the coupon. ε_{11}-2 is the strain reading from the single gage on the other surface of the coupon and is not a principal strain. The symbols only identify the corresponding line; the symbols are not data points. The lines consist of only data points.

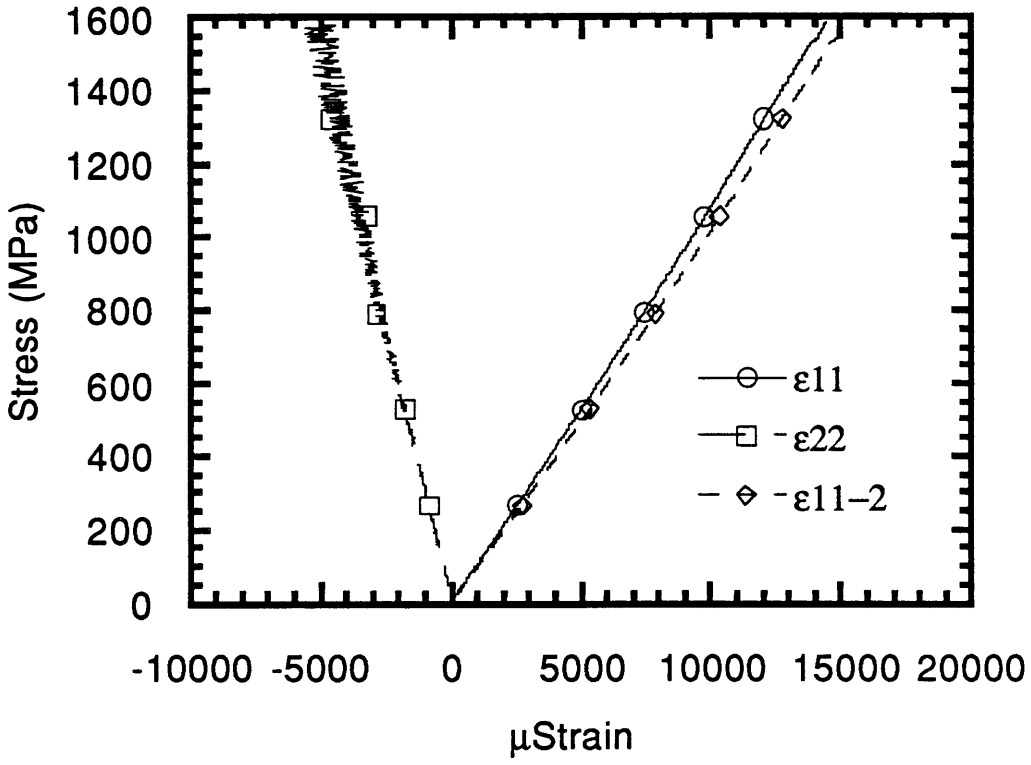

Figure H6 Stress vs. strain graph to failure of specimen T70/20/10-20. The stress is the applied stress by the MTS machine. ε_{11} and ε_{22} are principal strains calculated from the rosette strain gage in the longitudnal and transverse axes of the coupon. ε_{11}-2 is the strain reading from the single gage on the other surface of the coupon and is not a principal strain. The symbols only identify the corresponding line; the symbols are not data points. The lines consist of only data points.

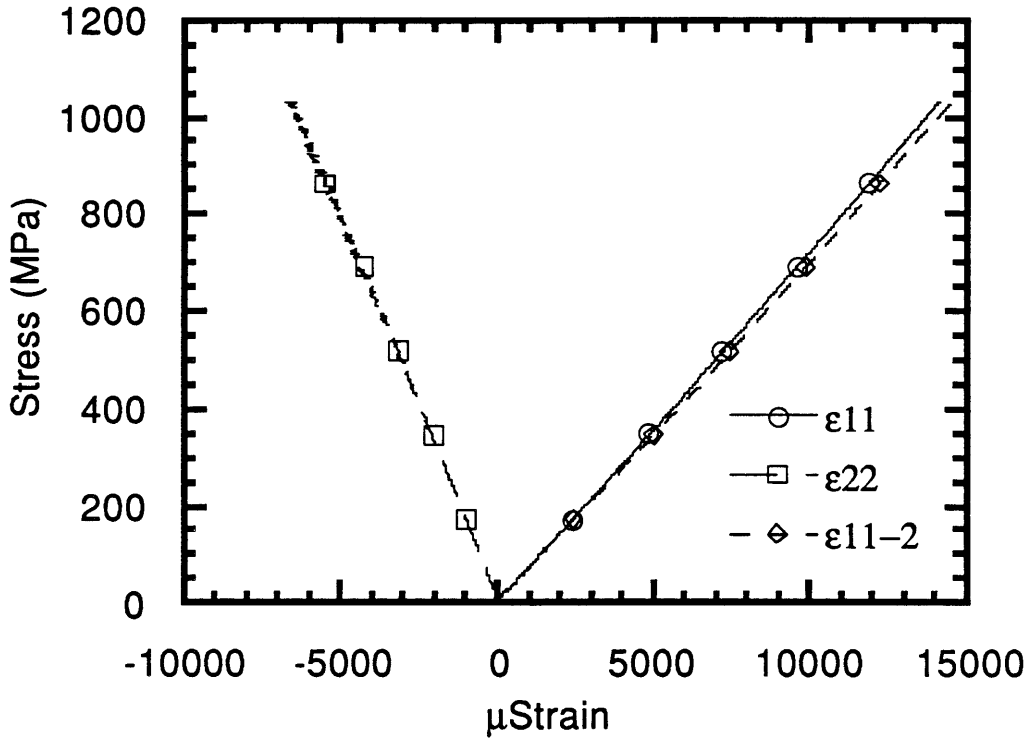

Figure H7 Stress vs. strain graph to failure of specimen T50/40/10-17. The stress is the applied stress by the MTS machine. ε_{11} and ε_{22} are principal strains calculated from the rosette strain gage in the longitudnal and transverse axes of the coupon. ε_{11}-2 is the strain reading from the single gage on the other surface of the coupon and is not a principal strain. The symbols only identify the corresponding line; the symbols are not data points. The lines consist of only data points.

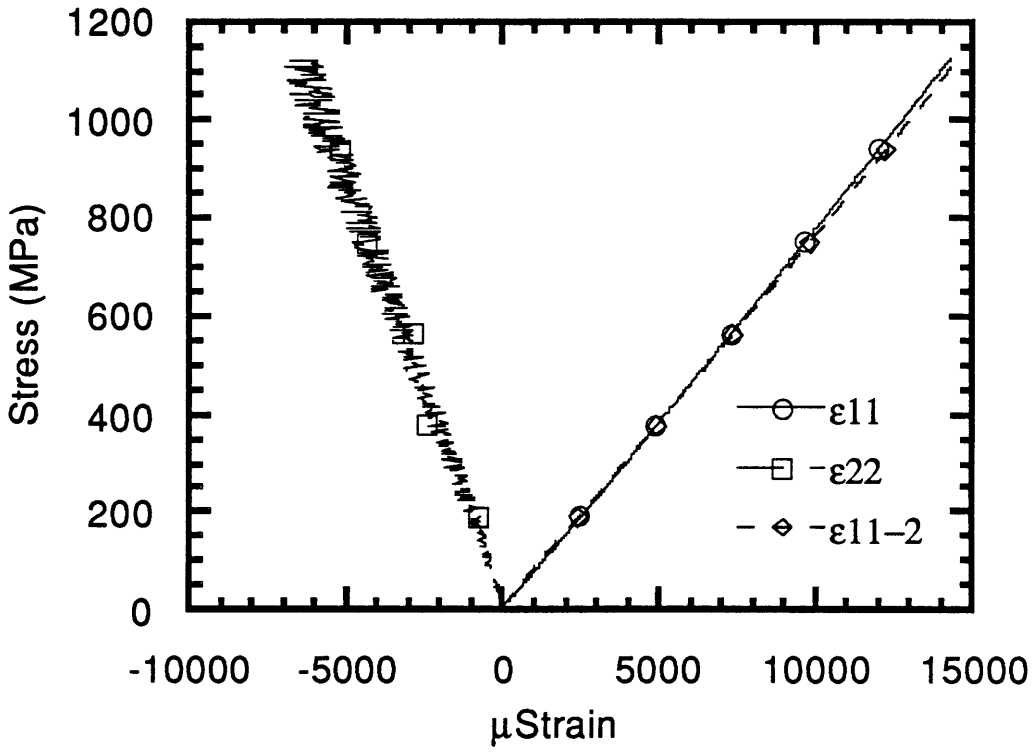

Figure H8 Stress vs. strain graph to failure of specimen T50/40/10-18. The stress is the applied stress by the MTS machine. ε_{11} and ε_{22} are principal strains calculated from the rosette strain gage in the longitudnal and transverse axes of the coupon. ε_{11}-2 is the strain reading from the single gage on the other surface of the coupon and is not a principal strain. The symbols only identify the corresponding line; the symbols are not data points. The lines consist of only data points.

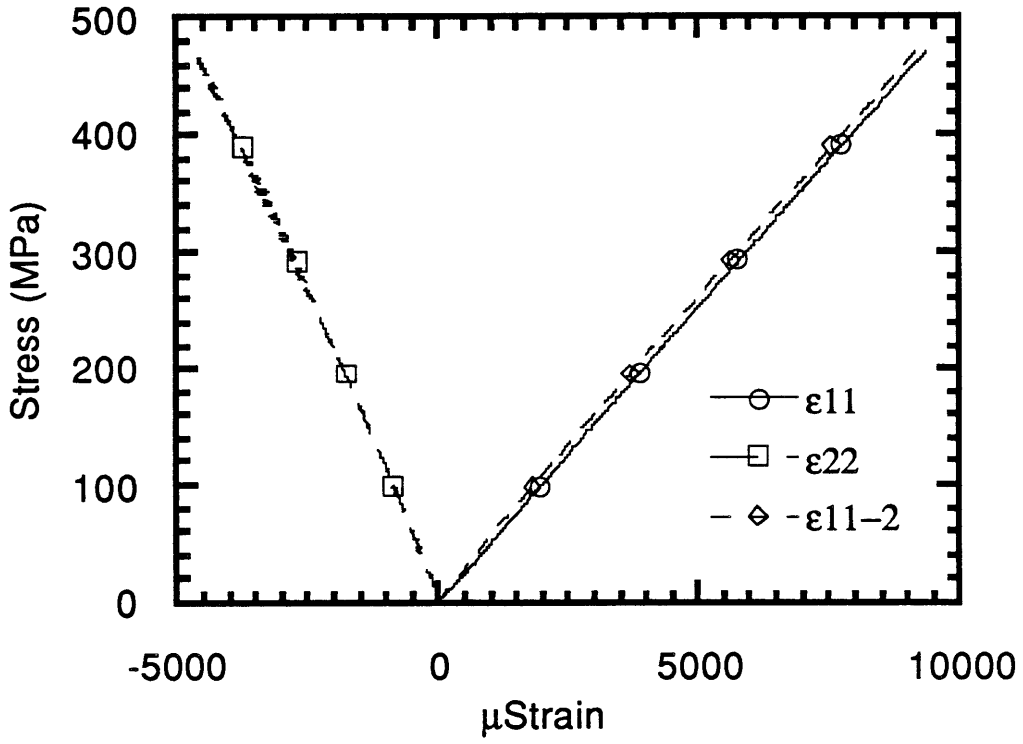

Figure H9 Stress vs. strain graph of specimen T30/60/10-13. The stress is the applied stress by the MTS machine. ε_{11} and ε_{22} are principal strains calculated from the rosette strain gage in the longitudnal and transverse axes of the coupon. ε_{11}-2 is the strain reading from the single gage on the other surface of the coupon and is not a principal strain. The symbols only identify the corresponding line; the symbols are not data points. The lines consist of only data points.

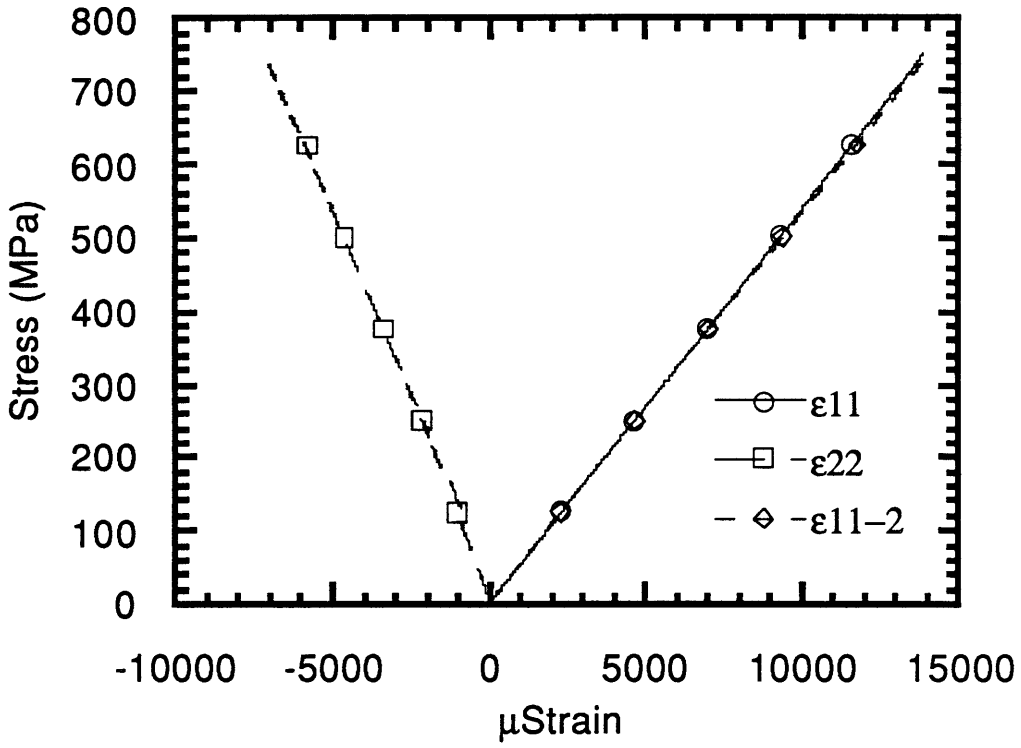

Figure H10 Stress vs. strain graph to failure of specimen T30/60/10-14. The stress is the applied stress by the MTS machine. ε_{11} and ε_{22} are principal strains calculated from the rosette strain gage in the longitudnal and transverse axes of the coupon. ε_{11}-2 is the strain reading from the single gage on the other surface of the coupon and is not a principal strain. The symbols only identify the corresponding line; the symbols are not data points. The lines consist of only data points.

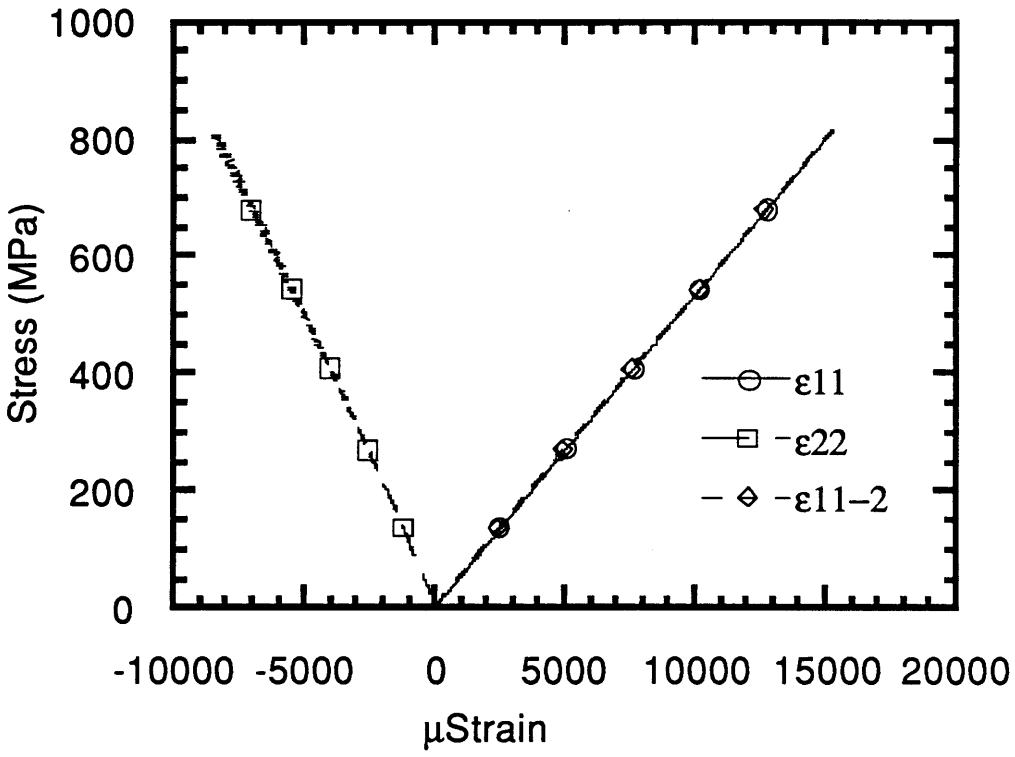

Figure H11 Stress vs. strain graph to failure of specimen T30/60/10-15. The stress is the applied stress by the MTS machine. ε_{11} and ε_{22} are principal strains calculated from the rosette strain gage in the longitudnal and transverse axes of the coupon. ε_{11}-2 is the strain reading from the single gage on the other surface of the coupon and is not a principal strain. The symbols only identify the corresponding line; the symbols are not data points. The lines consist of only data points.

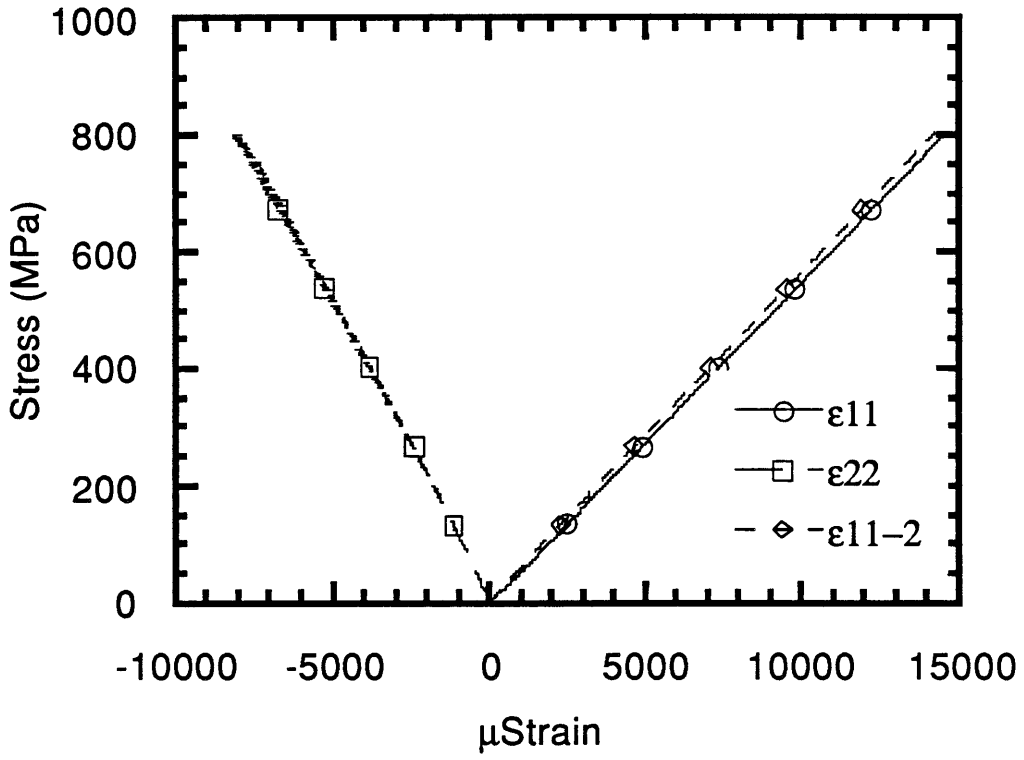

Figure H12 Stress vs. strain graph to failure of specimen T30/60/10-16. The stress is the applied stress by the MTS machine. ε_{11} and ε_{22} are principal strains calculated from the rosette strain gage in the longitudnal and transverse axes of the coupon. ε_{11}-2 is the strain reading from the single gage on the other surface of the coupon and is not a principal strain. The symbols only identify the corresponding line; the symbols are not data points. The lines consist of only data points.

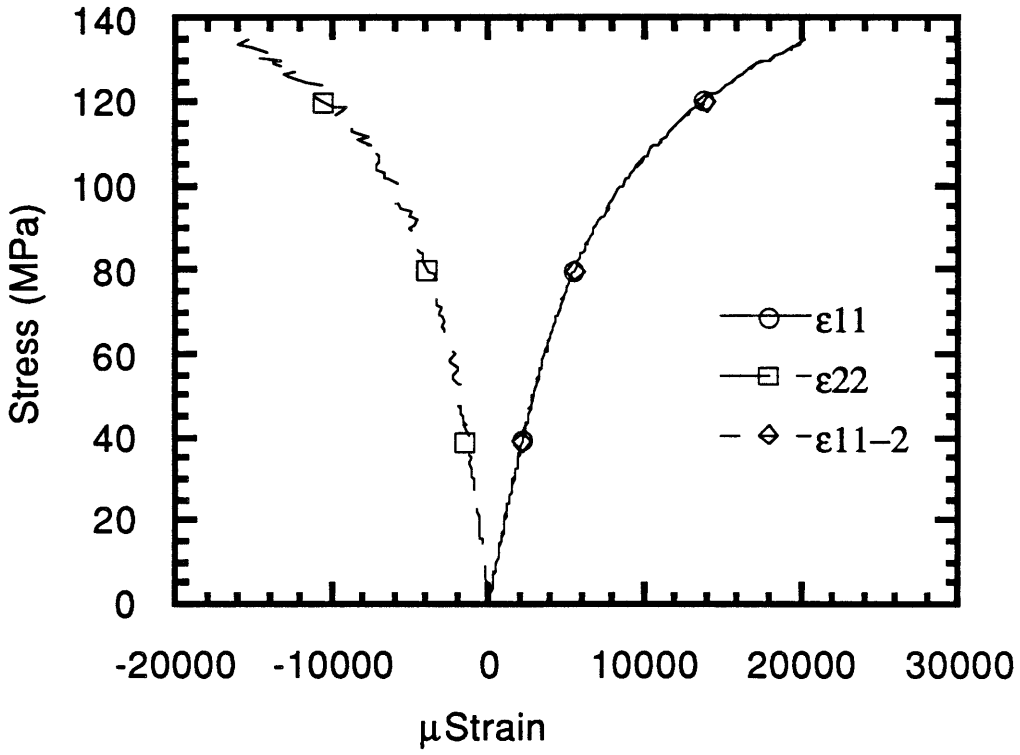

Figure H13 Stress vs. strain graph of specimen T0/100/0-1. The stress is the applied stress by the MTS machine. ε_{11} and ε_{22} are principal strains calculated from the rosette strain gage in the longitudnal and transverse axes of the coupon. ε_{11}-2 is the strain reading from the single gage on the other surface of the coupon and is not a principal strain. The symbols only identify the corresponding line; the symbols are not data points. The lines consist of only data points.

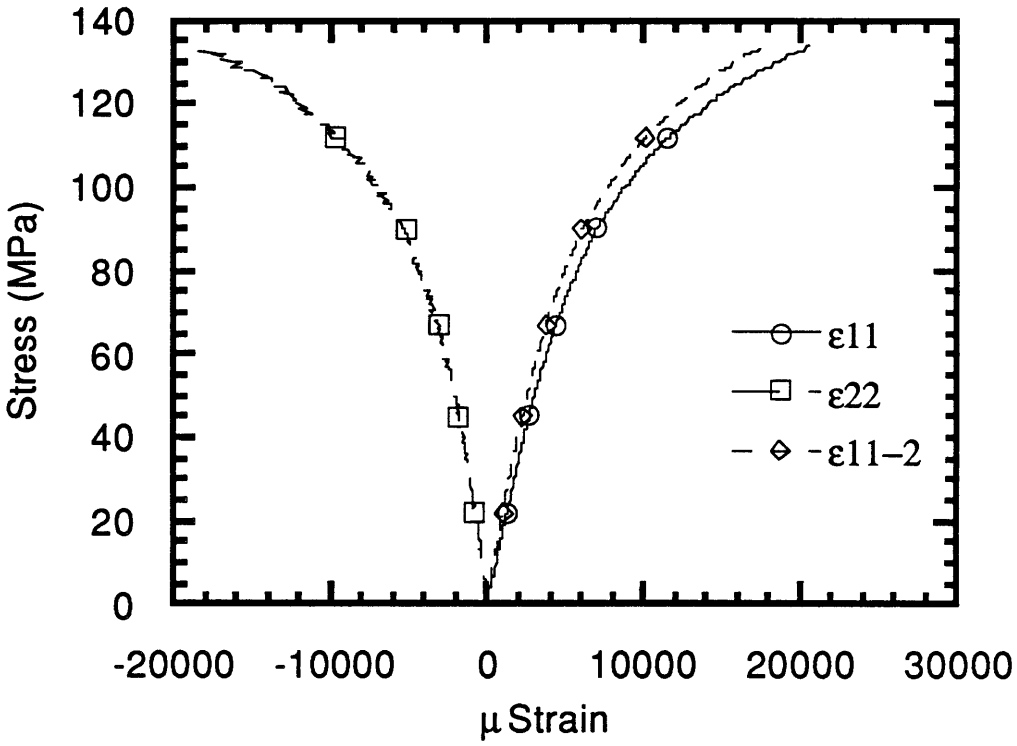

Figure H14 Stress vs. strain graph of specimen T0/100/0-2. The stress is the applied stress by the MTS machine. ε_{11} and ε_{22} are principal strains calculated from the rosette strain gage in the longitudnal and transverse axes of the coupon. ε_{11}-2 is the strain reading from the single gage on the other surface of the coupon and is not a principal strain. The symbols only identify the corresponding line; the symbols are not data points. The lines consist of only data points.

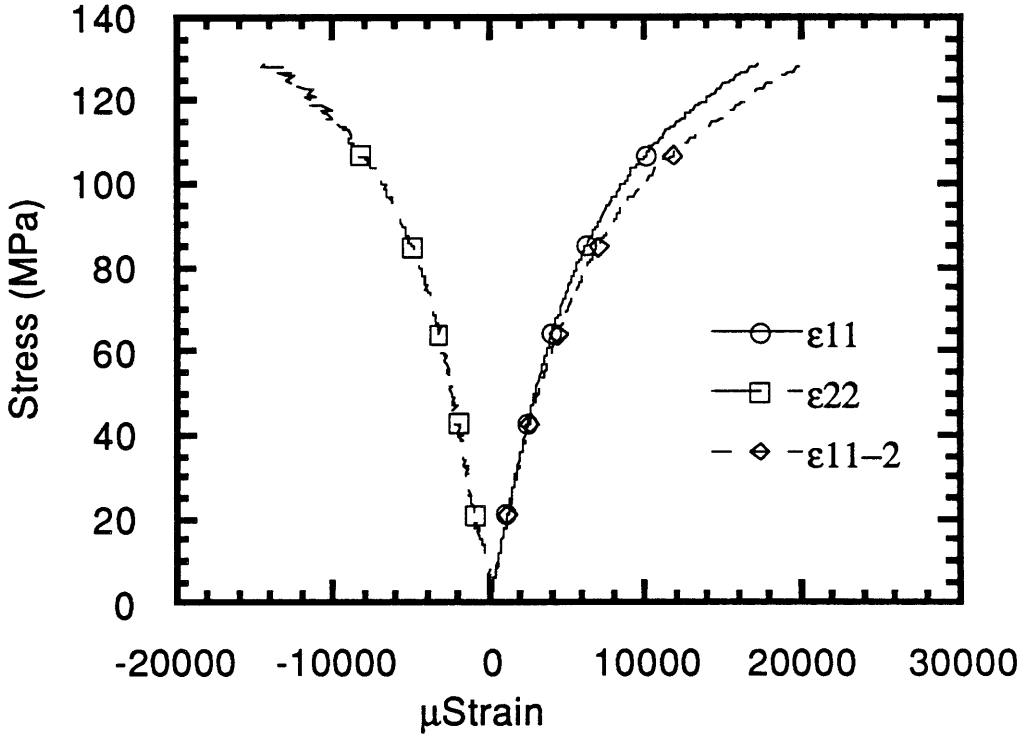

Figure H15 Stress vs. strain graph of specimen T0/100/0-3. The stress is the applied stress by the MTS machine. ε_{11} and ε_{22} are principal strains calculated from the rosette strain gage in the longitudnal and transverse axes of the coupon. ε_{11}-2 is the strain reading from the single gage on the other surface of the coupon and is not a principal strain. The symbols only identify the corresponding line; the symbols are not data points. The lines consist of only data points.

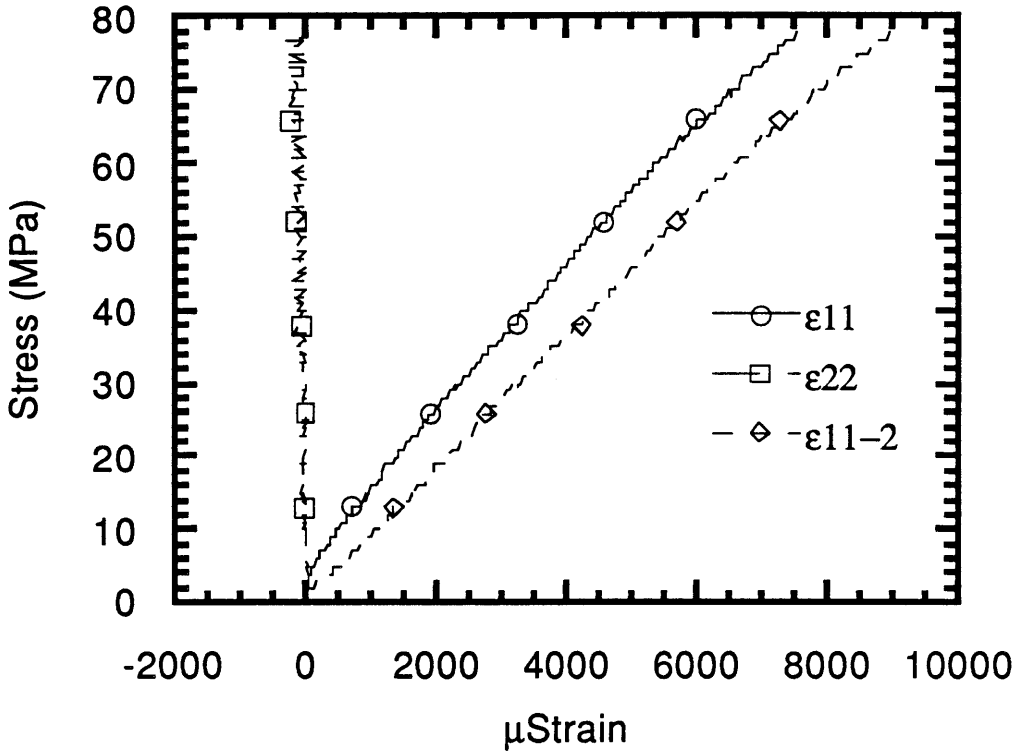

Figure H16 Stress vs. strain graph to failure of specimen T0/0/100-5. The stress is the applied stress by the MTS machine. ε_{11} and ε_{22} are principal strains calculated from the rosette strain gage in the longitudnal and transverse axes of the coupon. ε_{11}-2 is the strain reading from the single gage on the other surface of the coupon and is not a principal strain. The symbols only identify the corresponding line; the symbols are not data points. The lines consist of only data points.

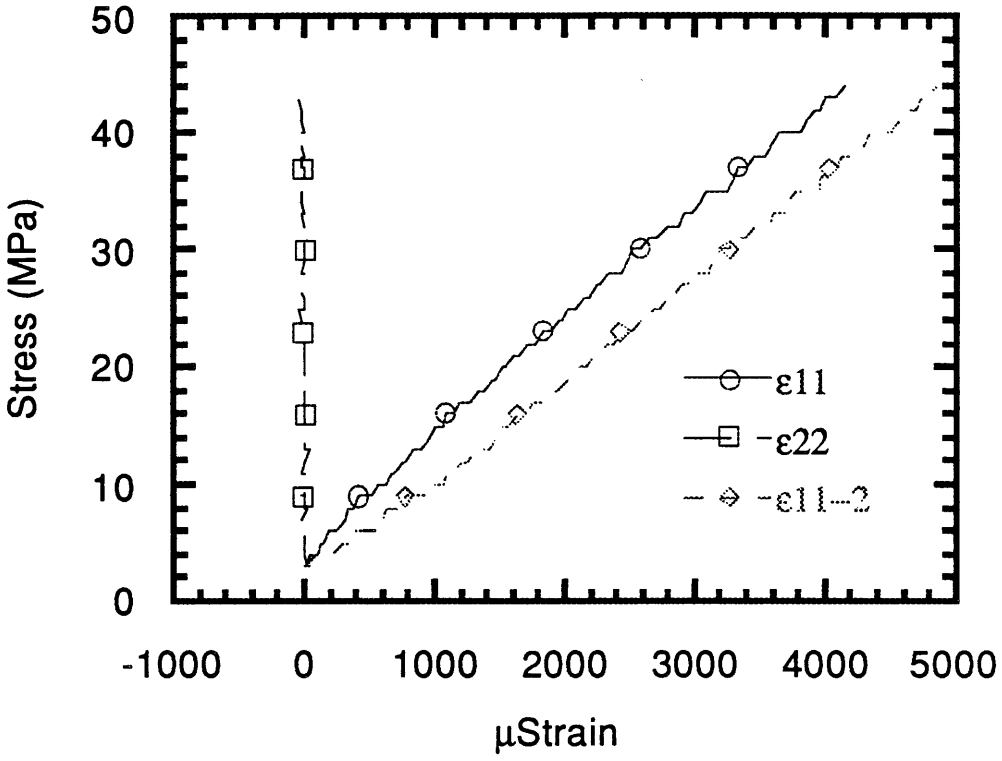

Figure H17 Stress vs. strain graph to failure of specimen T0/0/100-6. The stress is the applied stress by the MTS machine. ε_{11} and ε_{22} are principal strains calculated from the rosette strain gage in the longitudnal and transverse axes of the coupon. ε_{11}-2 is the strain reading from the single gage on the other surface of the coupon and is not a principal strain. The symbols only identify the corresponding line; the symbols are not data points. The lines consist of only data points.

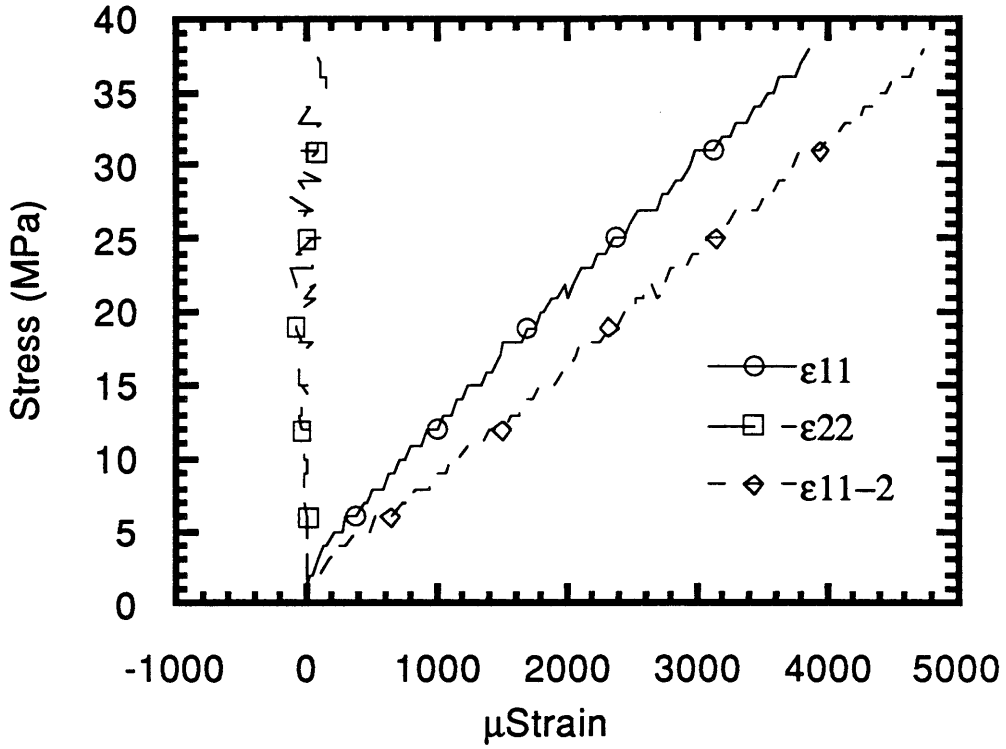

Figure H18 Stress vs. strain graph to failure of specimen T0/0/100-7. The stress is the applied stress by the MTS machine. ε_{11} and ε_{22} are principal strains calculated from the rosette strain gage in the longitudnal and transverse axes of the coupon. ε_{11}-2 is the strain reading from the single gage on the other surface of the coupon and is not a principal strain. The symbols only identify the corresponding line; the symbols are not data points. The lines consist of only data points.

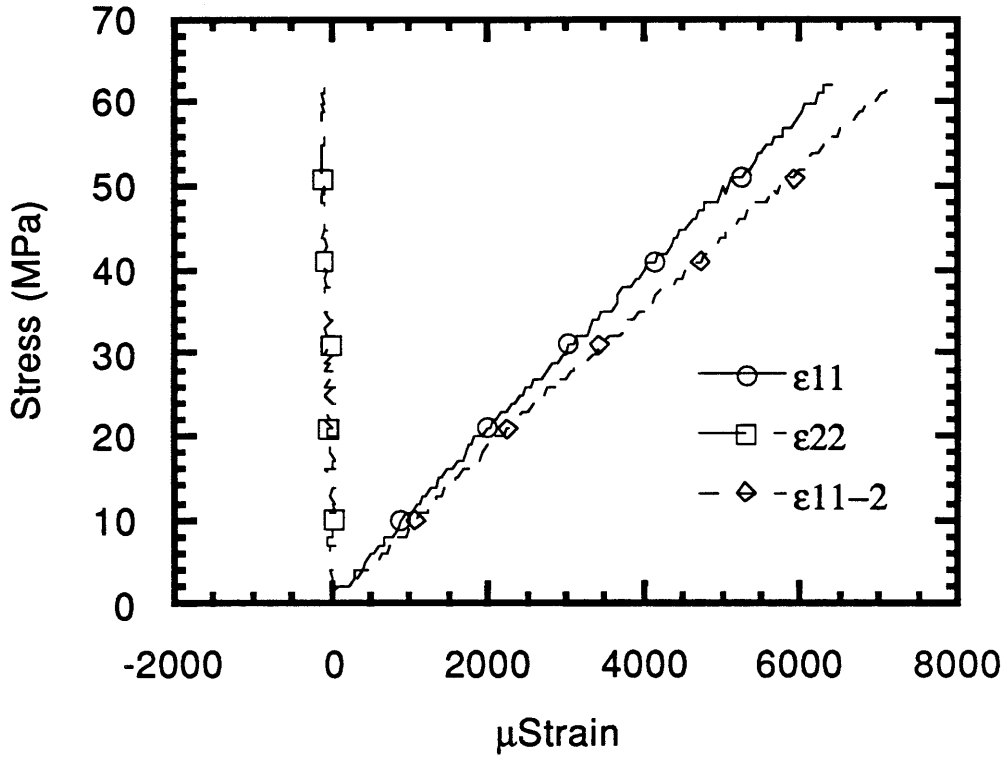

Figure H19 Stress vs. strain graph to failure of specimen T0/0/100-8. The stress is the applied stress by the MTS machine. ε_{11} and ε_{22} are principal strains calculated from the rosette strain gage in the longitudnal and transverse axes of the coupon. ε_{11}-2 is the strain reading from the single gage on the other surface of the coupon and is not a principal strain. The symbols only identify the corresponding line; the symbols are not data points. The lines consist of only data points.

Appendix I

Pictures of Tensile Coupon Edges

This Appendix contains pictures of the edges in the fiber direction of each type of laminate. The bottom half of each picture is a ruler; the vertical lines represent 1.59 mm (.0625 in).

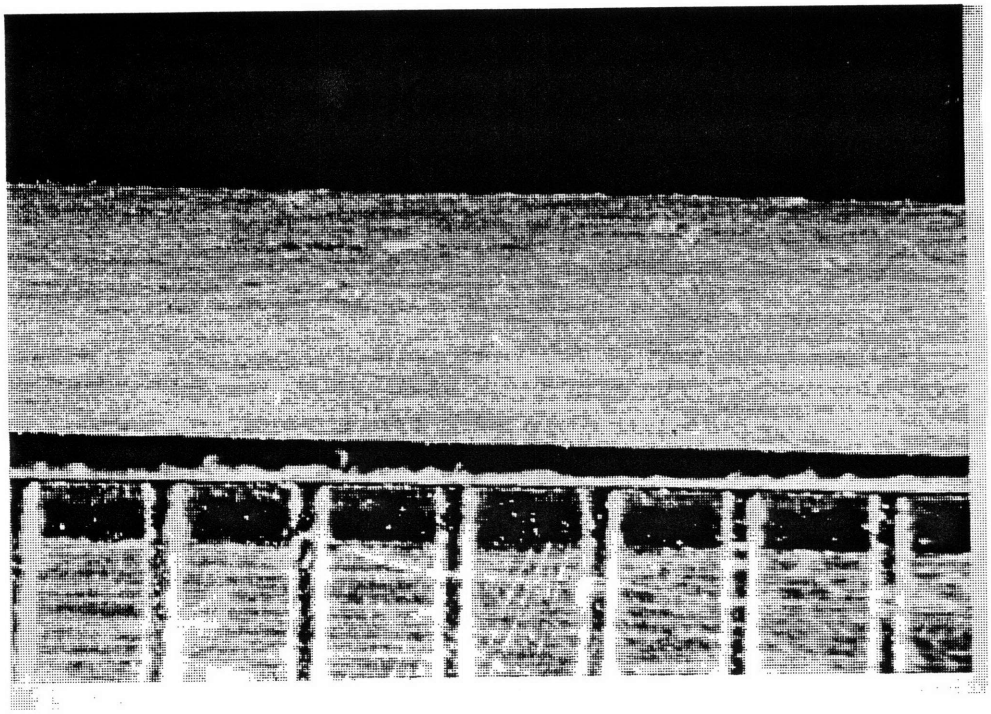

Figure I1 Picture of edge of specimen T0/100/0-2.

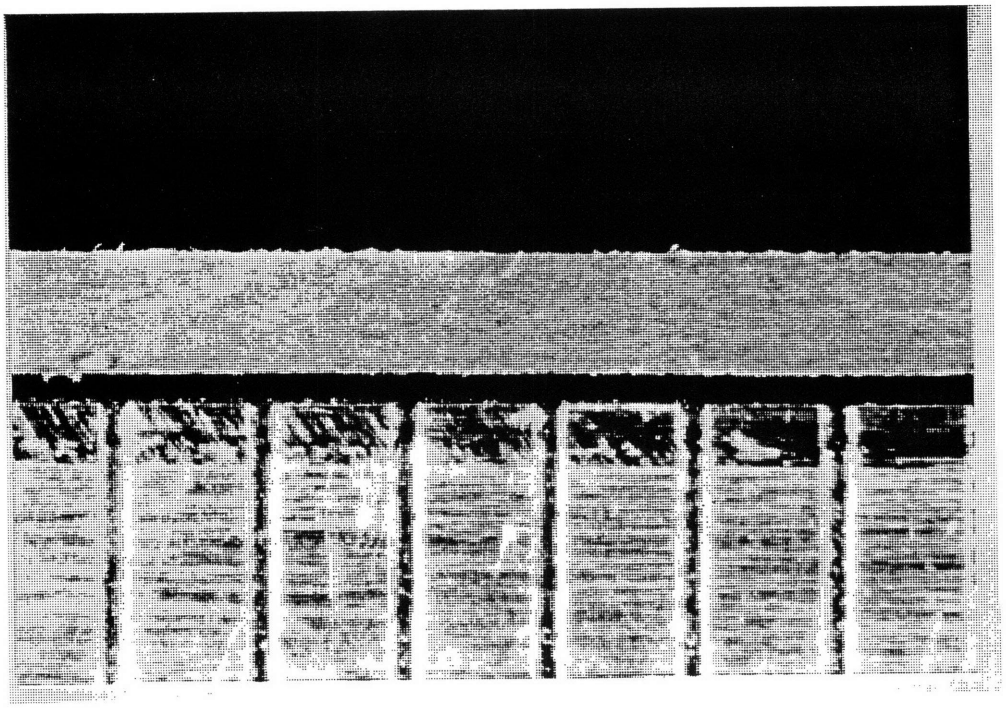

Figure I2 Picture of edge of specimen T0/0/100-6.

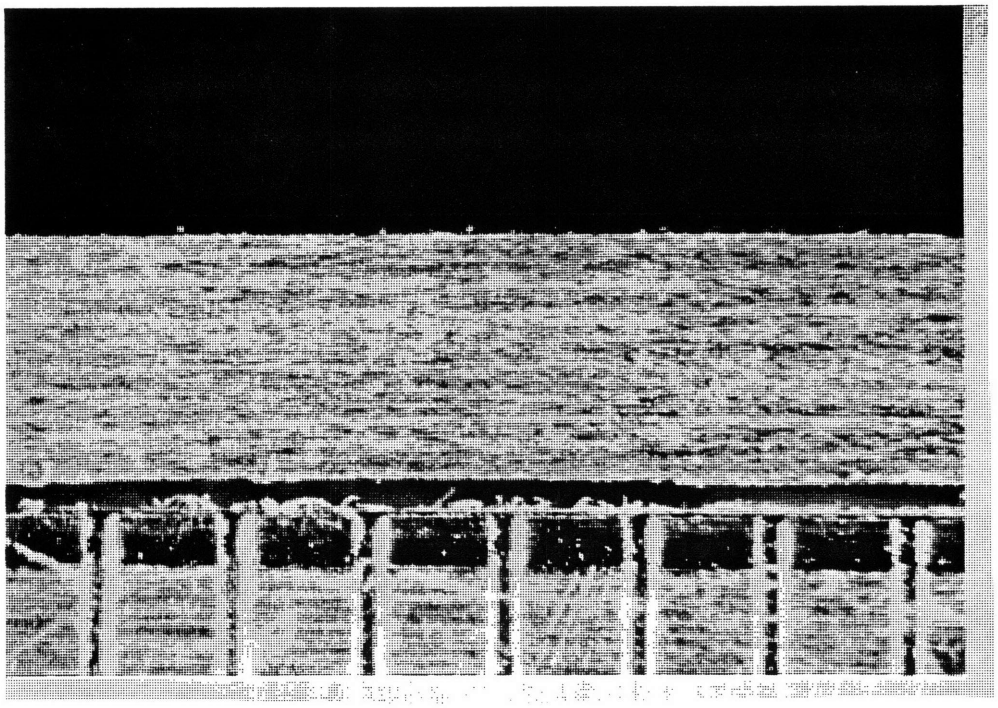

Figure I3 Picture of edge of specimen 100/0/0-10.

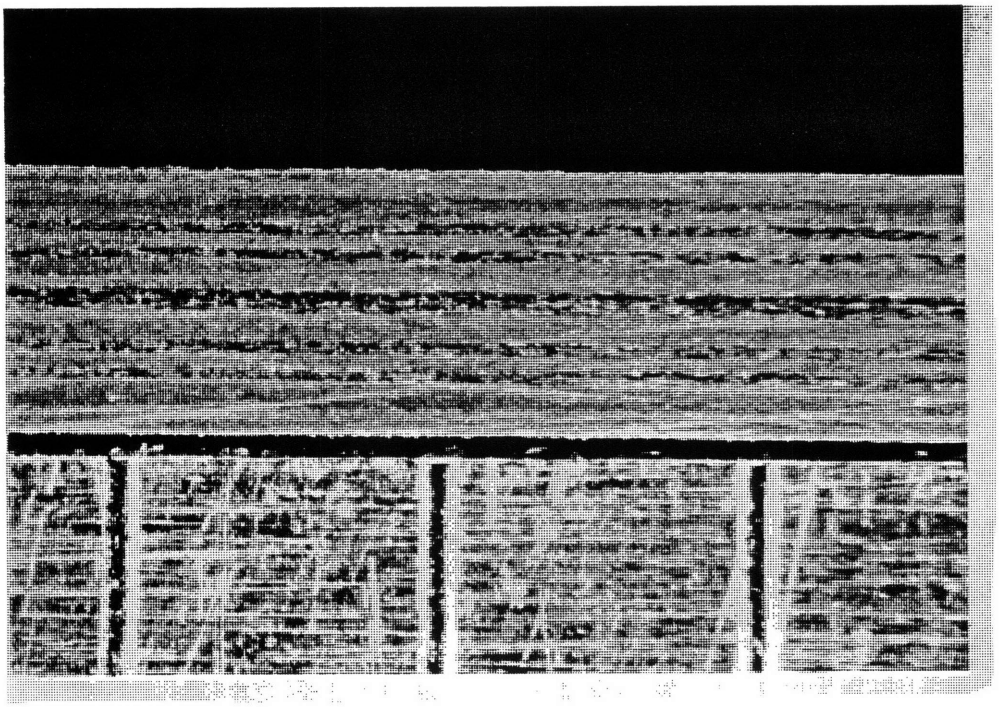

Figure I4 Picture of edge of specimen T30/60/10-15.

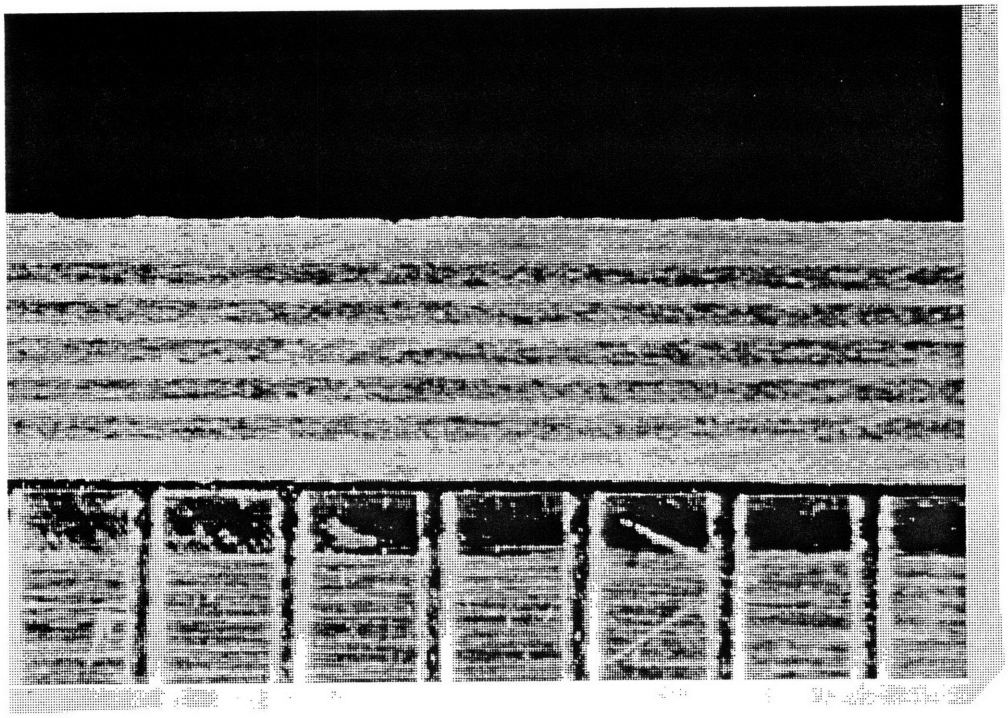

Figure I5 Picture of edge of specimen 50/40/10-18.

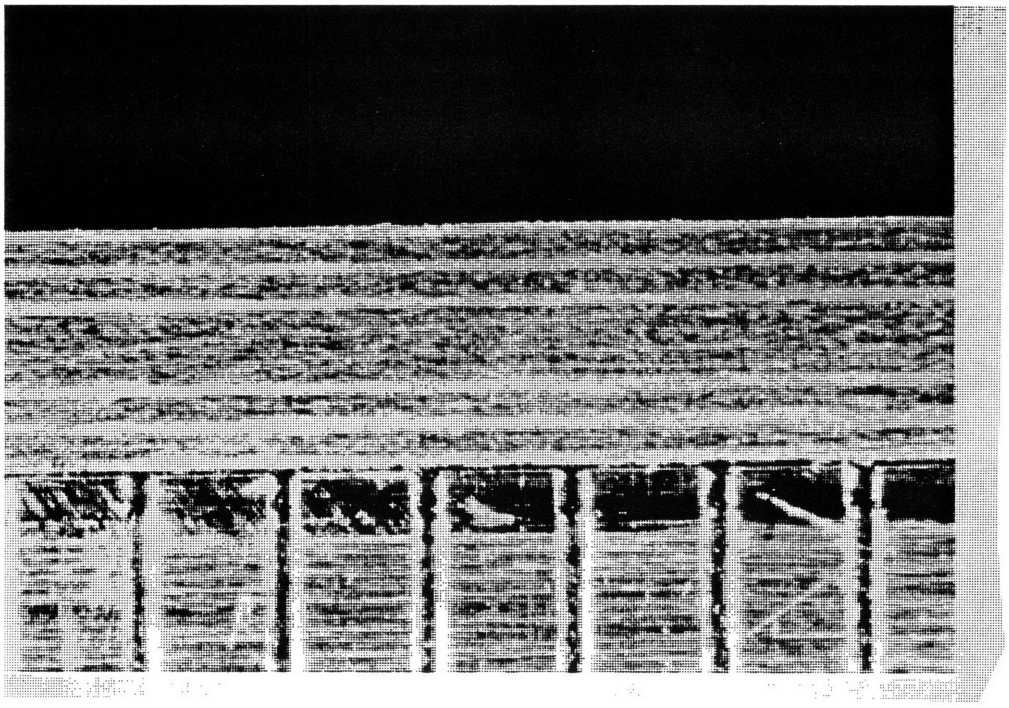

Figure I6 Picture of edge of specimen T70/20/10-19.

Appendix J

Pictures of Flaws in Tensile Coupons

This Appendix contains pictures of various types of manufacturing flaws on the surface and in the edges of the tensile coupons. The edges are along the fibers.

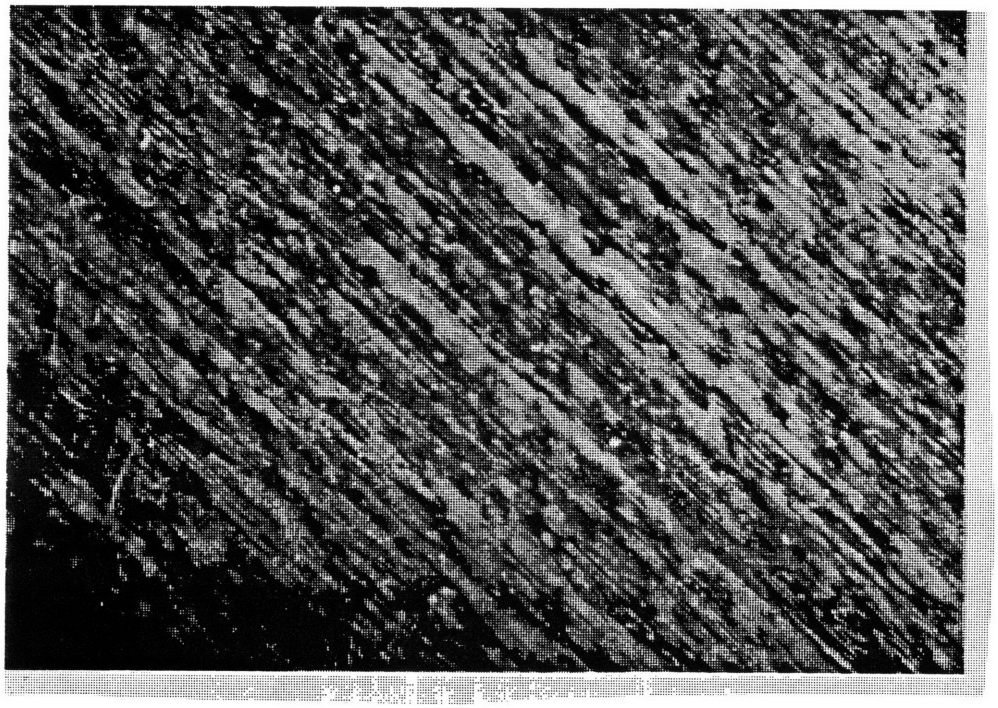

Figure J1 Picture of good surface of T30/60/10-15.

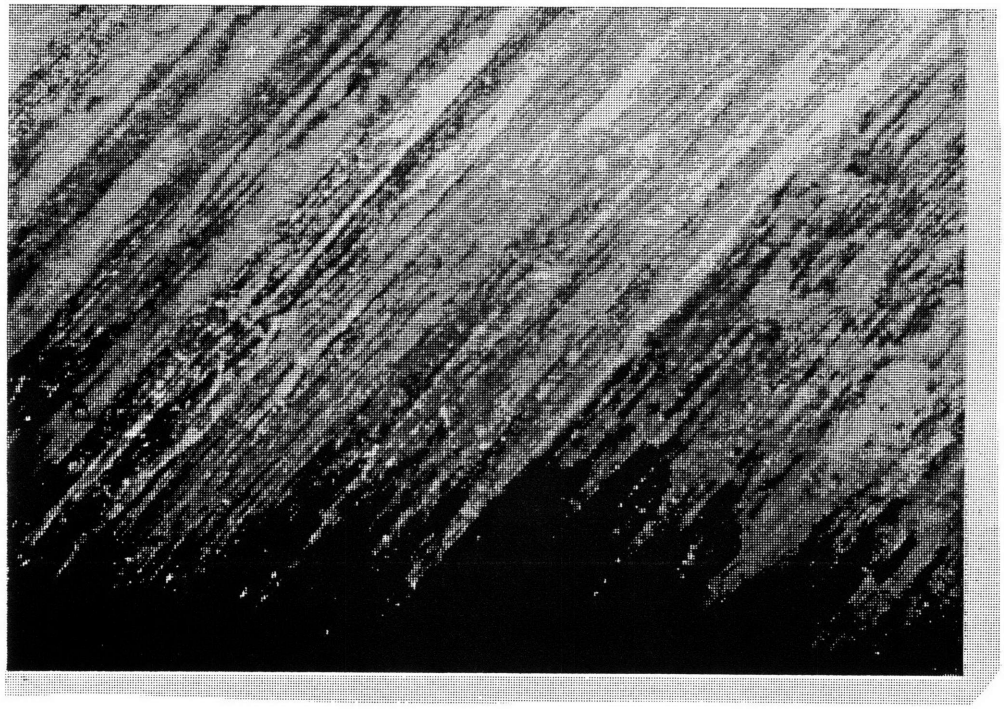

Figure J2 Picture of resin poor surface (burning) of T30/60/10-15.

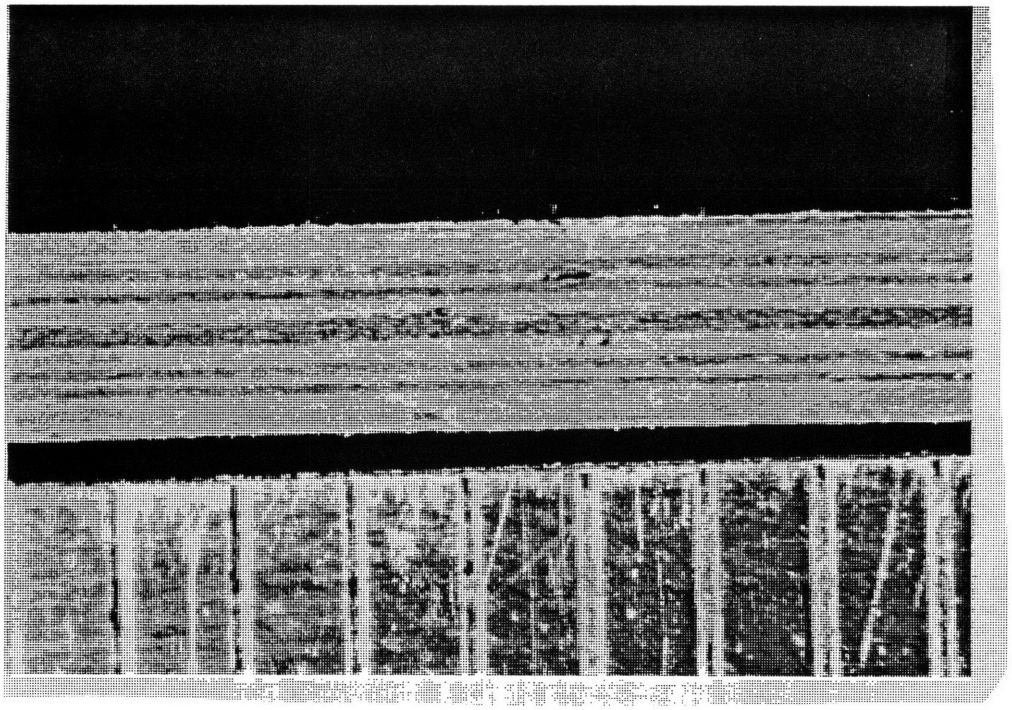

Figure J3 Picture of typical indents in specimen T30/60/10-13. The ruler increments are 1.59 mm (.063 in).

Appendix K

Pictures of Bend Edges, Including a Wrinkle

This Appendix contains a picture of an edge of a typical B100/0/0 angle bend and a picture of the edge of a wrinkle along the width of the specimen.

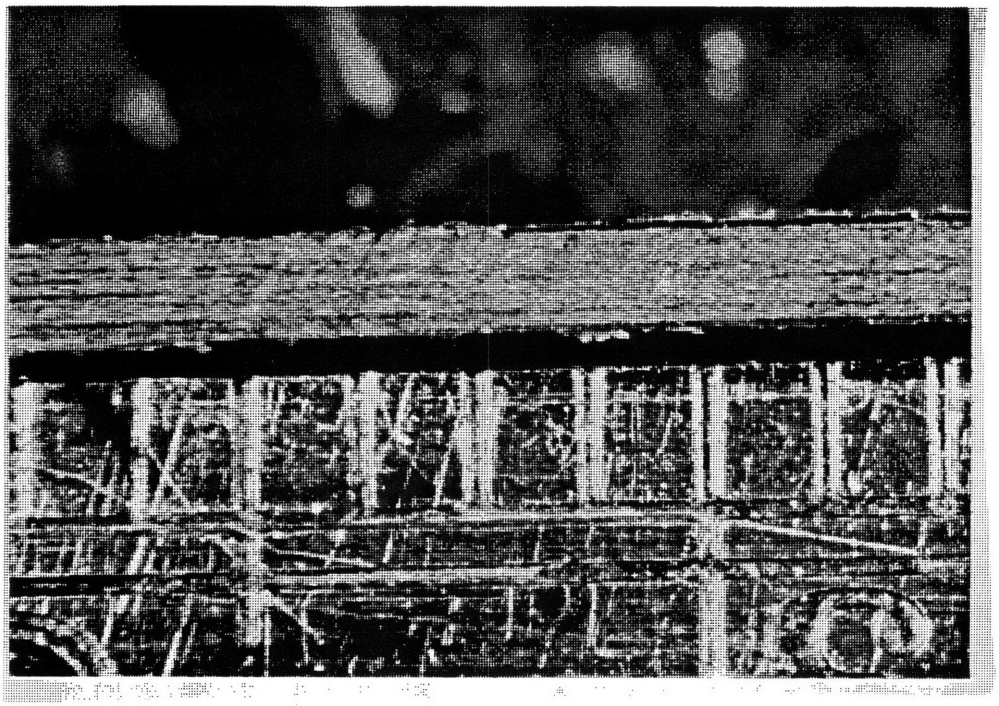

Figure K1 Picture of a typical edge of an angle bend.

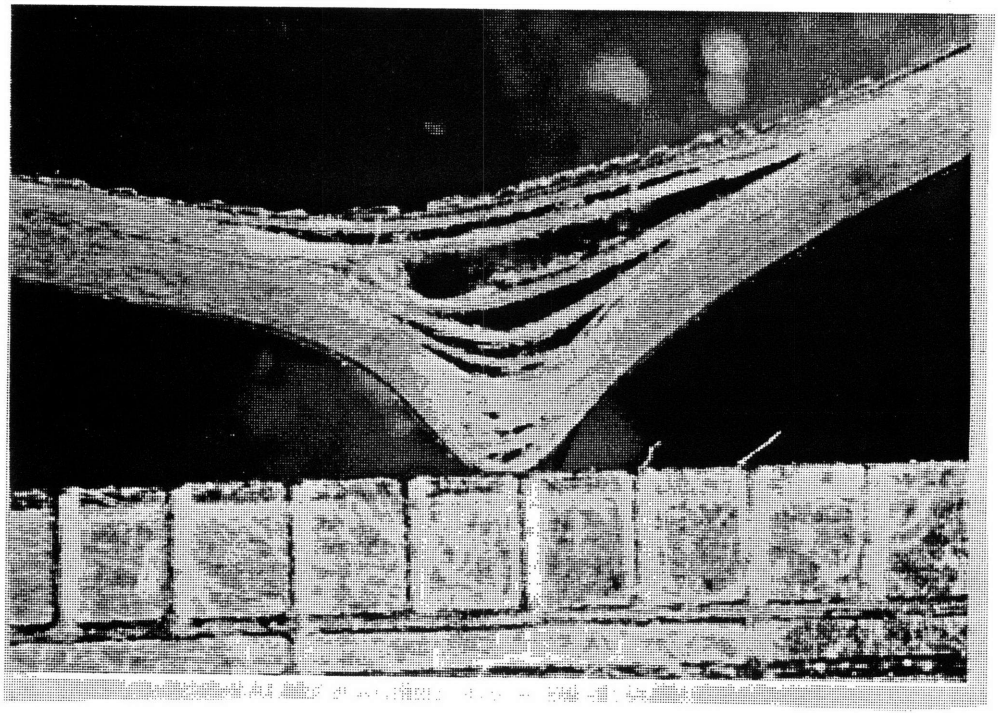

Figure K2 Picture of an edge of a wrinkle in an angle bend. The ruler's increments are 1.59 mm (.063 in).

Appendix L

Picture of Small Plate After Thermoforming

This Appendix contains a picture of a specimen after attempting to use stiff diaphragm forming to make a right angle bend.

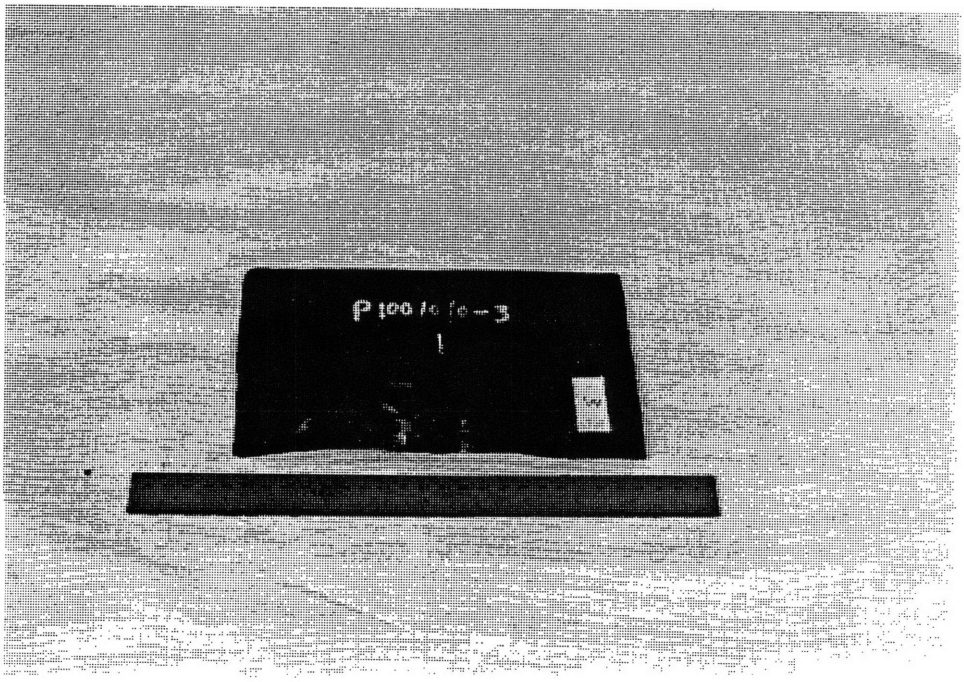

Figure L1 Picture of a specimen after attempting stiff diaphragm thermoforming to form a right angle bend. Originally, the specimen was a small plate with identification P100/0/0-3. Thermoforming was unsuccessful because the heat blanket burned through the Kapton vacuum bag.